

7-1-2015

Characterization of R-ketorolac as a single enantiomer selective inhibitor of Cdc42 and Rac1 in ovarian cancer

Shelby Kenney

Follow this and additional works at: https://digitalrepository.unm.edu/biom_etds

Recommended Citation

Kenney, Shelby. "Characterization of R-ketorolac as a single enantiomer selective inhibitor of Cdc42 and Rac1 in ovarian cancer." (2015). https://digitalrepository.unm.edu/biom_etds/132

This Dissertation is brought to you for free and open access by the Electronic Theses and Dissertations at UNM Digital Repository. It has been accepted for inclusion in Biomedical Sciences ETDs by an authorized administrator of UNM Digital Repository. For more information, please contact disc@unm.edu.

Shelby Ray Kenney Jr

Candidate

Biomedical Sciences

Department

This dissertation is approved, and it is acceptable in quality and form for publication:

Approved by the Dissertation Committee:

Laurie G. Hudson

, Chairperson

Helen Hathaway

Eric Prossnitz

Angela Wandinger-Ness

**CHARACTERIZATION OF R-KETOROLAC AS A
SINGLE ENANTIOMER SELECTIVE INHIBITOR
OF CDC42 AND RAC1 IN OVARIAN CANCER**

by

SHELBY RAY KENNEY JR

Bachelor of Science, Biology, Louisiana Tech University, 2004
Master of Science, Biology, Ball State University, 2009

DISSERTATION

Submitted in Partial Fulfillment of the
Requirements for the Degree of

**Doctor of Philosophy
Biomedical Sciences**

The University of New Mexico
Albuquerque, New Mexico

July 2015

Acknowledgements

I would like to take this opportunity to thank everyone who has made my time at UNM a success. First, to my mentor, Laurie Hudson, thank you for all your help these past years. It has been a privilege to work for you and I have learned so much. I'm not sure I will ever be able to repay you. To my committee, Helen Hathaway, Eric Prossnitz, and Angela Wandinger-Ness, thank you for your support and help in making my project a success. To all the members of the Hudson lab, thank you! Karen Cooper and Sabrina Samudio-Ruiz especially have helped me through a lot of difficulties, personal and professional. I appreciate your friendship more than you will know. To all of my New Mexico friends, especially Adam Flook and Erin Zekas, you helped me keep my sanity and I thank you from the bottom of my heart.

Most importantly, I would like to thank my parents, Shelby and Cindy Kenney. You have supported me through this long and tedious process and I just need to acknowledge that I wouldn't be here, or be the person I am if not for your guidance and help. I love you both, and I hope that I have made you proud. I would also like to acknowledge my brother, Louis Kenney for random calls and texts, they are always fun and interesting.

**Characterization of R-ketorolac as a Single Enantiomer Selective Inhibitor of Cdc42
and Rac1 in Ovarian Cancer**

By

Shelby Ray Kenney Jr.

Bachelor of Science, Biology, Louisiana Tech University, 2004

Master of Science, Biology, Ball State University, 2009

Doctor of Philosophy, Biomedical Sciences, University of New Mexico, 2015

ABSTRACT

Ovarian cancer is the 5th leading cause of cancer death for women in the United States and is frequently diagnosed at an advanced stage with multiple metastases. Rho family GTPases contribute to metastasis through regulation of the actin cytoskeleton, cell motility, cell-cell and cell-extracellular matrix adhesion and these GTPases are altered in a number of human cancers.

High throughput screening and *in silico* modeling identified the R-enantiomer, but not S-enantiomer, of the non-steroidal anti-inflammatory drug ketorolac as a novel inhibitor of Rac1 and Cdc42. Ketorolac is administered as a racemic mix of both enantiomers and is used clinically for surgical pain relief. The analgesic effect of ketorolac occurs through cyclooxygenase inhibition by S-ketorolac. R- ketorolac is a poor inhibitor of cyclooxygenase, but little is known about its pharmacologic activities or targets.

This project identified the expression of the Rho family GTPases Cdc42 and Rac1 in ovarian cancer and inhibition of these GTPases by R-ketorolac. The effects of R-/S-ketorolac, R-ketorolac, and S-ketorolac on Cdc42 and Rac1 regulated cellular events were investigated using SKOV3ip ovarian cancer cells. An intra-peritoneal xenograft mouse model of tumor implantation was used to determine the effects of ketorolac *in vivo*. A phase 0 clinical study examined ketorolac distribution to the peritoneal cavity of ovarian cancer patients following surgery. Additionally, primary ovarian cancer cells from these patients were examined *ex vivo* to determine GTPase activity and a retrospective analysis determined that patients who received ketorolac had improved clinical outcomes.

Together, this work identified Cdc42 and Rac1 as valid therapeutic targets in ovarian cancer. R-ketorolac is shown to inhibit Cdc42 and Rac1 regulated adhesion and migration related events. These results provide evidence to support the idea that the use of ketorolac in the clinic at the time of surgery will improve ovarian cancer patient outcome.

Table of Contents

Approval Form	i
Dissertation Title Page	ii
Acknowledgements	iii
Abstract	iv
Table of Contents	vi
List of Abbreviations	ix
List of Figures	x
List of Tables	xi
Chapter 1 – Introduction	
1.1 Ovarian Cancer	
1.1.1 Health Burden of Ovarian Cancer in the United States	1
1.1.2 Contributors to Mortality and Recurrence of Ovarian Cancer.....	1
1.1.3 Dissemination of Ovarian Cancer	
1.1.3.1 Peritoneal Fluid and Ascites in Ovarian Cancer	5
1.1.3.2 Multicellular aggregates in Ovarian Cancer Dissemination ..	7
1.1.4 Targeted Therapeutics in Ovarian Cancer	7
1.1.5 GTPases as Emerging Therapeutic Targets in Ovarian Cancer	
1.1.5.1 Ras Superfamily GTPases	10
1.1.5.2 Ras GTPases in Cancer.....	10
1.1.5.3 Cdc42 in Cancer	14
1.1.5.4 Rac1 in Cancer.....	14
1.2 Rho Subfamily GTPases	
1.2.1 Regulation of Rho Subfamily GTPases	15
1.2.2 Rho Subfamily GTPase Functions.....	16
1.2.3 Cdc42.....	18
1.2.4 Rac1	19
1.2.5 Interaction Between Cdc42, Rac1, and RhoA in Cell Migration.....	19
1.3 Targeting GTPases	
1.3.1 GTPases as Therapeutic Cancer Targets.....	21
1.3.2 Therapeutic Strategies for Rho Family GTPase Inhibition.....	22
1.3.2.1 GEFs and Effector Proteins	22
1.3.2.2 Statin Therapy in Cancer	24
1.3.2.3 Direct GTPase Inhibition.....	25
1.4 Drug Development	
1.4.1 High-Throughput Screening	27
1.4.2 Identification of Inhibitors of the Rho Family GTPases.....	28
1.4.3 Identification of Cdc42 and Rac1 Inhibitors.....	29
1.5 Ketorolac	30
1.6 Study Significance	34

Chapter 2 – Characterization of R-ketorolac in an <i>in vivo</i> model of recurrent ovarian cancer	
2.1 Introduction	36
2.2 Results	
2.2.1 Oral administration of ketorolac reduces tumor burden <i>in vivo</i>	39
2.2.2 Ketorolac has no effect on SKOV3ip growth kinetics in culture	40
2.2.3 Ketorolac does not change growth kinetics <i>in vivo</i>	42
2.2.4 Impact of ketorolac on GTPase gene expression	43
2.2.5 Ketorolac inhibits KOV3ip MCA adhesion and spreading	44
2.3 Discussion	46
2.4 Methods	
2.4.1 Ketorolac dosage	50
2.4.2 Animal model	50
2.4.3 High performance liquid chromatography.....	51
2.4.4 Cell migration assay	52
2.4.5 Cell culture fluorescent proliferation assay	52
2.4.6 MCA cytometry	53
2.4.7 Cell cycle assay.....	54
2.4.8 Immunohistochemical staining	54
2.4.9 RNA isolation	55
2.4.10 qPCR.....	56
2.4.11 MCA adhesion and spreading.....	57
2.5 Figure Legends	58
2.6 Figures	67
Chapter 3 – A novel pharmacologic activity of ketorolac for therapeutic benefit in ovarian cancer patients	77
3.1 Introduction	77
3.2 Results	
3.2.1 Expression of Rac1 and Cdc42 in ovarian cancer	79
3.2.2 Study design and patient population	80
3.2.3 Distribution of R- and S-ketorolac in peritoneal fluids	81
3.2.4 Analysis of patient derived cells.....	82
3.2.5 Retrospective patient outcomes review	83
3.3 Discussion	84
3.4 Patients and Methods	
3.4.1 Immunohistochemical analysis of GTPase targets	87
3.4.2 Quantitative PCR (qPCR) of ovarian cancer cDNA arrays	89
3.4.3 Patients, study design and treatment.....	89
3.4.4 High performance liquid chromatography.....	90
3.4.5 Analysis of GTPase activity	91
3.4.6 Isolation of patient derived cells.....	92
3.4.7 Retrospective patient outcomes review	93
3.4.8 Statistical Analysis.....	94
3.5 Figure Legends	100
3.6 Figures	107
Chapter 4 – Project Summary	
4.1 Overview	120
4.2 Ras GTPases in Cancer	121
4.3 Effect of Ketorolac on Ovarian Cancer in Culture	122

4.4 Effect of Ketorolac on Ovarian Cancer cells <i>in vivo</i>	125
4.5 Limitations of Animal Model	129
4.6 Ketorolac in Ovarian Cancer Patients	130
4.7 Future Directions.....	132
Literature Cited	135

List of Abbreviations

Cdc42 – cell division control protein 42 homolog
COX – cyclooxygenase
ECM – extracellular matrix
EGF – epidermal growth factor
EMT – epithelial-mesenchymal transition
FIGO - Federation Internationale de Gynecologie et d'Obstetrique
FTI – farnesyltransferase inhibitor
GAP – GTPase activating protein
GDI – guanine nucleotide dissociation inhibitors
GDP – guanosine diphosphate
GEF – guanine exchange factor
GFP – green fluorescent protein
GLISA – GTPase linked immunosorbent assay
GTP – guanosine triphosphate
GTPases – guanosine triphosphate-ases
GPCRs – G-coupled protein receptors
HMG-CoA – 3-hydroxymethylglutaryl-coenzyme A
HTS – high-throughput screening
KRAS – Kirsten-Ras
LMP – low malignant potential
MAPK – mitogen-activated protein kinase
MCA – multicellular aggregate
MLP – molecular libraries program
MMP – matrix metalloproteinases
NSAID – nonsteroidal anti-inflammatory drug
PAK – p21 associated kinase
PARP – poly(ADP-ribose) polymerase
PCR – polymerase chain reaction
PI3K – phosphatidyl-inositol-3-kinase
PIP3 –phosphatidyl-inositol-3,4,5-trisphosphate
PIX – PAK-interacting exchange factor
qPCR – quantitative polymerase chain reaction
Rac1 – Ras-related C3 botulinum toxin substrate 1
Ras – rat sarcoma protein
RhoA – Ras-homolog gene family member A
RFP – red fluorescent protein
ROCK – Rho-associated kinases
RTK – receptor tyrosine kinase
ROS – reactive oxygen species
TUNEL - Terminal deoxynucleotidyl transferase (TdT) dUTP Nick-End Labeling
VEGF - vascular endothelial growth factor
WASP - Wiskott-Aldrich syndrome protein
WAVE – WASP family verprolin-homologous protein

List of Figures

Figure 1.1 - Staging of ovarian cancer.....	2
Figure 1.2 - Distant peritoneal metastasis and dissemination in ovarian cancer due to the formation of multicellular aggregates.....	8
Figure 1.3 - Rho GTPase activation and cycling	11
Figure 1.4 - The Ras superfamily	13
Figure 1.5 - Cdc42, Rac1, and RhoA interactions in cell migration.....	17
Figure 1.6 – Different methods for inhibition of GTPase activity in the treatment of cancer	23
Figure 1.7 - Pathway of prostanoid synthesis	32
Figure 1.8 - Structure and <i>in vivo</i> IC ₅₀ values for ketorolac and naproxen enantiomers.....	33
Figure 2.1 - Oral administration of ketorolac reduces tumor burden <i>in vivo</i>	67
Figure 2.2 – Animals treated with R-naproxen have decreased tumor burden.....	68
Figure 2.3 – There is no interconversion of R-/S-Ketorolac, R-ketorolac, or S-ketorolac does not spontaneously interconvert when used in cell culture	69
Figure 2.4 – OVCA429 and SKOV3ip cell lines have similar responses ML141, NSC23766, and ketorolac treatments	70
Figure 2.5 – Ketorolac has no effect on SKOV3ip cell proliferation or cell cycle.....	71
Figure 2.6 – Ketorolac has no effect on proliferation <i>in vivo</i>	72
Figure 2.7 – Ketorolac has no effect on apoptosis <i>in vivo</i>	73
Figure 2.8 – Cdc42 or Rac1 inhibition does not change GTPase gene expression in cells or <i>in vivo</i>	74
Figure 2.9 – Ovarian cancer cell lines express the Rac1 splice variant Rac1b	75
Figure 2.10 – Ketorolac treatment reduces adhesion and MCA spreading	76
Figure 3.1 – Overexpression of Rac1 and Cdc42 protein in ovarian cancer specimens.....	107
Figure 3.2 – Expression of constitutively active Rac1b mRNA is elevated in ovarian cancer specimens	108

Figure 3.3 – Expression of Rho-family GTPases in primary patient cDNA samples analyzed by grade for serous cancer only	109
Figure 3.4 – Ketorolac distributes to peritoneal fluids and is enriched in the R-enantiomer.....	110
Figure 3.5 – Racemic distribution of clinical drug	111
Figure 3.6 – GTPases are activated in patient ascites and inhibited by ketorolac administration <i>in vivo</i>	112
Figure 3.7 – Purified Ovarian Tumor Cells Express EpCam and MUC16/CA125	113
Figure 3.8 – RhoA activity is insensitive to ketorolac treatment.....	114
Figure 3.9 – Example survival among ovarian cancer patients with and without perioperative ketorolac.....	115
Figure 3.10 – Survival estimates based on Cox-regression for Stage I (AJCC) with completion of chemotherapy.....	116
Figure 3.11 – Survival estimates based on Cox-regression for Stage II (AJCC) with completion of chemotherapy.....	117
Figure 3.12 – Survival estimates based on Cox-regression for Stage III (AJCC) with completion of chemotherapy.....	118
Figure 3.13– Survival estimates based on Cox-regression for Stage IV (AJCC) with completion of chemotherapy.....	119

List of Tables

Table 3.1 – Hazard ratios for ovarian cancer specific mortality for each characteristic adjusted for the other characteristics in the table.....	96
Table 3.2 – Patient Characteristics for IHC Microarrays OV1005 and OV8010	97
Table 3.3 – Patient Characteristics for cDNA Microarray	98
Table 3.4 – Ketorolac enantiomer concentration in serum or peritoneal fluids.....	99
Table 4.1 – Summary of the effect of Cdc42 and Rac1 inhibition on SKOV3ip ovarian cancer cells.....	123
Table 4.2 – Summary of the effect of Cdc42 and Rac1 inhibition on SKOV3ip ovarian cancer cells <i>in vivo</i>	126

Chapter 1

Introduction

1.1 Ovarian Cancer

1.1.1 Health Burden of Ovarian Cancer in the United States

In 2014, there were an estimated 22,000 newly diagnosed cases of ovarian cancer and 14,000 ovarian cancer related fatalities in the United States (1–3). Staging of ovarian cancer is based upon Federation Internationale de Gynecologie et d’Obstetrique (FIGO) guidelines. Patients with early stage disease (FIGO Stage I and II) have a 5 year survival rate of greater than 70%, while late stage disease (FIGO stage III and IV) have a 5 year survival rate of approximately 30% (1–3). Ovarian cancer is a heterogeneous disease, with many different sites of origin (2,4–6). The term ovarian cancer traditionally refers to epithelial ovarian cancer, due to the fact that carcinomas appear to arise from the epithelial cell layer of the ovary (2,4–6). New immunohistochemical evidence of patient samples suggests that histological subtypes of ovarian cancer arise from extra-ovarian sources (7,8). Staging and histological typing of the disease are common ways of indicating the severity and metastatic potential of the disease (2,4–6). Staging of ovarian cancer is based on the level of involvement of the ovaries and surrounding viscera (Fig 1.1) (1). Metastases in advanced disease are common at the omentum, intestinal mesentery, adipose tissue, lymph tissue, diaphragm, as well as spleen and liver surfaces.

1.1.2 Contributors to Mortality and Recurrence of Ovarian Cancer

While patients with early stage disease have a better prognosis for progression free survival, the majority of the patient population presents with late stage disease (2).

Figure 1.1

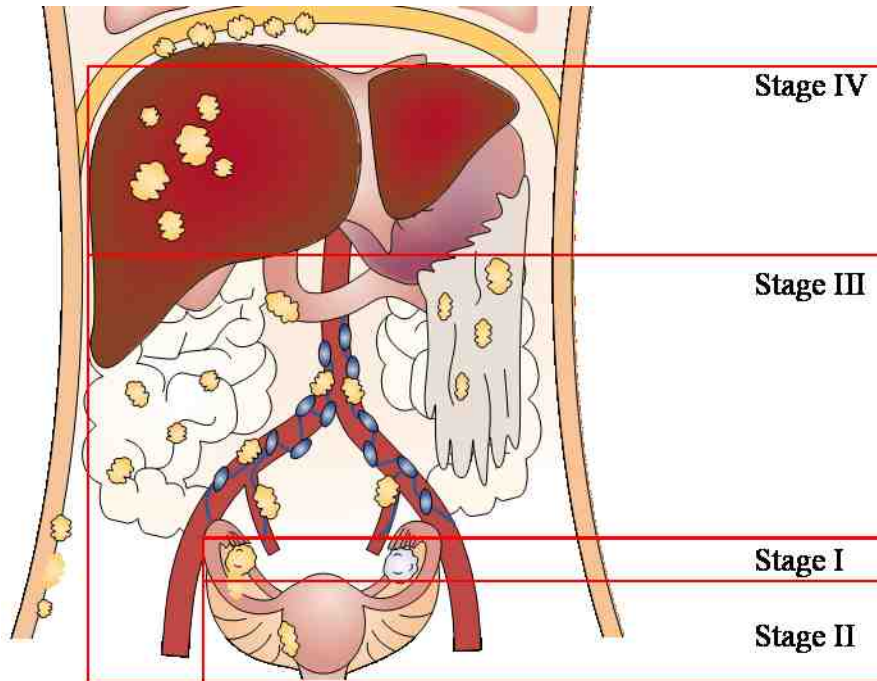


Figure 1.1 - Staging of ovarian cancer. The illustration depicts levels of tumor dissemination (yellow masses) used to determine stage in ovarian cancer. Stage I disease is limited to one or both ovaries with no breach of the epithelial ovarian capsule. Stage II disease includes one of both ovaries with limited metastasis to surrounding pelvic tissue, such as the endometrium, fallopian tubes, or uterus. Stage Ic and Iic disease are early stage disease but include malignant ascites. Stage III disease includes above with distant metastases to the intestinal mesentery, kidneys, lymph tissue (blue network), omentum, peritoneal surfaces, and surface implantation of the diaphragm. Stage IV includes all the above metastases with the inclusion of liver metastases. Image adapted from Naora and Montell (19).

Late stage diagnosis is common due to a lack of symptoms, few reliable biomarkers, and insufficient screening techniques for early diagnosis. Overall, patients diagnosed with ovarian cancer have a survival rate of approximately 40%. By comparison, women diagnosed with breast or uterine cancer have survival rates of approximately 80% (2). There are several major factors that contribute to the mortality of this disease, a few of which will be discussed.

Advanced ovarian cancer presents with varying degrees of metastasis (1–4). Metastasis in the context of ovarian cancer is unique from other cancers (6,9). Typically, metastasis refers to the ability of tumor cells to degrade the basement membrane, extravasate into the vasculature, spread hematogeneously, and seed secondary sites of implantation. Due to the nature of ovarian cancer and structure of the peritoneal cavity, metastatic cancer cells rarely enter the vasculature. Instead, ovarian cancer metastasis involves individual cancer cells or small multicellular aggregates (MCAs) moving from the tumor of origin to secondary sites within the peritoneal cavity (9). Cells float within the peritoneal cavity until they are able to attach to secondary sites. Ovarian cancer cells preferentially adhere to mesothelium and adipose tissue during secondary implantation (9,10). Additionally, changes that induce metastatic spread may also increase the invasive potential of these tumors (11–13). There are a number of signaling pathways altered in ovarian cancer cells prior to metastatic spread, which will be further discussed in section 1.1.4. Patients may not exhibit symptoms that allow for diagnosis of early stage ovarian cancer; however, increased tumor burden and strain on affected organs that comes with late stage disease, often leads to a cancer diagnosis.

Another factor leading to increased mortality is related to methods of treatment. Ovarian cancer patients are treated with surgery, chemotherapy, and/or radiotherapy (1,2,5). Surgery during early stage of the disease involves oophorectomy to remove the primary tumor and may be given as the sole treatment (1). In advanced disease, cytoreductive tumor debulking occurs, removing visible tumors. This does not account for microtumors which may be present, or for any tumor cells that are dislodged during surgery (1,9,13,14). Following a post-surgery recovery period, patients are given chemotherapy with or without radiotherapy (14). The most common chemotherapies include a combination of platinum based compounds and taxanes (14). Cisplatin and carboplatin are commonly prescribed platinum drugs, while paclitaxel is the most common taxane derivative (14,15). Many patients have tumors that are responsive to first line chemotherapy. However, more than 50% of patients will suffer from recurrent disease, and of these, approximately 70% will be resistant to platinum or taxane based therapy (5,14–16). Refractory disease leaves patients with few treatment options, the most common being liposomal doxorubicin (16). However, these alternative therapies are less successful and patients with refractory disease have a poor prognosis (5,16).

A third factor contributing to ovarian cancer mortality is the high level of heterogeneity between tumors and metastases (1,2,4–8). It has been suggested that rather than using histological subtype for ovarian cancer, carcinomas should be classified as type I and type II tumors (7). Type I tumors are characterized by young age of diagnosis, low malignant potential (LMP), low resistance to chemotherapeutics, and prolonged survival time (5,7). Type I cancers are confined to or near the ovary, possess varying levels of differentiation, and have high levels of genetic variability, which likely

accumulate as the tumor develops (7). In contrast, type II tumors are prevalent in postmenopausal women, highly malignant, initially sensitive but later refractory to chemotherapy, and patients have a shorter median survival time. Type II cancers are highly metastatic, show less differentiation, and are less well understood genetically, but typically have copy number aberrations and high genetic instability. This high genetic variation, even within a single patient, increases chemoresistance, complicates treatment, and ultimately leads to increased mortality (5,7).

Advanced disease at the time of diagnosis, multiple metastatic sites, organ involvement, peri- and post-surgical tumor environment, genetic and phenotypic variation between primary tumor and metastases within a patient, all potentially contribute to the high recurrence of ovarian cancer. With this in mind, development of new chemotherapies is needed to help increase the survival rate of women with ovarian cancer.

1.1.3 Dissemination of Ovarian Cancer

1.1.3.1 Peritoneal Fluid and Ascites in Ovarian Cancer

Dissemination of ovarian cancer cells can occur either through direct organ/tumor contact, or through cells circulating within the peritoneal fluid (6,7,17–20). Exfoliation of ovarian cancer cells from the primary tumor allows either single cells or MCAs to travel through the peritoneal cavity. Peritoneal fluid, moved through active respiration, will flow from the pelvis, along the right side of the body, along the intestinal mesenteries, to the right hemidiaphragm and across the omentum (17,18). Cancer cells will flow with the peritoneal fluid and seed not only adjacent tissues but any site within the peritoneal

cavity. Metastases are typically seen along the peritoneal cavity wall, in adipose and lymph tissue, intestinal mesentery, diaphragm, along the spleen and liver capsule, and within the omentum (1,17,18). Dissemination through the lymphatic system is also common in malignant stages of the disease. Rates of ovarian cancer within the paraaortic lymph node have been reported between 18%-70% depending on disease stage (20). Hematogenous spread is possible, but has only been reported in 2-3% of patients and occurs in patients with advanced stage disease (18,19,21). Significant risk factors for distant metastases are malignant ascites, peritoneal carcinomatosis, large metastatic disease within the abdomen, and retroperitoneal lymph node involvement at the time of initial surgery.

One contributing factor to metastasis is the development of ascites within the peritoneal cavity (20,22). Ascites is a fluid buildup between the peritoneal wall and the organs within the peritoneum. Under normal physiological conditions, a small amount of peritoneal fluid is produced from capillaries in the peritoneal wall to lubricate the viscera within the peritoneum. Fluid gets reabsorbed by blood vessels and the lymphatic system. In patients with ovarian cancer, leaky vasculature within the tumor and obstructed lymphatic vessels are unable to deal with the increased fluid production (20,22). This causes the formation of ascites, which is associated with poor disease prognosis. Ascites fluid is rich in inflammatory cytokines, growth factors, and extracellular matrix components which inhibit immune system function, promote cancer cell survival and proliferation, and stimulate cell adhesion and migration.

1.1.3.2 Multicellular Aggregates in Ovarian Cancer Dissemination

Advanced ovarian cancer is characterized by distant peritoneal metastases (3–5,18). Metastases occur because the primary tumor is able to breach the ovarian capsule and exfoliate cells into the peritoneal fluid. This leads to the formation of MCAs which circulate and implant at secondary sites (Fig 1.2) (5–7,11,13–15,19,23). Following release from the primary tumor, cancer cells will aggregate into MCAs. The formation of MCAs allows the cells to survive in an attachment independent manner (23). MCAs are able to evade radio- and chemotherapies (24,25) and their formation contributes to chemoresistance (26–28). Once formed, MCAs will home to specific sites in these tissues within the peritoneal cavity. This is consistent with the seed and soil hypothesis of cancer metastasis, and partially explains the pattern of ovarian cancer dissemination seen in late stage patients. The initial adhesion to secondary sites is mediated by integrin/extracellular matrix (ECM) interactions (23,29,30). Once MCAs have adhered to these preferred secondary sites, they disaggregate, and individual cells migrate along the mesothelial cell layer, away from the site of adhesion (9,13). Cancer cells then begin proteolytic digestion of the ECM, ultimately establishing metastatic tumors (5,7,9,11,23,30,31). Although these processes occur in primary dissemination of ovarian cancer, they also contribute to the high recurrence of this disease (2,5). Therapeutic targeting of MCA formation, adhesion, and disaggregation offers a novel approach to reduce recurrent ovarian cancer.

1.1.4 Targeted Therapeutics in Ovarian Cancer

Therapeutics for ovarian cancer have changed little since the 1970s (1,32–36). Surgery, followed by platinum or taxane therapy is standard treatment, but has not

Figure 1.2

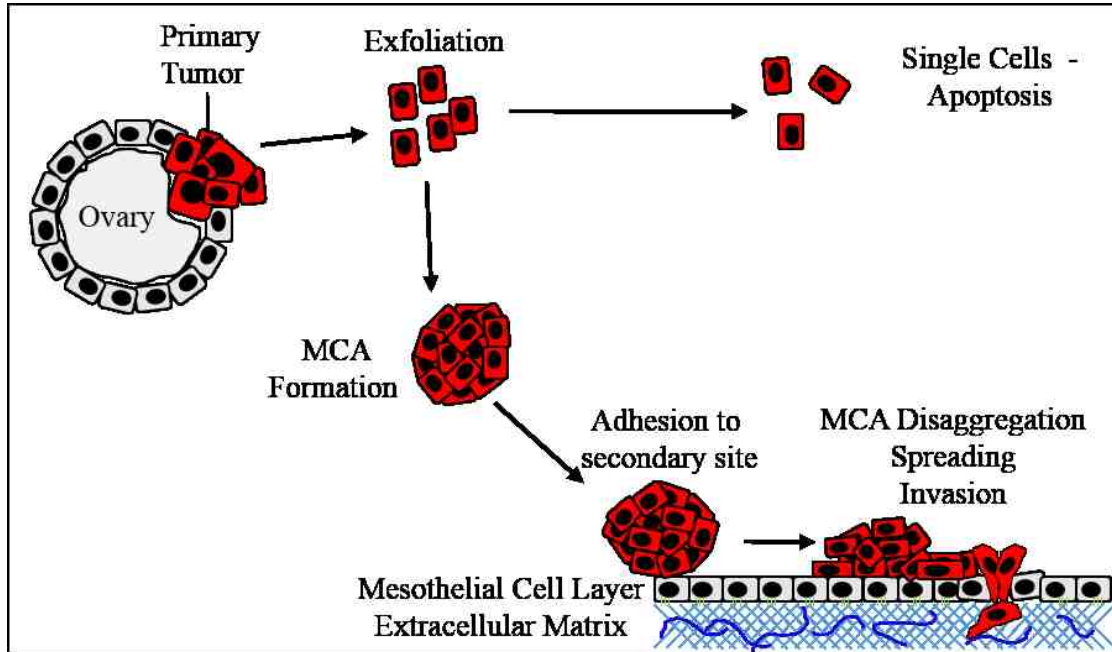


Figure 1.2 – Distant peritoneal metastasis and dissemination in ovarian cancer due to the formation of multicellular aggregates. Following a breach of the ovarian capsule, cancer cells are exfoliated from the primary tumor. Cells remaining as single cells will likely undergo apoptosis. Exfoliation of many cells may result in MCAs. MCA formation provides survival signals to the cells, are chemoprotective, and contribute to the development of chemoresistance. MCAs travel through the peritoneal cavity via the flow of peritoneal fluid. MCAs will home to specific tissues, typically mesothelium or adipose tissue. Adhesion of the MCA is mediated by integrin ECM interactions. MCA disaggregation leads to cell migration away from the site of implantation. Migrating cells express MMPs to break mesothelial cell contacts and to degrade ECM, establishing secondary metastatic tumors.

improved patient survival rates in over 20 years. Targeted therapeutics would provide alternatives during adjuvant chemotherapy that may reduce recurrence or to attack platinum-resistant recurrent disease (32). BRCA1 and p53 mutations are reliant on the action of poly(ADP-ribose) polymerase (PARP) to avoid apoptosis. BRCA1 mutations have been identified in high grade serous carcinomas (37) and PARP overexpression has been recognized as a poor prognostic marker for overall survival and progression free survival (38). With this in mind, the use of PARP inhibitors is currently being explored and have promise for providing survival benefit to patients. Immunotherapies looking at the use of the inflammatory cytokine interferon- γ is being explored as a possible first line treatment or in combination with current chemotherapies (39,40). Interferon- γ treatment has met with mixed results. When used in conjunction with cisplatin and cyclophosphamide, interferon- γ increased progression free survival time (39). In another clinical trial, the use of interferon- γ prior to carboplatin and paclitaxel had no effect on survival (40). Perhaps the most promising alternative treatment for ovarian cancer is bevacizumab (41). Bevacizumab is an anti-angiogenic monoclonal antibody to VEGF receptor. Activation of VEGF increases angiogenesis, which contributes to ovarian cancer tumor development (19,20,42). When used alone, bevacizumab increases progression free survival in ovarian cancer patients and there is a synergistic effect when used in conjunction with other chemotherapeutics (41). A number of patients experience a severe adverse event in the form of gastrointestinal bleeds. This has prompted the search for biomarkers to predict which individuals may benefit from the use of bevacizumab (43). It is clear that the individuals who are not at risk from the therapy,

benefit from bevacizumab. The difficulty is that not all patients who could benefit are able to receive this treatment.

1.1.5 GTPases as Emerging Therapeutic Targets in Ovarian Cancer

1.1.5.1 Ras Superfamily GTPases

The Ras Sarcoma (Ras) superfamily of GTPases are low molecular weight, monomeric, membrane bound, guanine nucleotide binding proteins (44–47). Ras GTPases possess an N-terminal G-domain consisting of G-box guanine nucleotide binding motif. Switch regions within the G-domain induce conformational changes depending on guanine nucleotide status. These proteins are localized to the cell membrane, where activation from G-protein coupled receptors (GPCRs), integrins, and receptor tyrosine kinases (RTKs) causes a nucleotide switch and activation (Fig 1.3) (46). Guanosine diphosphate (GDP) or guanosine triphosphate (GTP) binding determines GTPase interaction with regulator and effector proteins. Most Ras superfamily members possess a C-terminal CAAX (C=cysteine, A=aliphatic residue, X=any residue) box motif that permits the covalent addition of either an isoprenoid group, targeting the GTPase to a specific cellular membrane, where they interact with regulators and effector proteins (45).

1.1.5.2 Ras GTPases in Cancer

The Ras superfamily is composed of over 150 GTPases that regulate signal transduction pathways (Fig 1.4) (44–47). Ras is divided into five subfamilies based on the sequence and function of the founding members (44–47). The Ras subfamily are proto-oncogenes which regulate cell functions related to gene expression, proliferation,

Figure 1.3

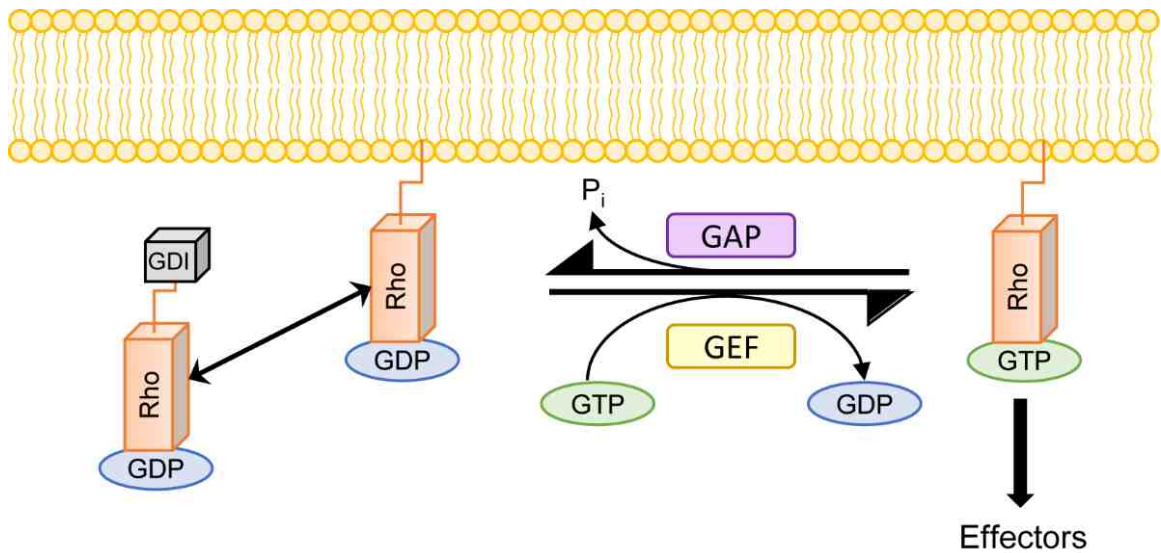


Figure 1.3 – Rho GTPase activation and cycling. Guanine nucleotide dissociation inhibitors (GDIs) bind the isoprenoid moiety of inactive, GDP bound, Rho GTPases, preventing binding to the plasma membrane. Removal of the GDI allows association with the plasma membrane. Interaction with guanine nucleotide exchange factors (GEFs) replace guanosine diphosphate (GDP) with guanosine triphosphate (GTP). This induces a conformational change in GTPases and allows for interaction with effector proteins.

differentiation, and cell survival (45–47). The Ras-homolog (Rho) subfamily, which integrate signals from the cellular microenvironment, facilitate crosstalk between signaling networks, and largely control actin dynamics and related signaling (45–47). Ras (44–52), and the Rho members Cdc42, Rac1 and RhoA (53–71), have been identified as playing a role in a number of cancers.

In ovarian cancer, mutations of Kirsten-Ras (*KRAS*) have been found in approximately half of the cases of mucinous and LMP tumors, but are uncommon in serous tumors (48,49). KRas regulates cell survival and gene expression related to tumorigenesis, making it a promising molecular target in ovarian cancer. Farnesylation of Ras proteins requires interaction with farnesyltransferase (44). It is thought that those ovarian tumors which have KRas mutations may be susceptible to treatment with farnesyltransferase inhibitors (FTIs), preventing association with the membrane and subsequent activation. While there has been success with FTI treatments in breast cancer (50) results have been mixed in ovarian cancer (51,52). The use of FTIs in conjunction with paclitaxel and gemcitabine was successful, initially, in increasing response rate and progression free survival of ovarian cancer patients (51). However, a more recent study saw no effect of the addition of FTIs to carboplatin and paclitaxel treatment (52).

Ras pathways make promising therapeutic targets because they regulate a number of cell signaling pathways (44). Inhibition of Ras signaling may be beneficial because of the disruption to other signaling pathways that may be linked to ovarian cancer. Development of targeted therapeutics is less problematic for most human cancers due to the homogeneity of the tumors and the distinct genetic or protein expression changes that are the hallmark of those diseases (2,3,32,37,50,72,73). Ovarian cancer is a

Figure 1.4

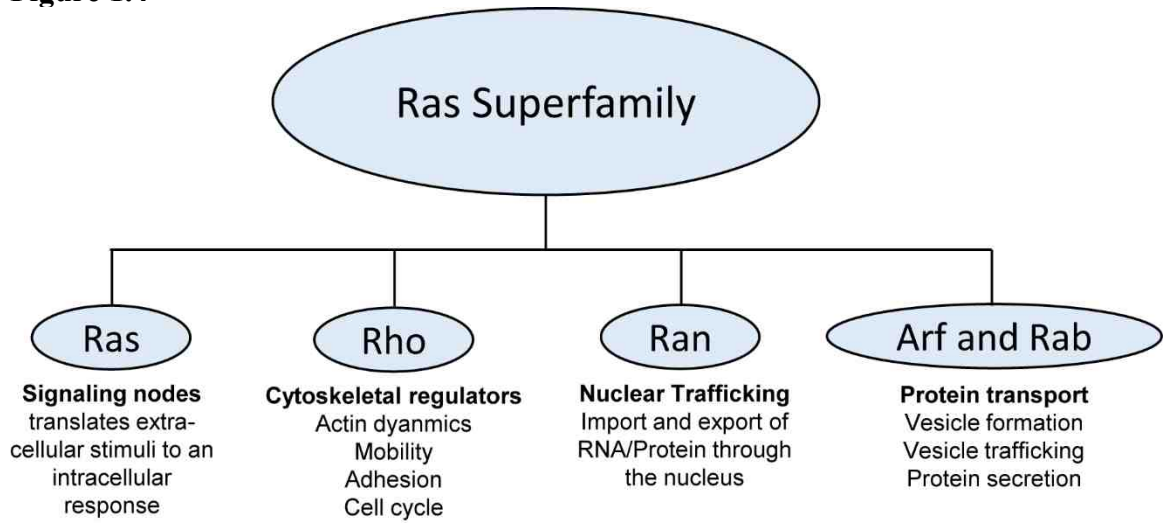


Figure 1.4 –The Ras superfamily. The subfamilies that comprise the Ras superfamily and their respective functions.

heterogeneous disease with many histological subtypes, which have distinct molecular profiles (14,15,19,20). Even within a single patient, primary tumors and metastases can exhibit vastly different molecular profiles, making a single treatment for all patients implausible. Perhaps the best option for treatment is to use cell signaling pathways that are broad spectrum and more likely to apply to the pathways required for recurrence.

1.1.5.3 Cdc42 in Cancer

Aberrant signaling of Cdc42 has only been identified in a few cancers (53,74). Kamai et al identified Cdc42, Rac1, and RhoA as being overexpressed in testicular cancer (53). As disease stage progresses, expression of all three GTPases increases, leading the authors to suggest that they are necessary for disease progression of testicular cancer. Fritz et al have shown that there is an overexpression of Cdc42 in breast cancer (74). This overexpression also increases with disease progression. RhoGDIs that associate with Cdc42 have been shown to be overexpressed in ovarian cancer (75). This would prevent activation of Cdc42, and may cause other Rho GTPases to compensate, leading to tumorigenesis. This identifies Cdc42 as a viable target for therapy and potential dysregulated in ovarian cancer.

1.1.5.4 Rac1 in Cancer

Despite having no genetic alterations, Rac1 has been identified as playing a role in a number of cancers (54,58). Rac1 overexpression is known to occur in breast, colon, lung, gastric, testicular, oral squamous cell carcinoma, and ovarian cancer (53,59–65). Overexpression of Rac1 in cancer can lead to increased levels of metastasis through

epithelial-to-mesenchymal transition (EMT), decreased levels of apoptosis, increased angiogenesis, and has been identified as a marker of poor prognosis (53,59–66).

A splice variant of Rac1, Rac1b, was initially identified as a neural-specific isoform of Rac1, and was thought to play a role in development (67). Since its identification, it has been described in breast (59), colon (61), lung (68), and ovarian cancer (65). Rac1b is unique from Rac1 in that, other than being present in developing neurons, it appears to be largely tumor specific. Rac1b is also constitutively active, having accelerated GDP/GTP exchange, decreased hydrolytic activity, and a decreased affinity for RhoGDI or GAPs. Because Rac1b is constitutively active, it has increased signaling, which promotes tumorigenesis and metastasis. Rac1b has been shown to protect cells from apoptosis through PI3K signaling, increase cell migration, and increases anchorage independent growth in breast and colon cancer cells (59). In relation to tumor progression, it has been shown to increase survival signaling through NF- κ B (70) and can be induced through stimulation by MMP-3 during EMT (71). This implies that EMT may actually drive the production of this splice variant, providing a positive feedback loop for tumor progression.

1.2 Rho Subfamily GTPases

1.2.1 Regulation of Rho Subfamily GTPases

GTPases have limited ability to naturally cycle between GDP and GTP bound states so the intrinsic nucleotide exchange and hydrolysis capability are very low (45–47). These processes are largely modulated by two classes of regulatory proteins, guanine nucleotide exchange factors (GEFs) and GTPase activating proteins (GAPs). When

bound to GDP, GEFs interact with GTPases to promote the exchange of GDP for GTP. This functionally activates the protein, allowing for the interaction between GTPases and their effector proteins. To return to an inactive conformation, GAPs interact with GTPases to accelerate the hydrolysis of GTP to GDP. Rho family members are also regulated through interactions with Rho guanine nucleotide dissociation inhibitors (GDIs) (Fig 1.3) (44–47). GDIs associate with GDP-bound proteins and shield the isoprenoid moiety, and regulate plasma membrane localization. In response to a stimulus, GDIs bring the GTPase to the appropriate membrane. Following a dissociation of the GDI, Rho GTPases integrate into the plasma membrane for GEF activation.

1.2.2 Rho Subfamily GTPase Functions

Rho GTPase is the founding member of the Rho family GTPases, and as mentioned previously, help to regulate actin dynamics, cell migration, cell adhesion and cell cycle (44–47). There are 20 members of the Rho family, divided into 5 subfamilies, based on function. Of the Rho GTPases, Cdc42, Rac1, and RhoA are the most well studied members. Together, they work in concert to direct the processes related to cellular migration (Fig 1.5). RhoA has a number of effectors, including the Rho-associated kinases (ROCK) (47). Through ROCK, RhoA regulates actin stress fiber maturation during migration and the development of focal adhesion complexes. Activated RhoA signals to ROCK. Activated ROCK then signals LIM kinases, which deactivates cofilin. Cofilin associates with filopodia and lamellipodia at the leading edge and trailing edge of a migrating cell, and one function is to destabilize actin for rapid turnover. At the leading edge, LIM kinase phosphorylated cofilin becomes inactive, stabilizing actin

Figure 1.5

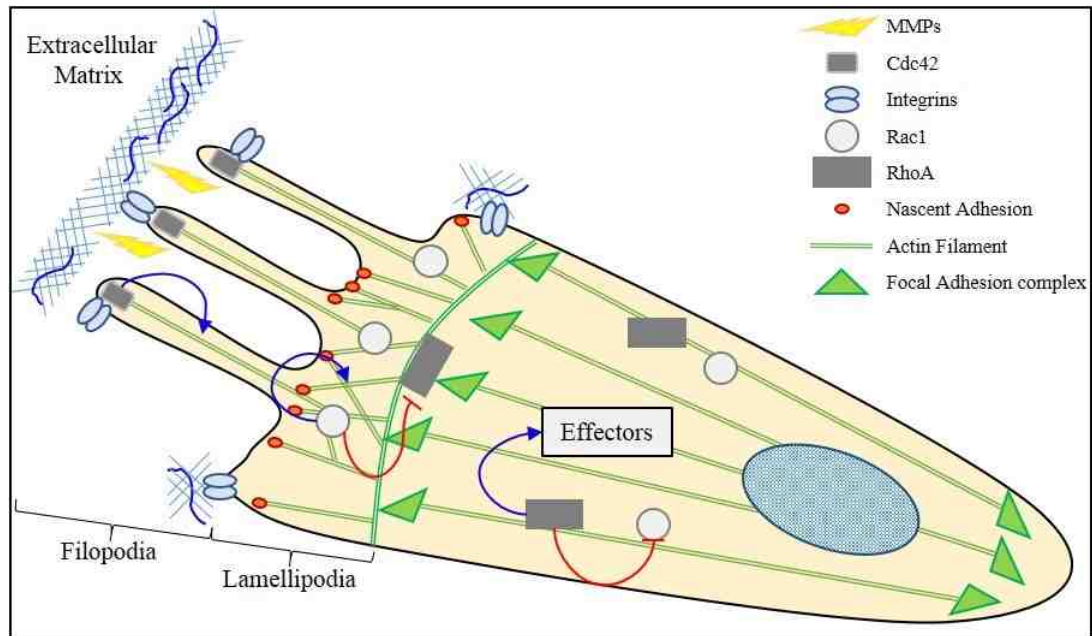


Figure 1.5 - Cdc42, Rac1, and RhoA interactions in cell migration. Extracellular stimuli initiate migration through integrins, GPCRs, and RTKs. Cdc42 begins actin polymerization, forming filopodia. This activates downstream effectors, forms nascent adhesions, and signals Rac1. Following Rac1 activation, actin polymerization progresses, amplifying filopodia and starting lamellipodia formation. Nascent formations within the lamellipodia mature into mature to focal adhesion complexes. Cdc42 and Rac1 activation at the leading edge of migration stimulates actin polymerization, actinomyosin contractility to move the cell forward, release of MMPs to degrade ECM, and inhibits RhoA activity, to prevent actin disassembly. In the middle of the cell, RhoA becomes activated. This stabilizes actin filaments into actin stress fibers, matures adhesion complexes into focal adhesion complexes, activates downstream signaling effectors, and inhibits Rac1 activity. RhoA is also active at the trailing edge of the cell, modulating actin disassembly.

filaments into actin stress fibers (46). At the trailing edge, active cofilin destabilizes actin filaments and allows for actin depolymerization. RhoA is also partially responsible for the regulation of endocytosis, exocytosis, and vesicle trafficking. There is evidence that the interaction of Cdc42, Rac1, and RhoA during migration, is similar to the interaction that determines cell polarity. While there is no evidence for its dysregulation in cancers, the role of RhoA in actin dynamics and cell migration suggests it may be a potential target in cancer therapy.

1.2.3 Cdc42

Cdc42 is a member of the Rho subfamily GTPases (44). Although first identified in yeasts, human Cdc42 was identified in 1990 (76). The Cdc42 CAAX-box motif allows for geranylgeranylation (76). This prenyl moiety anchors Cdc42 at the plasma membrane for rapid interaction with regulators and effectors (Fig 1.3). In conjunction with Rac1, Cdc42 regulates actin dynamics, cell adhesion, cell migration, and cell polarity in normal cells, as well as contributing to microtubule dynamics, gene expression, and lipid metabolism (44,76).

One of the main functions of Cdc42 is to regulate and maintain cell migration and adhesion (Fig 1.5) (47,76). Directed migration that occurs *in vivo* is a highly regulated process that requires the interaction of a number of the Rho GTPases as well as their effector proteins. Although Rac1 and Cdc42 interact with shared regulators, activate similar effectors, and have nearly identical structures, they have separate and distinct effects as well.

1.2.4 Rac1

Rac1 is a member of the Rho subfamily GTPases and was discovered in 1989 (77). Since then, it has become one of the most widely studied members of the Rho GTPase family and has a number of physiological functions in normal cells (46). The Rac1 CAAX-box motif allows for farnesylfarnesylation. This prenyl moiety anchors Rac1 at the plasma membrane for rapid interaction with regulators and effectors (Fig 1.3) (46). Rac1 is largely responsible for the regulation of actin dynamics, cell migration, and cell adhesion. Rac1 also contributes to stabilization of microtubules, gene regulation through transcription factors, reactive oxygen species (ROS) generation, cell growth and proliferation, adhesion independent anoikis, endo- and exocytosis, and nuclear signaling (78–85).

1.2.5 Interaction Between Cdc42, Rac1 and RhoA in Cell Migration

In the modulation of migration and adhesion, Cdc42, Rac1, and RhoA are differentially regulated within the cell (Fig 1.5) (44,47). Their respective roles in actin dynamics, as well as feedback from the other Rho GTPases, partially regulate the subcellular localization and activity of Cdc42, Rac1, and RhoA in migrating cells (45,46). Cdc42 and Rac1 are more active at the leading edge, where they inhibit RhoA activity. RhoA is more active within the maturing lamellipodium and trailing edge where it provides negative feedback to Cdc42 and Rac1. All three GTPases are integrated with the plasma membrane, unless prevented from integration by GDIs (47,76).

Cdc42 functions as an environmental sensor following GTP loading in response to GEFs which have been activated by GPCRs, integrins, or RTKS (44). Following

activation, Cdc42 signals to PAK and Wiskott-Aldrich syndrome protein (WASP) to induce actin nucleation and branching, causing filopodia formation (86–88). Although they are activated by similar pathways, filopodia generated by Cdc42 have a less robust response than those by generated by Rac1, and do not lead to the formation of lamellipodia which are necessary for migration. Cdc42 generated filopodia also allow the formation of nascent adhesion complexes necessary for Rac1 activation (54). Following filopodial generation, activation of Rac1 occurs, most likely through PAK-interacting exchange factor (PIX) (54,89). PIX scaffolds to Cdc42 and possesses GEF activity for Rac1(89). Activated Rac1 accumulates at the leading edge of the cell, which is sustained through a positive feedback loop involving Rac1, phosphatidylinositol-3-kinase (PI3K) and its product phosphatidylinositol-3,4,5-trisphosphate (PIP3). Rac1 directly activates p21-activated kinases (PAK), WASP family Verprolin-homologous protein (WAVE), and actin-related proteins 2/3 (Arp 2/3) (90–96). Arp 2/3 and WAVE are scaffolding proteins which cause nucleation and branching of actin filaments, resulting in the creation of filopodia and lamellipodia (54,58,89).

As lamellipodia form between filopodia, nascent adhesions mature to form focal adhesion complexes. Actinomyosin contractility pulls the cell forward, towards the leading edge. Cdc42 and Rac1 activity along the leading edge induces actin polymerization, adhesion complex formation and simultaneously provides negative feedback to inhibit Rho activity (86). In the mature lamellum, within the center of the cell, Rho is more active. Rho strengthens focal complexes and provides stability to actin filaments as the cell moves forward. Rho provides negative feedback to Rac1 in the center of the migrating cell to drive directed migration (45,84). At the trailing edge of the

cell, the majority of the actin filaments are being disassembled in a Rho dependent manner. While Rac1 activity has been reported at low levels at the trailing edge, its role remains unclear.

1.3 Targeting GTPases

1.3.1 GTPases as Therapeutic Cancer Targets

The Rho family GTPases lie at critical signaling points within cell migration, adhesion, and invasion signaling pathways. Rho GTPases are recognized as prognostic markers and lead to advanced disease for a number of cancers (44–47). Rho GTPases contribute to tumorigenesis through mechanisms that are dependent on changes in actin dynamics. Metastasis from primary tumors to secondary sites requires a loss of adhesion and an increase in migratory capacity, usually a result of EMT (19,20,22,97,98). EMT has a number of effects on cancer cells, primarily loss of adhesion signaling, which would normally induce apoptosis. However, in ascites, activators of Rho signaling pathways (19,20,22,42,71,99) may provide sufficient survival signals to avoid apoptosis (100,101). These activators also provide feedback loops to alter the expression of Rho GTPases. Increases in GAP and GEF expression and activity have also been found in some cancers (90,94). This suggests that Rho GTPase signaling is more active during tumorigenesis. Taken together, these data suggest that the Rho family GTPases are valid potential targets in the treatment of cancer.

1.3.2 Therapeutic Strategies for Rho Family GTPase Inhibition

There are three main strategies that have been explored for inhibiting Rho family GTPases as possible cancer adjuvant therapy (54,58,89,102–104). Inhibition of GEFs and effectors, inhibition of GTPases directly, or preventing the association of the GTPases with the plasma membrane have been investigated (Fig 1.6). These strategies for targeting GTPases will be discussed below.

1.3.2.1 GEFs and Effector Proteins

Inhibition of GEFs may abrogate the effects of increased GEF or GTPase activity (Fig 1.6). A number of GEF inhibitors have been identified, but few have been used *in vivo* or translated to human use as of yet (105). The inhibitor NSC23766 has been shown to inhibit Rac1 through binding the GEF groove, preventing Rac1 association with GEFs and activation (104). NSC23766 has been shown to inhibit the dissemination of lymphoma, as well as to induce cell-cycle arrest or apoptosis in some breast cancer cell lines (59). Despite the effective concentration being too high to be considered useful *in vivo*, the identification of NSC23766 has proven to be a useful tool in examining GTPase dynamics.

Due to the intersection with Cdc42/Rac1/RhoA actin dynamics, a number of studies have looked at ROCK and PAK for utility in cancer therapy (102–105). ROCK proteins are a coiled-coil serine/threonine kinase which help to regulate the formation of actin stress fibers and focal adhesion complexes (104). The inhibitor Y-27632 is a potent inhibitor of ROCK proteins (105). Y-27632 inhibits the formation of actin stress fibers, progression of the cell cycle in G₁-S, and cytokinesis. Inhibition occurs

Figure 1.6

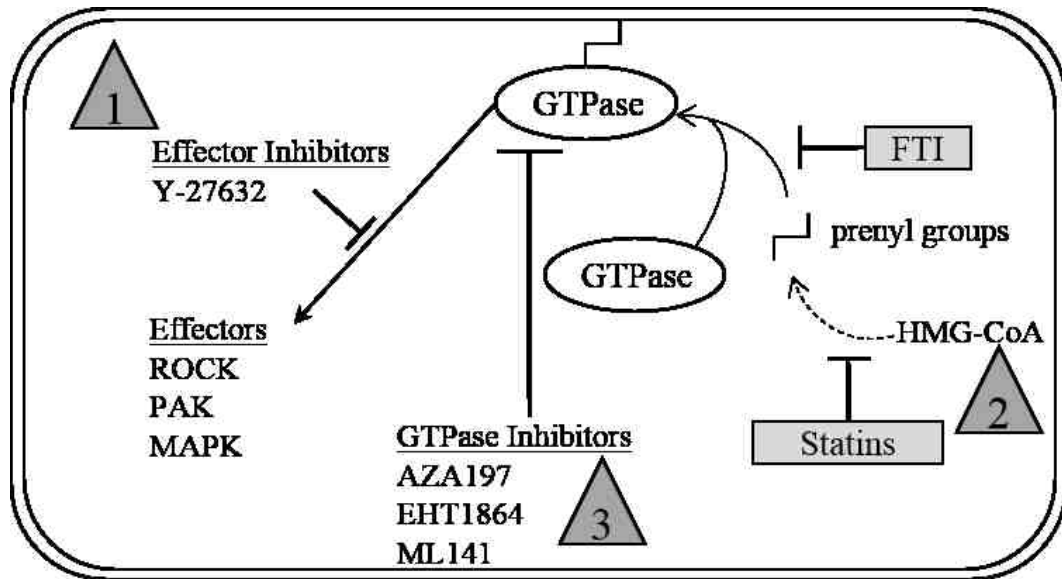


Figure 1.6 – Different methods of inhibition of GTPase activity in the treatment of cancer. **1.** Effector inhibition reduces downstream signaling. Several attempts have been made to find inhibitors for GTPase effector proteins in the treatment of cancer. For example, a ROCK inhibitor, Y-27632, inhibits stress fiber formation in Swiss 3T3 cells. **2.** Preventing GTPase posttranslational prenylation can prevent GTPase association with the membrane and therefore activation. Statins inhibit HMG-CoA reductase, the rate limiting step of cholesterol biosynthesis. This reduces the pool of farnesyl- and geranylgeranyl-isoprenoids necessary to prenylate GTPases but has had mixed results clinically. Farnesyltransferase inhibitors (FTIs) prevent prenylation of GTPases, but have not been successful clinically. **3.** Direct GTPase inhibition reduces the activity of GTPases with their effectors. In colon and prostate cancer cell lines, AZA197 and AZA1 have been identified as Cdc42 only and Cdc42/Rac1 specific inhibitors, respectively. EHT1864 has been identified as a Rac1 specific inhibitor in Swiss 3T3 cells. ML141 has been identified as a Cdc42 specific inhibitor in ovarian cancer cells.

through competitive binding to the ATP for the active binding pocket in ROCK. PAK plays an important role in Akt activation, anchorage dependent and independent proliferation, and evasion of apoptosis in KRas driven cancer (84). While Ras pathway inhibitors have been ineffective in reduction of KRas driven cancers, there is evidence to suggest that the use of PAK inhibitors simultaneously may have a positive effect on tumor inhibition (103). Tiam1 is a Rac1 GEF and is known to induce cancer invasiveness. In a murine model of breast cancer, Tiam1 knockouts not only showed delayed tumor development, but fewer tumors overall (106). This genetic data supports the idea that GEF inhibition is a viable therapeutic option in the treatment of ovarian cancer. Unfortunately, GEF and PAK inhibitors are fairly new and still in the preclinical stage, with one currently being evaluated in clinic (54).

1.3.2.2 Statin Therapy in Cancer

Inhibition of GTPase function through the use of statins has been attempted (Fig 1.6) (54,107–111). Statins have been used since the 1980s for the therapeutic reduction of cholesterol in patients with hypercholesterolemia (107,108). Statins inhibit the enzyme 3-hydroxyl-3-methylglutaryl-coenzyme A (HMG-CoA) reductase at the rate limiting step of *de novo* cholesterol synthesis, thereby reducing the serum levels of cholesterol. By blocking cholesterol synthesis at this point, intermediate prenyl products necessary for GTPase membrane anchoring are not produced (108). Because Rho family GTPases require prenylation to integrate with the cell membrane and subsequent activation, decreasing the available prenyl pool attenuates GTPase activation (107,108). The use of statins in the treatment of cancers with Rho family dysregulation has met with mixed

results (51,83,109–111). Reduced cancer risk has been associated with breast, colorectal, and pancreatic cancers when patients received statins (109–111). In certain ovarian cancer subtypes, improved overall survival was seen in patients who received statins (111). This would imply pleiotropic effects of statins, specifically a reduction of plasma lipids, prevents GTPase activation, resulting in decreased risk or improved survival. However, similar results were not seen when GTPase prenylation was prevented using FTIs (51). Similar to statins, the use of zoledronic acid has been shown to inhibit Rac1 activity in ovarian cancer cells (66). This inhibition is thought to be through a reduction of Rac1 prenylation (66).

1.3.2.3 Direct GTPase Inhibition

Direct inhibitors of Rho GTPases are further in development than ROCK and PAK inhibitors (Fig 1.6) (89–91,112–116). Direct inhibition of Rho family proteins that are overexpressed or have increased activity in cancer cells may provide therapeutic options to improve patient outcome. A collaborative research project between Drs. Angela Wandinger-Ness and Larry Sklar identified a Cdc42 specific inhibitor, ML141 (112). This inhibitor functions by preventing GTP binding to Cdc42, thus preventing activation. This reduces Cdc42 dependent activities in filopodia formation, migration, and viral particle internalization and infection. Two compounds, Aza1 and its derivative Aza197, have recently been identified as a Rac1/Cdc42 and a Cdc42 specific inhibitor respectively (113,114). Aza1 has been shown to suppress Rac1/Cdc42 dependent cell proliferation and cytoskeleton dynamics of prostate cancer cells *in vitro* and increase survival in an *in vivo* mouse model of prostate cancer (113). Similar results have been

seen in colon cancer cells using the Cdc42 specific inhibitor, Aza197 (40). EHT1864 has been identified as a Rac1 specific inhibitor (115). It functions through nucleotide displacement and prevents nucleotide exchange by inhibiting interactions with the Rac1 GEF, Tiam1. Inhibition of Rac1 in NIH 3T3 cells prevented lamellipodia formation, GTP binding, and PAK activation (115). EHT1864 has been shown to reduce estrogen receptor expression in ER+ breast tumors through an inhibition of Rac1 (116). While it has not been completely tested in a cancer setting, a Rho-specific inhibitor derived from a *Clostridium botulinum* enzyme, is currently being tested clinically in the treatment of spinal cord injury (117). The inhibitor is a fusion protein between *C. botulinum* exoenzyme C3 and a targeting peptide to increase cellular uptake. This fusion protein catalyzes ADP-ribosylation and creates a high affinity bond between Rho and Rho-GDI-1, preventing association with GEFs and an association with the plasma membrane. Through Rho inhibition, Rac1 activation helps to drive wound healing of axons. Taken together, there is sufficient evidence to support the use of Cdc42, Rac, or Rho specific inhibitors in the treatment of cancer. However, these treatments are still in early development and not yet available for human use.

With the identification of Rho family GTPase dysregulation in a number of cancers, it is desirable to look for Rho family inhibitors that can be used to decrease patient risk and improve patient survival (89,90). Cdc42, Rac, and Rho preclinical inhibitors have been identified, but most are unable to be used clinically. Those that can be used in the clinic have undesirable side effects and have shown only modest and non-specific results. Clinically approved GTPase inhibitors need to be identified. High throughput screening (HTS) of FDA approved compounds is possible and has been

utilized to identify small molecules which are both Rho subfamily inhibitors and are available for immediate clinical trials.

1.4 Drug Development

1.4.1 High-Throughput Screening

Development of novel therapeutic agents is an expensive and time consuming process. Since the early 1900s, pharmaceutical companies have used large numbers of small molecules in laborious experimentation to investigate new therapeutic options (118). Small molecules are usually described as chemical compounds that have a low molecular weight. Small molecule libraries are maintained and may contain hundreds of thousands of compounds. Traditional laboratory methods require a significant time and resource commitment to run tests on an entire library. Coupled with the high cost of testing for regulatory clearance, the cost of drug development becomes quickly prohibitive.

In an effort to alter the cost-to-benefit ratio, the need for new testing methodologies was realized (118,119). HTS refers to the ability to quickly test hundreds or thousands of compounds using specially designed assays to look at cellular events of interest. One method of HTS involves the use of 96-, 384-, or 1536-well microwell plates to quickly examine compounds against highly sensitive chemical or cellular assays. This is done using any combination of manned workstations and robotic equipment, such as the HyperCyt®, developed by University of New Mexico Center for Molecular Discovery (UNM-CMD). These assays can be cell based or in vitro assays, but are designed by the investigator.

The National Institutes of Health realized the benefit of having a small molecule library available to principal investigators who are not working in industry. To fill this need, the NIH Molecular Libraries Program (MLP) maintained HTS centers at institutions across the United States. A central resource of the MLP are small molecule libraries of thousands of small molecule compounds to be used in assays. The Prestwick library of Food and Drug Administration (FDA) approved compounds is a commercially available library which can be used for primary screening (119). The Prestwick library contains 1,280 compounds that are FDA approved for human use. This library allows for an investigator to rapidly translate active compounds from the screen to a clinical setting.

1.4.2 Identification of Inhibitors of the Rho Family GTPases

The UNM-Center for Molecular Discovery was a Molecular Library Program funded center. Previously, the center, in a collaboration between and Drs. Wandinger-Ness and Sklar, developed a cell-free multiplex polystyrene bead array that could be performed in a 384-well format (120–122). This array uses glutathione beads of different fluorescent intensities bound to GTPases as a quantitative measurement of GTPase activation. Ras family GTPases fused to glutathione-S-transferase were bound to the glutathione beads. Compounds within the small molecule libraries at UNM were tested for activation or inhibition of GTPase nucleotide binding activity using this system. Compounds were loaded into wells containing GTPase conjugated beads and then incubated with BODIPY-conjugated-GTP. Compounds were considered potentially active if there was a 20% change in fluorescence from baseline. This study identified 2 compounds, a Rho family selective inhibitor and a Cdc42 specific inhibitor (120–122).

1.4.3 Identification of Cdc42 and Rac1 Inhibitors

Drs. Wandinger-Ness and Sklar utilized the described small molecule screen to examine the Prestwick library for GTPase inhibition (120,123). This version of the Prestwick library contained 1208 compounds which have all been previously approved by the FDA and qualify for off patent use. The Prestwick library contained 24 compounds classified as non-steroidal anti-inflammatory drugs which had activity in the primary screen (NSAIDs) (123). Of these, 11 NSAIDs were tested in a confirmatory dose response screen to test for activity against 8 GTPases: Cdc42 wild-type, Cdc42 activated mutant, Rab2, Rab7, Rac1 wild-type, Rac1 activated mutant, Ras wild-type, and Ras activated mutant (123). There were 4 NSAIDs confirmed to have activity against the selected GTPases: R-naproxen, S-ibuprofen, S-naproxen, and sulindac sulfide. R-naproxen was the only identified NSAID with an EC_{50} less than $3\mu\text{M}$ and selectively inhibited GTP-binding of Cdc42 and Rac1 (123). This effect was enantiomer specific, as S-naproxen did not exhibit the same inhibitory effect. This activity is notable because the anti-inflammatory activity of naproxen is due to the S-enantiomer, not the R-enantiomer (124). R-naproxen was previously thought to be largely inert, with no known pharmacologic activity (124). But further testing showed inhibition of Cdc42 and Rac1 activation in NIH 3T3 cells and Cdc42 and Rac1 regulated cytoskeletal events in OVCA429 and OVCA433, two ovarian cancer cell lines (123). Because the Cdc42 and Rac1 inhibition was enantiomer specific, the UNM investigators postulated that the aryl ring structure and rotational constraints around the chiral center of R-naproxen, place it within a hydrophobic pocket on the GTPase surface (124). Using R-naproxen as the basis for an *in silico* query, another enantiomer specific compound, R-ketorolac, but not S-

ketorolac was identified (123). Further docking studies suggested that mechanism of Cdc42 and Rac1 inhibition by R-ketorolac and R-naproxen is through the neutralization of a magnesium ion necessary for nucleotide release within the nucleotide binding pocket.

HTS is an important tool that can be extremely beneficial (118). Using HTS, it was possible to identify FDA approved enantiomer specific NSAIDs which have previously unknown activity against Cdc42 and Rac1. NSAIDs can be protective in some cancers, suggested to be due to the anti-inflammatory effects (125–128)(153-156). However, NSAIDs may have COX independent effects, such as disruption of cell adhesion, cytotoxic or anti-proliferative effects which need to be explored. The enantiomer selective binding of R-ketorolac to Cdc42 and Rac1 shows that NSAIDs can affect proteins not related to inflammation (123).

1.5 Ketorolac

NSAIDs are a heterogeneous group of drugs that are commonly used for their anti-inflammatory, antipyretic, and analgesic effects (128–131). NSAIDs function through the inhibition of eicosanoid synthesis (Fig 1.7) (128–131). In the arachidonic acid pathway, cyclooxygenase-1 and -2 (COX-1 and COX-2) generates prostaglandins which ultimately result in inflammation and pain (128). The anti-inflammatory effects of NSAIDs is a result of selective inhibition of COX-1/COX-2 (128–131).

Ketorolac is a heterocyclic acetic acid derivative class NSAID first described in 1978 (Fig 1.8) (132). Ketorolac has the trade name Toradol® and is used primarily as an analgesic, but has exhibited some antibiotic and antipyretic abilities. It is a chiral, non-

selective COX-1/-2 inhibitor (132–134). Ketorolac is administered as a racemic mixture, with approximately a 50:50 ratio of the R-/S- forms. COX inhibition by ketorolac is by the S-enantiomer only at similar levels for COX-1 ($IC_{50} = 0.46\mu\text{M}$) and COX-2 ($IC_{50} = 1.46\mu\text{M}$), while R-ketorolac has no detectable COX at peak serum levels ($IC_{50} > 100\mu\text{M}$) (133,134). Administration is oral, intramuscular, intravenous, and as a topical ophthalmic solution (132). Ketorolac rapidly reaches a maximum plasma concentration following oral or intramuscular administration, and is mostly cleared within 6 hours, with a preferential clearance of the S-enantiomer over the R-enantiomer (134). Due to its potent analgesic effects, it is given perioperatively, intraoperatively, and postoperatively for pain management of moderate to severe surgical and cancer related pain. Despite a lack of inhibition of serotonin, δ -opioid, μ -opioid, or κ -opioid receptors, ketorolac treatment confers opioid level pain relief (133), being 3-30 times more potent than some NSAIDs (132). Ketorolac is non-habit forming, and patients do not develop tolerance. Coupled with its cost effectiveness relative to opioids or steroids, it is a popular choice for alternative short term pain relief. As an NSAID, long term use is associated with gastrointestinal bleeding, perforation, and peptic ulcers (132,135,136). These GI effects are assumed to be associated with the COX inhibition. However, there is evidence of long term, prophylactic use for pain relief in athletes with few adverse effects (137).

This project examines how R-ketorolac inhibition of Cdc42 and Rac1 alters ovarian cancer cell behaviors related to adhesion, migration and invasion. Because ketorolac is an FDA approved drug in current use, it is a strong candidate to be rapidly translated to clinical studies. Ketorolac is not often been used for off-label purposes, but based on our studies it may have promise in the treatment of ovarian cancer (132).

Figure 1.7

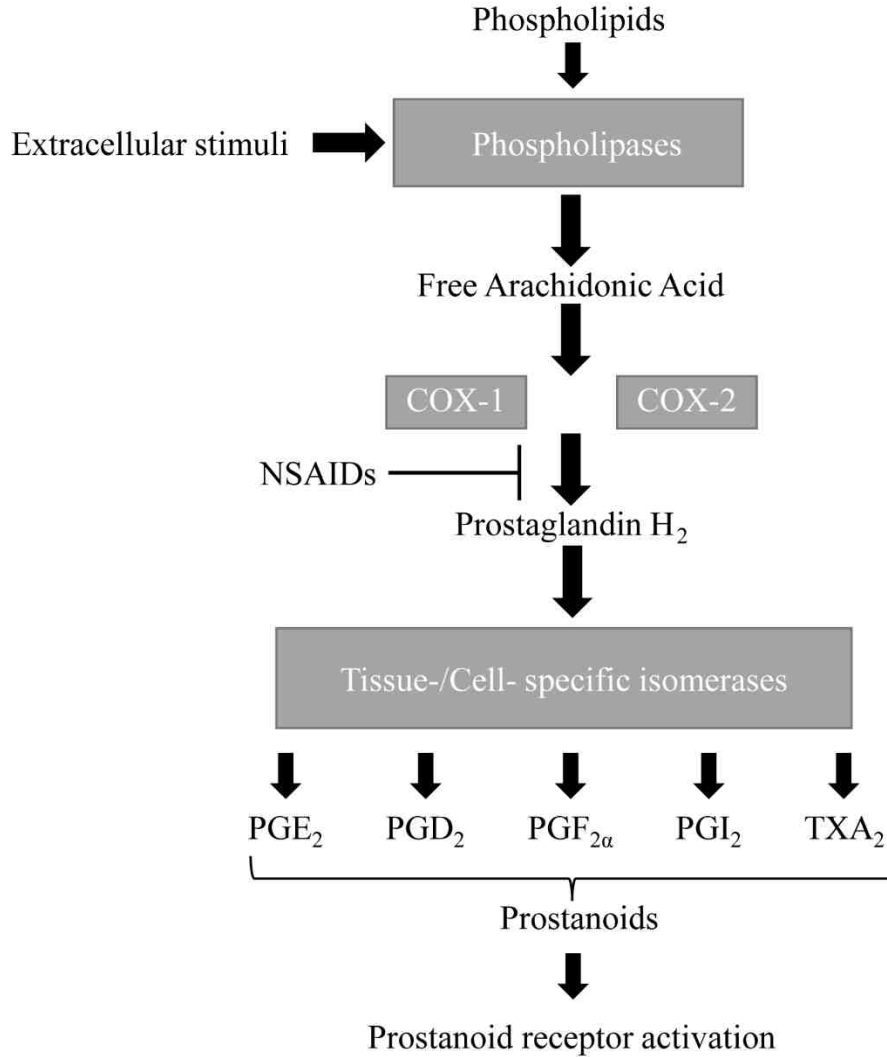


Figure 1.7 – Pathway of prostanoid synthesis. Following extracellular stimulus, phospholipases generate arachidonic acid from the cleavage of membrane phospholipids. Cyclooxygenase 1 and 2 (COX-1 and COX-2) utilize arachidonic acid as a substrate to generate prostaglandin H₂ (PGH₂). PGH₂ is then metabolized by tissue specific prostaglandin isomerases tissue specific prostanoids. These then bind their cognate receptors to initiate downstream signaling involved with inflammation and nociception. NSAIDs, such as naproxen and ketorolac, block this pathway through the inhibition of COX-1/COX-2. (adapted from Brune and Patrignani, 135)

Figure 1.8

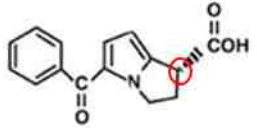
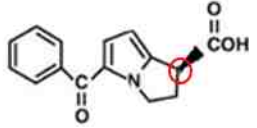
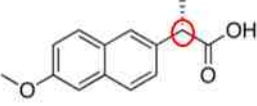
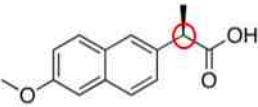
		COX-1	IC ₅₀	COX-2
R-ketorolac		>100μM		>100μM
S-ketorolac		0.46μM		1.46μM
R-naproxen		>100μM		>100μM
S-naproxen		35.48μM		64.62μM

Figure 1.8 - Structure and *in vivo* IC₅₀ values for ketorolac and naproxen enantiomers.

Structure of each enantiomer is presented here. Red circles indicate chiral centers for the enantiomers. S-ketorolac exhibits COX inhibition at similar levels for COX-1 (IC₅₀ = 0.46μM) and COX-2 (IC₅₀ = 1.46μM), R-ketorolac exhibits no inhibition of COX-1/2. S-naproxen is a non-selective COX antagonist which inhibits COX-1 (IC₅₀ = 35.48μM) and COX-2 (IC₅₀ = 64.62μM), R-naproxen exhibits no inhibition of COX-1/2.

1.6 Study Significance and Hypothesis

Women diagnosed with ovarian cancer have a tumor free survival rate of approximately 40% (2). The mortality due to ovarian cancer is partially due to women being diagnosed with advanced disease, which presents with multiple metastases within the peritoneal cavity (1). The majority of metastases are surgically removed, but cellular exfoliation from the tumors and microtumors which are not removed contribute to recurrence. The process of surgical debulking initiates an inflammatory response that floods the peritoneal cavity with cytokines, growth factors, and extracellular debris that promotes cancer cell survival, migration, adhesion and invasion, contributing to recurrence (5,7,11).

Rho family GTPases Cdc42, Rac1, and RhoA regulate actin dynamics and regulate cellular migration, adhesion, and invasion(45–47). Cdc42 has been acknowledged as being overexpressed in a number of cancers (57,58). Rac1 has been identified in promoting cancer progression and recurrence in a number of cancers (54–61,70,95,96). RhoA effectors are known to be upregulated in some cancers (58). Upregulation of these GTPases and activation of their downstream effectors has also been shown to reduce apoptosis and be protective in chemotherapy (58,74). Taken together, these data indicate that Cdc42 and Rac1 may be valid therapeutic targets in the treatment of recurrent ovarian cancer.

NSAIDs have been found to provide survival benefit to patients in some cancers (125,138–143). Collaborative efforts at UNM have identified an enantiomer specific inhibition of Cdc42 and Rac1 using the NSAIDs R-naproxen and R-ketorolac (123). NSAIDs primarily target COX-1 and COX-2 (127–129), however there is evidence of an

enantiomer-specific response to non-COX targets in cells (129,131,135,136) and in animal models (114,144,145). Ketorolac administered clinically has been shown to provide survival benefit in recurrent breast cancer (126) and it is known that there is benefit for ovarian cancer patients (65).

The purpose of the present work is to elucidate the cellular mechanisms responsible for the protective effect of ketorolac treatment in breast and ovarian cancer patients. Use of *in vivo* models of ovarian cancer and patient data will identify the mechanisms driving ovarian cancer metastasis and recurrence. I hypothesize that the use of R-ketorolac will inhibit Cdc42 and Rac1, thereby inhibiting the cellular events related to migration, adhesion, and invasion, which provides survival benefit to ovarian cancer patients.

Characterization of R-ketorolac in an
***in vivo* model of recurrent ovarian cancer**

Introduction

In 2014, there were an estimated 22,000 newly diagnosed cases of ovarian cancer and 14,000 ovarian cancer related fatalities in the United States (1,2,5). Overall, patients diagnosed with ovarian cancer have a 5 year survival rate of less than 50%. The high mortality rate in later stages of the disease is influenced by numerous factors including multiple metastases and acquired resistance to chemotherapeutics, frequently leading to recurrence (5).

Metastatic spread and the recurrence of ovarian cancer can be partially attributed to the formation and dissemination of MCAs (23,146). These structures form naturally within the peritoneal cavity and ascites fluids of patients. Extracellular components within the ascites fluid provides MCAs with growth factors, survival signals, adhesion signals, and may increase invasion potential (25,92,146,147). The formation of these structures also decreases sensitivity to chemotherapeutics and radiation (24,148). The formation, development, adhesion and invasion of MCAs are widely used as an *in vitro* model of metastasis (9,146,149). MCAs and single cell suspensions of ovarian cancer cells consistently show preferential adhesion to specific ECM components through integrin signaling (10,23,31,148). Integrin signaling is known to activate the Rho family GTPase transduction pathways, which regulate actin dynamics and cellular adhesion (47,93,94).

Actin dynamics are regulated through interplay of the GTPases Cdc42, Rac1, and RhoA (47,93,94). These GTPases are responsible for cell-cell adhesion, cell-matrix adhesion, cell migration, and cell invasion. Cdc42 and Rac1 have both been identified as having aberrant expression or activity in a number of cancers (54–61,70,95,96). Most significantly, a recent study has linked Rac1 overexpression in ovarian cancer patients with poor prognostic outcome and increased recurrence (64). Similarly, our group identified Cdc42 and Rac1, but not RhoA, as being dysregulated in ovarian cancer (65). With these studies in mind, the promise of exploiting Cdc42 and Rac1 as therapeutic targets in cancer has been well recognized (54–61,70,95,96).

R-ketorolac inhibits Cdc42 and Rac1 related events in ovarian cancer cells (65,123,150). Previous work has shown that R-ketorolac inhibits Cdc42 and Rac1 activity *in vitro* as well as in SKOV3ip and *ex vivo* primary ovarian cancer cells (65). In patients treated with racemic ketorolac, *ex vivo* cells show decreased Cdc42 and Rac1 activity (65). Additionally, R-ketorolac, but not S-ketorolac, was shown to inhibit filopodia formation, migration, adhesion, and invasion in SKOV3ip and primary ovarian cancer cells (150). These cell behaviors are necessary for ovarian cancer dissemination within the peritoneal cavity.

Breast cancer (126,143) and ovarian cancer patients (65) who received racemic ketorolac for postoperative pain relief have improved 5 year survival. It has been postulated that this survival benefit is due largely to COX inhibition by ketorolac (126, 143). Ketorolac is administered as a racemic mix, and at therapeutic concentrations, the S-enantiomer alone inhibits COX activity (123,133,134,151). It is likely that survival benefit is conferred by a combination of COX inhibition by S-ketorolac and Cdc42/Rac1

inhibition by R-ketorolac (65, 123). This combined activity conferred by ketorolac explains why other NSAIDs do not improve patient survival (123,126,143).

The goal of this work is to further investigate the impact of R-ketorolac in ovarian cancer. Because R-ketorolac inhibits Cdc42 and Rac1 related cellular events (150) and racemic ketorolac improves survival benefit in ovarian cancer (65), we investigated SKOV3ip ovarian cancer cell behavior *in vivo* and as MCAs *in vitro*. We find that Cdc42 and Rac1 inhibition disrupts MCA adhesion and spreading events, and decreases tumor burden *in vivo*. This further demonstrates that R-ketorolac has activity against Cdc42 and Rac1 and suggests the anti-cancer benefits observed following administration of racemic ketorolac to ovarian cancer patients is partially due to the R-enantiomer.

Results

Oral administration of ketorolac reduces tumor burden in vivo

To determine the effects of ketorolac treatment *in vivo*, we utilized a xenograft mouse model of recurrent ovarian cancer. Mice were given intraperitoneal (IP) injections of GFP-expressing SKOV3ip ovarian cancer cells. Preliminary studies established that mice had significant tumor growth by 14 days post-injection (Fig 2.1A). Mice received either placebo, R-/S-ketorolac, R-ketorolac, or S-ketorolac pills twice daily. Tumor burden was assessed through image analysis of fluorescent tumors within the peritoneal cavity. Quantification of the images shows that racemic ketorolac and R-ketorolac treated animals possessed significantly fewer tumors compared to placebo treated animals ($p \leq 0.05$) (Fig 2.1B). Initial HTS of NSAIDs identified R-naproxen, not S-naproxen, as having enantiomer selective activity against Cdc42 and Rac1. Similar to ketorolac, mice treated with R-naproxen, but not S-naproxen, showed fewer tumors (Fig 2.2A).

In humans, deposition of ovarian cancer metastases occurs at specific sites within the peritoneum (9,10,19). We observed that tumor growth and distribution in the animals was consistent with patterns of human metastasis. The largest tumor develops at, and then envelops, the omentum. The omental tumor appears to be smaller and less solid in ketorolac treated animals compared to placebo treated animals (Fig 2.2B). Smaller metastases formed at adipose or highly vascularized tissues (Fig 2.1A). However, in this model, it is unclear if the smaller metastatic sites form as a result of injection or as secondary deposition from the omental tumor.

S-ketorolac is the active enantiomer for COX inhibition (133,134,151) while R-ketorolac inhibits Cdc42 and Rac1 (123). However, pharmacokinetics are different

among species (151) and the distribution of ketorolac in these mice was examined. Studies in humans, mice, and rats, demonstrates that S-ketorolac is cleared more rapidly than R-ketorolac following single dose administration (133,134,151). We confirmed that there is no significant difference in the total ketorolac serum concentration between ketorolac treatment groups (Fig 2.1C, grey bars). However, there was a predominance of R-ketorolac over S-ketorolac in all ketorolac treated animals (Fig 2.1C, black bars). R-ketorolac represented approximately 78%, 94%, and 62% of the total recovered ketorolac from racemic ketorolac, R-ketorolac, and S-ketorolac treated animals, respectively. Additionally, in mice there is spontaneous interconversion of S-ketorolac to R-ketorolac (151). Interconversion causes a shift to the R-enantiomer in racemic ketorolac and S-ketorolac treated animals, with no change in R-ketorolac treated animals (Fig 2.1C) and does not occur outside of an *in vivo* setting (Fig 2.3).

Ketorolac has no effect on SKOV3ip growth kinetics in culture

There is evidence that specific NSAIDs can induce apoptosis, decrease proliferation, or induce cell cycle arrest (131,152,153). Therefore, the effects of ketorolac on cell proliferation and cell cycle were examined. SKOV3ip ovarian cancer cells were treated for 48h or 96h with R-/S-ketorolac, R-ketorolac, or S-ketorolac. Concentrations of ketorolac that spanned and exceeded the normal therapeutic serum concentrations were used (132). Cells treated with ML141 (10 μ M) or NSC23766 (30 μ M), specific inhibitors for Cdc42 and Rac1, respectively, were used as controls (112,147). These concentrations were selected based on approximate IC₅₀ values obtained through migration studies (Fig 2.4). There was no significant difference in cell viability after 96h for any ketorolac

treatment (300 μ M) group, when compared to the no treatment control (Fig 2.5A). However, specific inhibition of either Cdc42 or Rac1 caused an approximately 20-30% decrease in viability ($p \leq 0.01$). The Cdc42 inhibitor ML141 (112,139), and direct inhibition of Rac1 have been reported to inhibit cancer cell proliferation in other tumor models (113–115,130,154).

The formation of MCAs is known to protect cells from radiation or taxane induced apoptosis (9), increase chemoresistance compared to cells grown in monolayer, and reduce proliferation compared to monolayer (13,30). SKOV3ip cells cultured as MCAs were counted using flow cytometry to determine the effect of ketorolac enantiomers on cell proliferation. After 96h growth, ketorolac treatments had no effect on basal cell proliferation or EGF-stimulated cell proliferation (Fig 2.5B). However, EGF-stimulated proliferation of ML141 treated cells is inhibited compared to non-treated MCAs.

COX inhibitors can cause cell cycle arrest in chondrocytes, osteoblasts, and osteoblasts (154–156). Cell cycle analysis was performed by Amanda Peretti to determine if this occurs in ovarian cancer cells. SKOV3ip cells were cultured for 48 hours, with increasing concentrations of racemic ketorolac, and measured using flow cytometry (Fig 2.5C). Taxol, a mitotic inhibitor, was used as a positive control for cell cycle arrest at a concentration of 0.5 μ M. Taxol treated cells were significantly different than no treatment controls in all cell cycle populations. There is no significant change in the cell cycle populations of ketorolac treated cells when compared to the no treatment control group. Based on these data, above therapeutic concentrations, ketorolac does not inhibit cell proliferation or alter cell cycle in SKOV3ip ovarian cancer cells.

Ketorolac does not change growth kinetics in vivo

The peritoneal fluid contains a number of soluble factors that contribute to cancer cell survival through survival pathways to evade apoptosis (9,20,100). It is possible that changes in growth kinetics due to ketorolac treatment can occur in a biological setting. Ki-67 and TUNEL staining were performed on mouse omental tumors to determine the effects of ketorolac treatment on growth and apoptosis of ovarian cancer cells *in vivo*.

Sections of omental tumors and spleen with attached tumor were sectioned and subjected to immunohistochemical staining for the proliferation marker Ki-67 (Fig 2.6A-B). Because we observed significant interconversion of S-ketorolac to R-ketorolac in the mice, further experiments did not include mice treated with S-ketorolac. Slides were scanned using an Aperio slide scanner and analyzed using Imagescope software. Area of analysis included tumor tissue only and not spleen tissue (Fig 2.6C). Nuclei were scored no staining, low, moderate, or strong positive staining for Ki-67. Low to strong Ki-67 staining was considered positive, and data are presented as percent positive nuclei. There is no statistically significant difference in levels of proliferation between treatment groups and placebo group (Fig 2.6D).

Because ketorolac has no effect on proliferation, TUNEL staining was performed to examine levels of apoptosis (Fig 2.7A-B). Sections were counterstained using DAPI (4',6-diamidino-2-phenylindole) and imaged with an Olympus IX70 inverted fluorescent microscope. Olympus CellSens software was used to analyze images. Total fluorescence intensities were captured for fluorescein and DAPI channels. Data are presented as percent positive fluorescein (Fig 2.7C). There is no significant difference between levels of apoptosis in treatment groups compared to placebo groups. Consistent with our

observation in ovarian cancer cells alone, use of ketorolac *in vivo* does not significantly reduce levels of proliferation in the tumor (Fig 2.6D) nor does treatment increase levels of apoptosis (Fig 2.7C).

Impact of ketorolac on GTPase gene expression

Increases of Rho family GTPase expression have been identified in multiple cancer types (54). Our own work has shown stage specific changes to *Rac1* and *Cdc42* at the mRNA and protein level in ovarian cancer, including the expression of the constitutively active splice variant of *Rac1*, *Rac1b* (65). We examined changes in Rho family GTPase gene expression following ketorolac treatment (Fig 2.8). Initial PCR analysis confirmed that a number of ovarian cancer cell lines, including SKOV3ip, express *Rac1b* (Fig 2.9). SKOV3ip cells were treated with ketorolac (100 μ M), or specific inhibitors, for 24h. Cells were changed to serum free medium containing drug for 24h, followed by the addition of 10nM EGF for 24h. RNA isolated from cells using Qiagen RNeasy kit and cDNA was generated using Applied Biosystems High Capacity cDNA kit. Quantitative PCR was performed using primers for *Cdc42*, *Rac1*, *Rac1b*, and *RhoA*. An apparent decrease of *Rac1b* occurred following treatment with R-ketorolac (Fig 2.8A). Gene expression of *Rac1b* following R-/S-ketorolac or S-ketorolac alone showed a similar, although not as robust, decrease. EGF stimulated gene expression of *RhoA*, increased, but did not reach significance, following treatment with R-/S-ketorolac, R-ketorolac, or S-ketorolac. Inhibition of Cdc42 with ML141 showed modest, but not significant, reduction in gene expression of all 4 targets compared to EGF stimulated, no treatment controls.

Long term treatment *in vivo* may result in a different gene expression profile. To examine this, a portion of the omental tumor collected from animals was used to evaluate gene expression. Isolation of RNA was performed as above, utilizing the QiaShredder column to lyse tumor cells. We observed that in ketorolac and R-ketorolac treated animals, there was a trend towards an increase in *Cdc42* and *RhoA* expression compared to the placebo group which was not statistically significant (Fig 2.8B). There was no change in *Rac1* or *Rac1b* expression in these animals.

We primarily examined these four GTPases because of their relationship to metastasis and cancer progression (54). It has been reported that inhibition of Rac1 can reverse a malignant phenotype (115). While not statistically significant, SKOV3ip cells exhibited a large but not significant decrease in *Rac1b* following 24h EGF stimulation. RNA from treated SKOV3ip cells was also used in a microarray containing known cytoskeletal regulators and markers of metastasis (Qiagen). There were no significant changes to any of the 192 genes assayed (data not shown). Although there were trends for inhibition of GTPase gene expression *in vivo*, there were no significant differences observed (Fig 2.8B).

Ketorolac inhibits SKOV3ip MCA adhesion and spreading

Inhibition of *Cdc42* and *Rac1* decreases cell adhesion, migration, and invasion in monolayer culture (150) and increases survival time in animal models of prostate and colorectal cancer (113,114). We used an organotypic cell culture model of ovarian cancer to test MCA adherence and spreading (31,157,158). Mesothelial cells were cultured in the presence of collagen I and fibronectin in 96-well dishes. To test MCA adherence,

SKOV3ip MCAs were placed on top of a confluent mesothelial cell layer in the presence of the Cdc42 inhibitor, ML141, or the Rac1 inhibitor, NSC23766. At 4h, wells were washed with 1X phosphate buffered saline (PBS). The majority of the no treatment MCAs adhered and had begun to clear the mesothelial cells, while treated cells did not (Fig 2.10A). SKOV3ip MCAs were also allowed to spread and clear the mesothelial cell layer for 24h (Fig 2.10B). MCA area was measured prior to plating and the cleared mesothelial area was measured after 24h. The percent increase from MCA area to cleared mesothelial area was calculated. Inhibition of Cdc42 and Rac1, either by specific inhibitors or ketorolac enantiomers, reduced the increase in area (Fig 2.10C). It has been reported that, in GTPase activity assays, 10 μ M S-ketorolac is sufficient for approximately 30% inhibition of Cdc42 and Rac1 (150).

Due to the level of ovarian cancer colonization of the mouse omental tumor, and the proximity to the spleen, we analyzed cancer cell attachment to the splenic capsule. Sections of spleen with attached tumor were H&E stained to look at cellular architecture (Fig 2.10D). There was a distinct difference between the human cancer cells and the mouse cell types. Red arrows identify SKOV3ip cells which are adhered to the splenic capsule. Donna Kusewitt, DVM, PhD and veterinary pathologist scored slides as positive for adhesion if there were ovarian cancer cells present on the splenic capsule. Chi square analysis of adhesion versus no adhesion for placebo, R-/S-ketorolac, R-ketorolac or S-ketorolac was performed. There was a substantial, but not significant ($p=0.052$), decrease in the levels of adhesion in animals treated with a single enantiomer of ketorolac (Fig 2.10E). This observation suggests that, despite not reaching significance, there may be an influence on adhesion that should be further explored.

Discussion

The use of NSAIDs in the treatment of cancer has provided mixed results in regards to survival benefit (60,125–127,129,138,159,160). Retrospective studies have shown that patients who receive ketorolac have early survival benefit in breast cancer recurrence (143) and our own studies show that ovarian cancer patients who have received ketorolac had a decreased risk of ovarian cancer related mortality within 5 years of treatment (65). Ketorolac is clinically administered as a strong, non-addictive analgesic (132) and is given as a 50:50 racemic mix of the R-enantiomer and S-enantiomer (65). The pain relieving effects are attributed non-selective COX inhibition by S-ketorolac, while R-ketorolac, a Cdc42/Rac1 selective inhibitor, has no activity against COX-1/2 (123,132). R-ketorolac concentrations within the peritoneal cavity are sufficient to inhibit GTPase activity, resulting in reduced adhesion and filopodia formation (65,150). These data indicate that ketorolac given clinically could target multiple signaling pathways related to cancer recurrence.

We provide evidence that oral administration of R-/S-ketorolac provides approximately 30% reduction of tumor burden in a mouse model of ovarian cancer (Fig 2.1B). This effect was similar to what has been reported with Cdc42 and Rac1 inhibition in mouse models using subcutaneous injection of colorectal and prostate cancer cells(113,114). Treatment with R-ketorolac alone provides an approximately 20% reduction in tumor burden (Fig 2.1B). It has been postulated that the benefit of NSAIDs in cancer therapies is due to the anti-inflammatory properties conferred by COX-1/2 inhibition (126). COX inhibition with ketorolac is entirely from S-ketorolac, as R-ketorolac does not reach a plasma concentration to provide COX inhibition (Fig 2.1C)

(132). In serum recovered from treated animals, we observe over 50% of the S-ketorolac undergoes interconversion to become R-ketorolac (Fig 2.1C). This is consistent with published data reporting a species specific interconversion of ketorolac (151).

Pharmacokinetics studies show a preferential clearance of S-ketorolac over R-ketorolac, indicating that the time in the therapeutic window for COX inhibition in animals is fairly low (151). These data indicate that the decrease in tumor burden is largely due to the COX-independent effects of R-ketorolac. To explore COX-dependent events related to tumor burden, a different animal model would be required.

In multiple cancer cell types, NSAIDs can induce apoptosis, impair proliferation and cause cell cycle arrest (131,152,153). These effects are both COX-dependent and COX-independent. In cell culture, we show that ketorolac has no effect on cell proliferation (Fig 2.5A-B). Ketorolac concentration presented in the live/dead assay is above therapeutic serum levels. After 96h monolayer culture in the presence of racemic ketorolac or single enantiomers, there is no decrease in cell proliferation (Fig 2.5A) and there is no cell cycle arrest observed (Fig 2.5C). When cells are cultured as MCAs, there is no difference in cell number when compared to no treatment controls (Fig 2.5B).

However, in monolayer, specific inhibitors of Cdc42 or Rac1 show a small but significant decrease in cell proliferation after 96h (Fig 2.5A). The use of ketorolac *in vivo* does not have a significant effect on cancer cell proliferation (Fig 2.6D) or apoptosis (Fig 2.7C).

Animals treated with R-ketorolac alone showed an increase in proliferation (Fig 2.6D) that is mirrored by a slight decrease in apoptosis (Fig 2.7C). If confirmed, these findings would be in opposition to the idea that NSAIDs induce apoptosis (refs). Further staining of animal tissues is required to determine if this is a significant effect. Animals which

received R-ketorolac alone, received a larger dose of R-ketorolac than R-/S-ketorolac treated animals (Fig 2.1C). The increase in proliferation (Fig 2.6D), along with a decrease in apoptosis (Fig 2.7C), following treatment with R-ketorolac alone, would account for the smaller decrease in tumor burden (Fig 2.1B).

In a COX-independent effect, the use of some NSAIDS are known to inhibit the transcription factor NF- κ B (70). Thus, the use of ketorolac may decrease Rho family GTPase gene expression. We observed that treatment with R-/S-ketorolac or R-ketorolac alone decreased EGF stimulated expression of *Rac1b* in cell culture, although this did not meet significance (Fig 2.8A). Interestingly, specific inhibition of Cdc42 using ML141 decreased EGF stimulated expression of *Cdc42*, *Rac1*, *Rac1b*, and *RhoA*. These data suggest that Rho family GTPase expression is partially regulated by Cdc42. When examined *in vivo*, chronic treatment with R-/S-ketorolac or R-ketorolac alone appeared to stimulate expression of *Cdc42* and *RhoA*, although this finding did not reach significance (Fig 2.8B).

Cdc42 and Rac1 are largely responsible for the adhesion, migration and invasion events related to ovarian cancer metastasis (31,54,90,93). Inhibition of Cdc42 and Rac1 can decrease the adhesion and migration of SKOV3ip cells grown in monolayer (151). MCAs are a model of ovarian cancer (9,13). We observe, in the presence of specific inhibitors of Cdc42 or Rac1, that adhesion of MCAs to an organotypic cell culture layer is decreased at 4h (Fig 2.10A). Similarly, MCA disaggregation and spreading is inhibited at 24h (Fig 2.10C). Decreased spreading following treatment with S-ketorolac was unexpected, but likely due to the concentration exceeding 10 μ M, the reported concentration of S-ketorolac inhibition of Cdc42 and Rac1 (150). MCA spreading was

performed at 100 μ M (Fig 2.10B) and it has been previously observed that 10 μ M S-ketorolac is sufficient to inhibit GTPase activity by ~30% (150). Further studies with lower ketorolac concentrations will be needed to correctly assess the impact of GTPase inhibition by R-ketorolac. The *in vivo* correlate to MCA adhesion and spreading was SKOV3ip cell adhesion to the splenic capsule (Fig 2.10D). We observe that adhesion to the splenic capsule is reduced, but not significant, in R-ketorolac and S-ketorolac treated animals compared to placebo treated animals.

The use of NSAIDs as anticancer agents has largely focused on their anti-inflammatory effects, which are caused by inhibition of COX-1/2 and reduced prostaglandin synthesis (126,128,143). The significant decrease in tumor burden we see in the racemic and R-ketorolac treated animals cannot be attributed to COX inhibition alone, and is likely the result of COX-independent mechanisms. Because S-ketorolac is largely converted to R-ketorolac in the animals, the work presented in this chapter suggests that GTPase-dependent events largely contribute to a decrease tumor burden. Although we are unable to currently define this mechanism, our work may provide insight on what needs to be pursued next. Currently there are no inhibitors of Cdc42 or Rac1 being used in a clinical setting. The use of ketorolac in the treatment of ovarian cancer provides a unique opportunity to test whether Cdc42 and Rac1 inhibition can confer therapeutic benefit in humans.

Methods

Ketorolac dosage

Racemic or single enantiomer ketorolac was orally administered to mice using transgenic dough diet (Bio-Serv, Flemington, NJ, cat #S3472) compressed into pills. (193) Briefly, R-/S-ketorolac tris salt (Sigma, St. Louis MO, cat# K1136) dissolved in water, R-Ketorolac (Toronto Research Chemicals, Toronto Canada, cat# K235600) or S-Ketorolac (Toronto Research Chemicals, cat# K235602) dissolved in 100% ethanol, at a concentration of 5mg/ml. Bromophenol blue was added to the ketorolac solution at a concentration of 0.1% to ensure even distribution into the dough. Pills were made using 1ml of ketorolac solution and 30g of transgenic dough. Solution was mixed with dough to ensure even incorporation. Placebo pills were made using an equivalent volume of 100% ethanol containing 0.1% bromophenol blue. Dough was then pressed using 100mg pill forms (Gallipot, St. Paul, MN). Pills were allowed to dry at room temperature on the bench overnight. Pills were removed from the forms and stored at 4°C until used.

Animal model

Foxn1^{nu} NU /J athymic nude mice, aged 6-9 weeks, were purchased from The Jackson Laboratory (Bar Harbor, ME, stock number 002019). To condition mice to accept pills containing drug, they were given placebo pills every 12 hours for two days. On day 3, mice were switched to pills containing 20µg drug or left on placebo pills as appropriate. On day 4, mice were given IP injections of 1×10^6 SKOV3ip cells expressing GFP. On day 15 of receiving drug, mice were sacrificed and imaged using a Light Tools imaging system (Synopsys Optical Solutions, Westminster CO) with long pass GFP

filters. Three images per mouse were captured to ensure all tumors were counted. Using the images of the mice, green fluorescent tumors were identified as single tumors if there was a distinct border of non-fluorescent tissue. The omental tumor typically is a bundle of distinct tumors, and therefore was removed, counted separate from the images, but included in the total tumor counts. Blood was collected via cardiac puncture and used for HPLC analysis. Tumor and tumor adjacent tissue was collected and stored in 10% neutral buffered formalin, RNAlater (Qiagen, cat# 76104), RIPA buffer or snap frozen using liquid nitrogen for further analysis. Animal work has been approved by the University of New Mexico, Institutional Animal Care and Use Committee (protocol #12-100881-HSC). For tumor burden studies, data presented are combined from 3 separate trials, with 6 animals/treatment group/trial (n=18).

High performance liquid chromatography

Blood from mice was collected at sacrifice via cardiac puncture and stored at 4°C overnight. Samples were then centrifuged at 4000xg for 10 minutes. Serum was separated from red cells into a fresh Eppendorf tube. Serum was then mixed 1:1 with 600mM sulfuric acid and vortexed for 30 seconds. Solution was vortexed with 3ml diethyl ether and separated by centrifugation at 1000xg for 5 minutes. The organic layer was removed and evaporated to dryness in a speedvac, then reconstituted in 37°C 200µl 0.1% formic acid in water.

HPLC analysis was performed with a 50mm long 5µm silica guard column (Phenomenex, 03B-4053-N0) attached to a Partisil® 5 µm ODS(3) 85 Å LC Column 150 x 4.6 mm (Phenomenex, 00F-0120-E0) followed by a reverse phase Lux 5 µm Cellulose-

3 50 x 4.6mm column (Phenomenex, 00G-4493-E0). The columns are equilibrated with acetonitrile/0.1% Formic acid in water (25:75) at a flow rate of 2ml/min. A standard curve of racemic ketorolac in water was generated based on an injection volume of 10 μ l. Ketorolac was detected using a UV spectrometer set at UV310. Retention times for R-ketorolac and S-ketorolac were 5.0 minutes and 5.9 minutes respectively, and were validated against each individual enantiomer. Data presented are combined from two animal studies (n=12).

Cell migration assay

SKOV3ip cells were plated at 1x10⁴ cells / well in 24-well Boyden chambers and allowed to attach for 4h. ML141, NSC23766, or ketorolac enantiomers were added to growth media at final concentrations ranging from 0.001 to 300 μ M. After 48 h, inserts were removed and stained with DAPI. Membrane filters were imaged on an Olympus IX70 inverted fluorescent microscope using a 20x objective. Three representative fields were counted from each treatment group. One-way ANOVA followed by Dunnett's multiple comparison analysis in Graphpad Prism were used to assess statistical significance ($p \leq 0.05$). For each panel, data are combined from three independent trials, each trial was performed in triplicate.

Cell culture fluorescent proliferation assay

SKOV3ip cells were seeded at a density of 1x10⁴ cells/ml in a black-walled 96 well plate. Cells were allowed to adhere for 4h then media was changed for media containing drug. Cells were cultured for 48h in the presence of R-/S-ketorolac, R-

ketorolac, or S-ketorolac at varying concentrations (1-300 μ M). The Cdc42 specific inhibitor ML141 (Sigma-Aldrich, SML0407) was used at a concentration of 10 μ M. The Rac1 specific inhibitor NSC23766 (Tocris Bioscience, #2161) was used at a concentration of 30 μ M. Media only wells were included on the plate for background subtraction. After 48h, calcein AM dye (Invitrogen, C3100MP) was added to each well at a final concentration of 14 μ M and incubated at 37°C for 30m. Plates were read using a plate spectrophotometer (Molecular Dynamics) at an excitation of 490nm and emission of 530nm. Data were subjected to one-way ANOVA followed by Dunnett's multiple comparison test to determine significance ($p \leq 0.01$).

MCA cytometry

SKOV3ip cells were resuspended in Eppendorf tubes at a concentration of 2.5x10⁴cells/ml. Cells were treated with R-/S-ketorolac, R-ketorolac, or S-ketorolac at 300 μ M, ML141 at 10 μ M, or NSC23766 at 30 μ M. Cells were seeded in triplicate into individual wells of a 96-well, U-bottom, non-adherent plate (Corning, cat# 7007) and incubated at 37°C for 48h. After 48h, MCAs were treated with DAPI (Invitrogen, D1306) at a final concentration of 300nM for 30m. Media was aspirated and MCAs were rinsed once using 1X PBS. MCAs were disaggregated using 50 μ l of 0.25% trypsin EDTA (Invitrogen, 25200-056) for 1m at 37°C. Media was added to each well and the disaggregated MCAs were transferred to Eppendorf tubes. Cells in each tube were quantified using a Becton Dickinson FACScan flow cytometer (Immunocytometry Systems). Data were subjected to one-way ANOVA followed by Dunnett's multiple comparison test to determine significance ($p \leq 0.01$).

Cell cycle assay

SKOV3ip cells were seeded at 2.5×10^5 cells/mL with 1 mL/well into 24-well plates and allowed to adhere overnight. After 24h, media was changed for media containing drug. Cells were treated with R-/S-ketorolac at 10 μ M, 30 μ M, 100 μ M, and 300 μ M and 0.5 μ M Taxol (Enzo Lifesciences, Cat# T-104). Old media was removed and new media containing drug was added to the wells in triplicate at 1 mL/well. Cells were incubated for 48 hours then washed once with 1X PBS. A few drops of trypsin were used in each well to detach adherent cells then neutralized with media. Samples were then put into 15 mL conical tubes, pelleted and supernatant was removed. Each sample was re-suspended in 5 mL of PBS as a washing step and centrifuged at 2500 rpm for 5 minutes. Pellets were re-suspended in 1 mL of freshly made 30 μ M propidium iodide (PI) staining solution and incubated for 30 minutes. PI dye was made new every time the experiment was repeated by mixing 20 mL of 0.1% Triton X-100 in 1X PBS, 40 μ L DNase-free RNase-A (100 mg/mL in PBS) (2 mg total) and 800 μ L of 500 μ g/mL PI stock. Samples were transferred to falcon tubes and analyzed on a Becton-Dickson C6 Accuri flow cytometer at 20,000 events. Three independent experiments were conducted and a two-way ANOVA with a Bonferroni post-test was used to calculate significance.

Immunohistochemical staining

Formalin fixed tissues which were stored in 70% ethanol were sent to the University of New Mexico Human Tissue Repository (UNM-HTR) for tissue processing. UNM-HTR embedded tissues in paraffin wax and sectioned blocks into 10 μ m sections. Tissue sections were mounted on hydrophobic slides for further staining. UNM-HTR

stained sections of omental tumor and omental tumor with spleen adjacent with human specific Ki-67 antibody to measure proliferation. UNM-HTR also performed hematoxylin and eosin (H&E) staining on sections. Slides stained at UNM-HTR were then imaged using the Aperio slide scanner. Ki-67 proliferation analysis was done using Aperio ImageScope slide software and proliferation macro. Nuclei were scored as no, low, intermediate or high staining. Low, intermediate, and high staining were considered positive for Ki-67. Data are presented as percent positive staining compared to total number of nuclei. TUNEL staining on tumor and tumor with adjacent tissue was performed using Millipore Apoptag® Fluorescein *In Situ* Apoptosis Detection kit (Millipore, cat #EMD-S7110) according to manufacturer protocol. Slides were counterstained and mounted in Vectashield Hardset Mounting media containing DAPI (Vector Labs, cat # H-1500). Images of TUNEL stained sections was captured using an Olympus IX70 inverted fluorescent microscope at 5.5x. Montage images of each section were created, and fluorescence threshold limits were set using DAPI nuclei. Count and measure module in CellSens software was used to count nuclei of the tumor sections in FITC and DAPI channels. Data presented as percent fluorescein positive nuclei. Data were subjected to one-way ANOVA followed by Dunnett's multiple comparison test to determine significance.

RNA isolation

SKOV3ip cells were seeded at a density of 1×10^5 cells/ml in a 6- well tissue culture dish and allowed to adhere 4h. Cells were treated with 10 μ M ML141, 30 μ M NSC23766, 100 μ M R-/S-ketorolac, 100 μ M R-ketorolac, or 100 μ M S-ketorolac and

incubated at 37°C for 24h. Cells were switched to serum free media containing drug and incubated at 37°C for 24h. After 24h, EGF was added to control wells to a concentration of 10nM and cells were incubated 24h. Media was aspirated and cells were rinsed with 1X PBS. Cells were treated with 1ml TRIzol (Invitrogen, cat #15596-026), cells were scraped from the plate and transferred to a microcentrifuge tube. TRIzol isolation of RNA was performed according to Invitrogen protocol. Collected RNA was stored at -80°C. Animal tumor tissue was stored in RNAlater. From this tissue, 30mg of animal tumor tissue was weighed into a microcentrifuge tube. Tissue was flash frozen in liquid nitrogen and ground using RNase free microcentrifuge tissue homogenizer (Daigger, cat# EF2486Q). The tissue homogenate was resuspended in RLT buffer from the RNeasy kit (Qiaagen, cat# 74104) and centrifuged through a Qiasredder lysis column (Qiagen, cat# 79654). Tissue homogenate was then processed using Qiagen RNeasy kit according to manufacturer protocols. RNA was stored at -80°C. cDNA was generated from 1µg cell and animal RNA using ABI High Capacity cDNA kit (Invitrogen, cat # 4368814).

qPCR

Following cDNA generation, qPCR amplification of Cdc42, Rac1, Rac1b, RhoA, and GAPDH was performed. ABI Fast SYBR® Green Master Mix was diluted with 1µl Qiagen Quantitect primer per reaction. Primers used were Cdc42 (QT01674442), Rac1 (QT00065856), and RhoA (QT00044723), and GAPDH (QT00079247). Rac1b primer set was custom designed and ordered from Invitrogen. Rac1b forward primer, 5'-TCCGCAAACAGTTGGAGA-3', was coupled with Rac1 reverse primer, 5'-CTACATGTTTGC GGATAGGATAGGG-3'. cDNA was diluted 1:5 in nuclease free

water. For qPCR, 6µl of PCR mastermix was added to 4µl cDNA in a 384-well plate, in quadruplicate, for each gene. qPCR was conducted on an ABI 7900HT Fast PCR system under the following conditions: 95°C for 10m, 40 cycles of (95°C for 15s, 60°C for 1m), followed by dissociation curve analysis. Ct values were used for gene analysis.

MCA adhesion and spreading

To form MCAs, SKOV3ip cells were trypsinized from a culture dish and diluted in media to a density of 2.5×10^4 cells/ml. Cells were treated with 10µM ML141, 30µM NSC23766, or 100µM R-/S-ketorolac, R-ketorolac, or S-ketorolac, +/- 10nM EGF simultaneously. For each treatment group, 100µl cell dilution/well was added to a 96-well Ultra-low adhesion, U-bottom dish (Corning, cat#7007) and incubated for 24h. At 24h prior to transferring MCAs, the organotypic cell culture system was setup.

LP9 cells were maintained in 1:1 M199 media (Gibco, cat# 11150-059):DMEM (Gibco, cat# 11965-092) supplemented with 10% fetal bovine serum (Gibco, 16000-044), 0.4µg/ml hydrocortisone (Calbiochem 3867), and 10nM EGF. On ice, 8ng/µl each of rat tail collagen type I (Corning, cat# 354236) and fibronectin (Corning, cat# 356008) were mixed together in LP9 media. To each well of a 96-well flat bottom tissue culture dish, 50µl ECM mix was added and incubated at 37°C for one hour. To a 10cm plate of LP9 cells 2.5µM CellTracker™ CMTPX (Invitrogen, C34552) was added and incubated at 37°C for 1h. LP9 cells were rinsed with 1X PBS and trypsinized. Cells were resuspended to a concentration of 2×10^5 cells/ml and 100µl LP9 cell dilution was added to ECM coated wells. Plates were incubated at 37°C for 24h. MCAs were stained with 2.5µM CellTracker™ BODIPY (Invitrogen, C2102) and incubated 1h at 37°C. MCAs were

imaged and rinsed with 1X PBS. MCAs were suspended in 100µl LP9 media containing drug, +/- 10nm EGF simultaneously. Media was aspirated from LP9 cells, MCAs were transferred to LP9 cell layers, and incubated at 37°C.

For the adhesion assay, MCAs were incubated on the organotypic cell layer at 37°C for 4h. Wells were rinsed with 1X PBS, fixed with 4% paraformaldehyde for 5m, mounted in Vectashield hardset mounting media with DAPI (Vector labs, cat# H-1800). For the spreading assay, MCAs were incubated on the organotypic cell layer at 37°C for 24h, rinsed with 1X PBS, fixed with 4% paraformaldehyde for 5m, mounted in Vectashield hardset mounting media with DAPI. MCAs were imaged using an Olympus IX70 inverted fluorescent microscope. MCAs and area of clearance were measured using Olympus CellSens Dimension software.

Figure Legends

Figure 2.1 - Oral administration of ketorolac reduces tumor burden *in vivo*. **A.** A xenograft mouse model of recurrent ovarian cancer indicates that ketorolac treatment can reduce tumor burden in mice. Mice injected with GFP-expressing SKOV3ip cells show abundant tumor formation after 14 days. Representative images of animals which received either placebo or R/S-ketorolac pills. **B.** Tumor burden is decreased in racemic and R-ketorolac treated animals. There are significantly fewer tumors in animals that received either racemic ketorolac or R-ketorolac. Tumor burden was quantified by counting visible tumors images of the peritoneal cavity. Three images of each animal were captured to reveal tumors in each region of the peritoneal cavity. Total tumor counts from the peritoneal cavity were normalized to placebo treated animals within individual

experiments. These data are combined normalized tumor counts from three separate experiments, n=18. * indicates $p \leq 0.01$ when compared to placebo group. C. Ketorolac recovered from mouse serum. There is no significant difference in the concentration of total ketorolac recovered from mouse serum. For each treatment group, grey bars represent total ketorolac recovered, black and white bars represent R-enantiomer and S-enantiomer, respectively. A predominance of R-ketorolac in all treatment groups indicates that interconversion of the S-enantiomer to the R-enantiomer occurs in this strain of mice.

Figure 2.2 – Animals treated with R-naproxen have decreased tumor burden. A. A xenograft mouse model of recurrent ovarian cancer indicates that R-naproxen, but not S-naproxen, treatment can reduce tumor burden in mice. Mice injected with GFP-expressing SKOV3ip cells show abundant tumor formation, 14 days post-injection (n=3). B. Omental tumor is smaller in R-/S-ketorolac and R-ketorolac treated animals. Omental tumor was removed from animals and weighed prior to being separated for RNA isolation, protein isolation, or histology. Animals treated with R-/S-ketorolac or R-ketorolac had smaller omental tumors when compared to placebo treated animals. R-naproxen treated animals appeared to have smaller tumors, but did not reach statistical significance (n=3, $p \leq 0.05$).

Figure 2.3 –Ketorolac racemates are stable in cell culture. There is no significant difference between area under the curve measurements for R-ketorolac or S-ketorolac peaks when compared to stock solutions. Cells were treated with 100 μ M of R-/S-

ketorolac, R-ketorolac, or S-ketorolac for 48h. HPLC chromatograms are representative of ketorolac treatments recovered from treated SKOV3ip cells, or conditioned media (shown). Racemates show no interconversion to the opposite enantiomer when compared to stock solutions.

Figure 2.4 – OVCA429 and SKOV3ip cell lines have similar reductions in migration following treatment with ML141, NSC23766, or ketorolac. Inhibition of migration dose response curves following treatment with ML141, NSC23766, and R-/S-ketorolac, R-ketorolac, S-ketorolac. IC₅₀ values for OVCA429 and SKOV3ip ovarian cancer cell lines are similar for each drug tested. Cells were plated at 1x10⁵ cells/well in 24-well Boyden chambers and allowed to attach for 4h. Drug was then added at appropriate concentrations and cells were incubated at 37°C for 48h. After incubation, inserts were removed and stained with DAPI. Membrane filters were imaged on a Zeiss inverted microscope using a 20x objective. Three representative fields were counted from each treatment group. IC₅₀ values were obtained using GraphPad Prism 5.0 software. Data presented are combined from 3 independent trials.

Figure 2.5 - Ketorolac has no effect on SKOV3ip cell proliferation or cell cycle. SKOV3ip cells are allowed to grow in culture for 48h in the presence of a CDC42 specific inhibitor ML141 (10μM), a Rac1 specific inhibitor NSC23766 (30μM), R-/S-ketorolac (300μM), R-ketorolac (300μM), or S-ketorolac (300μM). **A.** SKOV3ip cells plated in monolayer and allowed to grow in culture for 48h in the presence of either racemic or single enantiomers. Cells were stained using 4mM calcein AM dye for 30

minutes at 37°C. Plates were read using an excitation of 490nm and emission of 530nm. Cells treated with ketorolac enantiomers showed no significant difference compared to no treatment control cells. A significant decrease was noted in cells treated with either ML141 or NSC23766. These data were normalized from three separate experiments. Significance was determined using a one-way ANOVA followed by Dunnett's multiple comparisons post-test, * indicates $p \leq 0.01$. **B.** SKOV3ip cells were plated in a 96-well, non-adherent U-bottom plate and cultured for 96h. Cells were trypsinized for 3 minutes, triturated to disaggregate cells, and counted using an Accuri C6 cell analyzer. There was no significant difference between ketorolac treatment groups and no treatment control, at basal or EGF stimulated levels. ML141 inhibition of Cdc42 does significantly decrease cell proliferation as compared to no treatment, EGF-stimulated levels. Significance was determined using a one-way ANOVA followed by Dunnett's multiple comparisons post-test. * indicates significant increase in growth between basal and EGF stimulated levels, $p \leq 0.05$. **C.** Cell cycle analysis performed by Amanda Peretti. Flow cytometry was performed to determine if racemic ketorolac causes cell cycle arrest. SKOV3ip cells were treated for 48h with racemic ketorolac or 0.5 μM taxol as a positive control. There was no difference in the cell cycle populations of ketorolac treated cells compared to the no treatment. Taxol treated cells were significantly different than no treatment group in all cell cycle populations. Significance was determined with two-way ANOVA followed by Bonferroni post-test. * indicates $p \leq 0.001$.

Figure 2.6 - Ketorolac has no effect on proliferation *in vivo*. Omental tumor and spleen tissue were collected from animals, fixed in 10% neutral buffered formalin for 24h

and transferred to 70% ethanol. Tissues were processed by the UNM-HTR and embedded in paraffin wax. Sections from placebo, R-/S-ketorolac, and R-ketorolac were analyzed for Ki-67 staining. **A-B.** Tumor tissue was stained for Ki-67 proliferation marker. Tissue sections were stained by UNM-HTR for human Ki-67 and counterstained using hematoxylin. Slides were imaged using an Aperio slide scanner. Nuclei were stained blue and those positive for Ki-67 are brown. **C.** Images were analyzed using Aperio ImageScope. For analysis of proliferation, only tumor tissue was used. Tumor tissue is circled in green, adjacent tissue is spleen and was not used for analysis. Analysis was automated using a proliferation algorithm in ImageScope. Nuclei were scored as negative, low, moderate, or strong staining. **D.** Analysis of proliferation performed by ImageScope. Data are presented as percent Ki-67 positive nuclei, sampled from all three trials (placebo, n=4, R-/S-ketorolac, n=5, R-ketorolac, n=5). There is no difference between treatment groups. Groups were compared using One-way ANOVA followed by Dunnett's multiple comparisons post-test.

Figure 2.7 - Ketorolac has no effect on apoptosis *in vivo*. Serial tissue sections from the tissue blocks used for Ki-67 staining were obtained from the UNM-HTR. Sections were 10µm thick, deparaffinized, and TUNEL staining was performed using Millipore Apoptag® Fluorescein In Situ Apoptosis detection kit and counterstained using DAPI. Sections were imaged using an Olympus IX70 inverted fluorescent microscope using CellSens Dimension software. Image montages were captured at 10x magnification **A-B.** Representative images of placebo section and R-/S-ketorolac treated animals analyzed for apoptosis. Positive nuclear staining is green and compared to total blue staining (not

shown). Similar to Ki-67 staining, only tumor tissue was analyzed. Due to non-specific staining of extracellular matrix and erythrocytes, a threshold was set for positive nuclear staining. C. There is no difference in levels of apoptosis between treatment groups (n=5). Data are presented as percent positive nuclei. Groups were compared using One-way ANOVA followed by Dunnett's multiple comparisons post-test.

Figure 2.8 - Cdc42 or Rac1 inhibition does not change GTPase gene expression in

cells or *in vivo*. **A.** Inhibition of Cdc42 or Rac1 does not affect gene expression of GTPases after 24h EGF stimulation. Cells were plated and cultured for 24h in the presence of drug and switched to serum free media for 24h. After 24h, 10nM EGF were added cells and cultured for another 24h. RNA was isolated using TRIzol according to manufacturer protocol. Following isolation, cDNA was generated using ABI High Capacity cDNA kit. qPCR was performed with 4 replicates for each sample using primers for Cdc42, Rac1, Rac1b, RhoA, and GAPDH on an ABI7900HT fast real time PCR system. CT values were obtained using SDS2.2 software and relative expression to EGF stimulation was determined using $\Delta\Delta CT$ values. Data are combined from 4 separate collections (n=4). Gene expression for each gene was subjected to One-way ANOVA followed by Dunnet's multiple comparisons post-test. **B.** Ketorolac treatment does not change gene expression *in vivo*. Tumor tissue preserved in RNAlater was homogenized using an RNase free micropestle in liquid nitrogen. RNA isolation from tumor tissue was then performed using QIAshredder columns followed by RNeasy mini kit from Qiagen according to manufacturer protocol. Following isolation, cDNA was generated using ABI High Capacity cDNA kit. qPCR was performed with 4 replicates for each sample using

primers for Cdc42, Rac1, Rac1b, RhoA, and GAPDH on an ABI7900HT fast real time PCR system. CT values were obtained using SDS2.2 software and relative expression to placebo group was determined using $\Delta\Delta CT$ values. Data presented are from 4 animals from each treatment group. Gene expression for each gene was subjected to One-way ANOVA followed by Dunnett's multiple comparisons post-test.

Figure 2.9 – Ovarian cancer cell lines express the Rac1 splice variant Rac1b. DNA isolated from immortalized ovarian surface epithelium (IOSE), human keratinocytes (HACAT), and the ovarian cancer cell lines DOV13, OVCA3, SKOV3ip, OVCA433, and OVCA429, expressed the constitutively active Rac1 splice variant, Rac1b, at different levels. Primers used were Rac1 forward primer – 5' AACCAATGCATTTCTGGAG, and Rac1 reverse primer, 5'-TACATGTTTGCGGATAGGATAGGG-3'. PCR product was run on a 1% agarose gel stained with SYBR Safe gel stain. Rac1 is identified as a band at 467bp, Rac1b is a band at 526bp.

Figure 2.10 - Ketorolac treatment reduces adhesion and MCA spreading. A. Inhibition of Cdc42 and Rac1 using ML141 and NSC23766 prevents MCA adhesion at 4h. LP9 mesothelial cells were cultured in a 96-well dish, on top of collagen and fibronectin for 24h to create an organotypic cell culture system. LP9s were stained using CellTracker™ CMTPX red fluorescent dye. SKOV3ip MCAs were cultured 48h in the presence of drug with 10nM EGF. MCAs were stained with CellTracker™ BODIPY green fluorescent dye and transferred to LP9 cell layer in the presence of drug and incubated 4h. Cell cultures were rinsed with 1x PBS. Cells were fixed in 4%

paraformaldehyde and covered with Vectashield mounting media with DAPI. Wells were imaged using an Olympus IX70 inverted fluorescent microscope at 5.5x magnification. MCAs treated with ML141, NSC23766, or ketorolac enantiomers were washed from LP9 cell layer. No treatment MCAs were adherent after 4h. **B.** Inhibition of Cdc42 and Rac1 impairs MCA spreading on organotypic cell layer after 24h. Cell culture was performed as in 2.10A, except MCAs were cultured on organotypic cell layer for 24h. Cells were rinsed and fixed as above. Images are mesothelial clearance and representative of no treatment and R-/S-ketorolac treated MCAs. **C.** Percent area increase from MCA to clearance area. MCAs were imaged prior to transfer to mesothelial cells. Mesothelial clearance was imaged after 24h incubation with MCAs. Area of MCAs and mesothelial clearance were calculated using Olympus CellSens software. Data from mesothelial clearance assay are presented as percent area increase and subjected to One-way ANOVA followed by Dunnett's multiple comparisons post-test. All treatment groups showed decreased clearance compared to no treatment control, * indicates $p \leq 0.05$. **D.** Ketorolac treatment does not affect SKOV3ip cell adhesion *in vivo*. Serial sections from tumor tissue stained for Ki-67 (Fig 2.6) were H&E stained and imaged using the Aperio Slide Scanner at the UNM-HTR. Slide images were scored by Dr. Donna Kusewitt for adhesion versus no adhesion to the splenic capsule. SKOV3ip cells are marked by red arrows. Analyzed sections had clear connective tissue between tumor and spleen. Images are representative of placebo and R-/S-ketorolac sections. **E.** Ketorolac treatment does not affect SKOV3ip cell adhesion *in vivo*, ($p=0.052$ in R-ketorolac and S-ketorolac groups). Treatment groups were placebo, n=10, R-/S-ketorolac, n=10, R-ketorolac, n=14,

S-ketorolac, n=11. Chi-square analysis compares adhesion vs no adhesion across treatment groups and is a measure of adhesion across different animal studies.

Figure 2.1

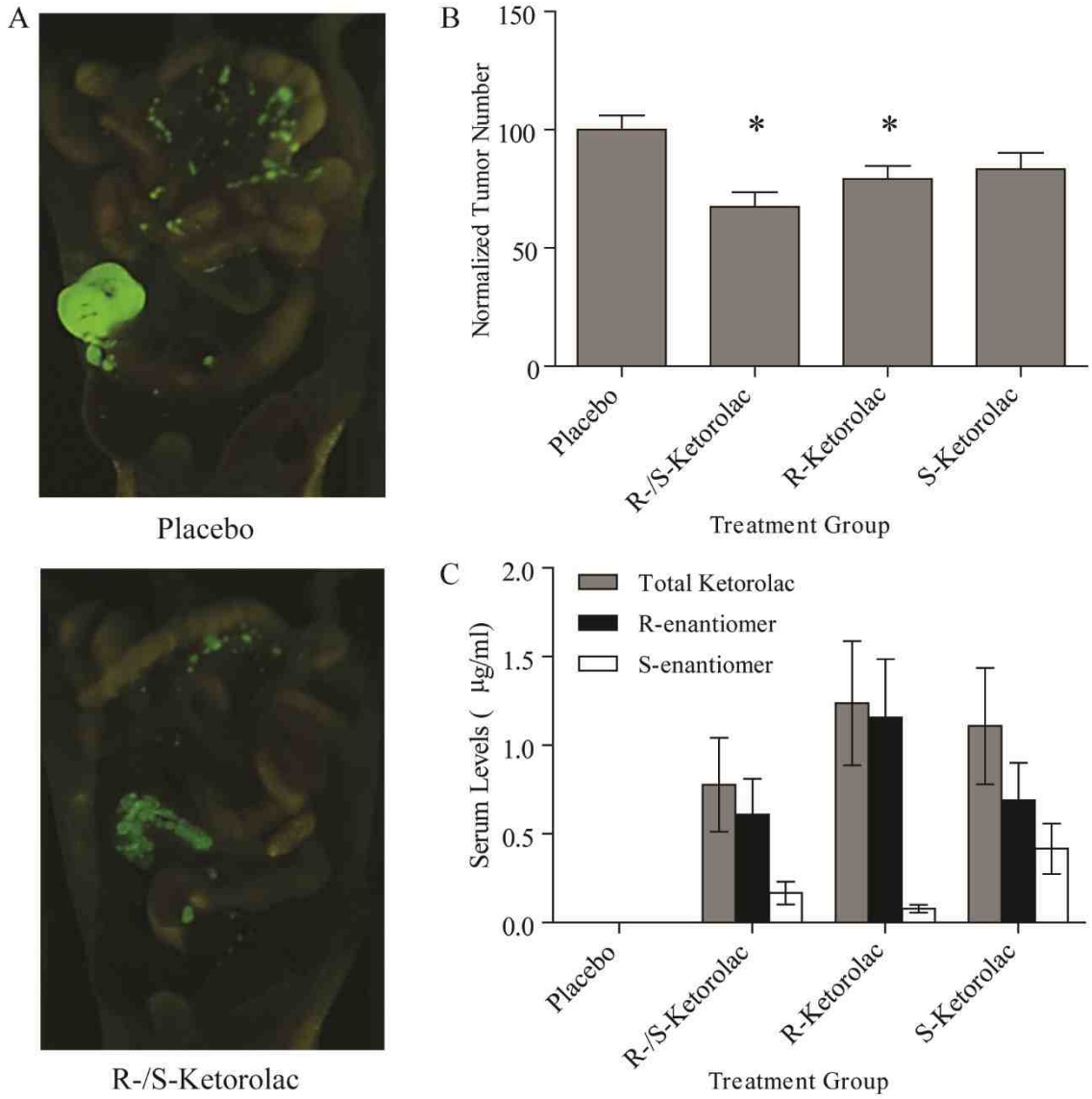


Figure 2.2

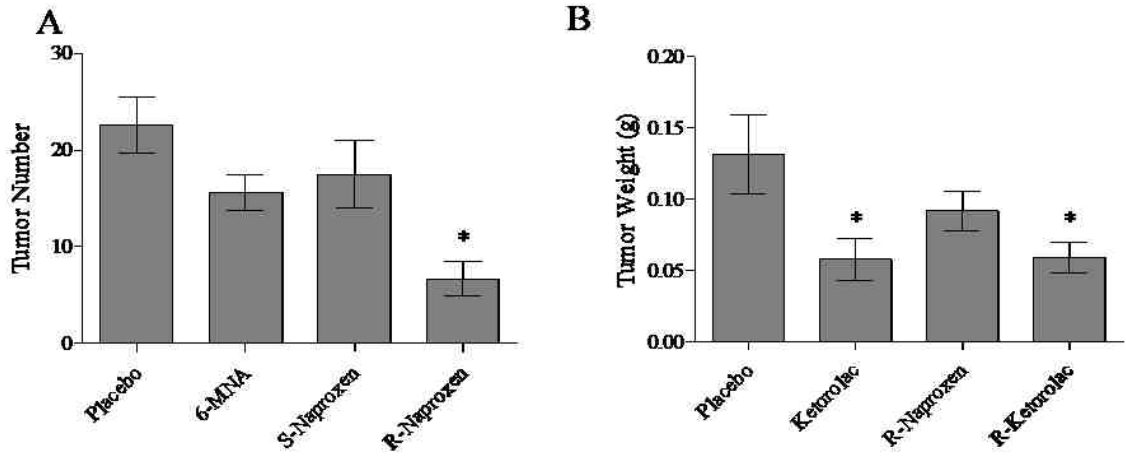


Figure 2.3

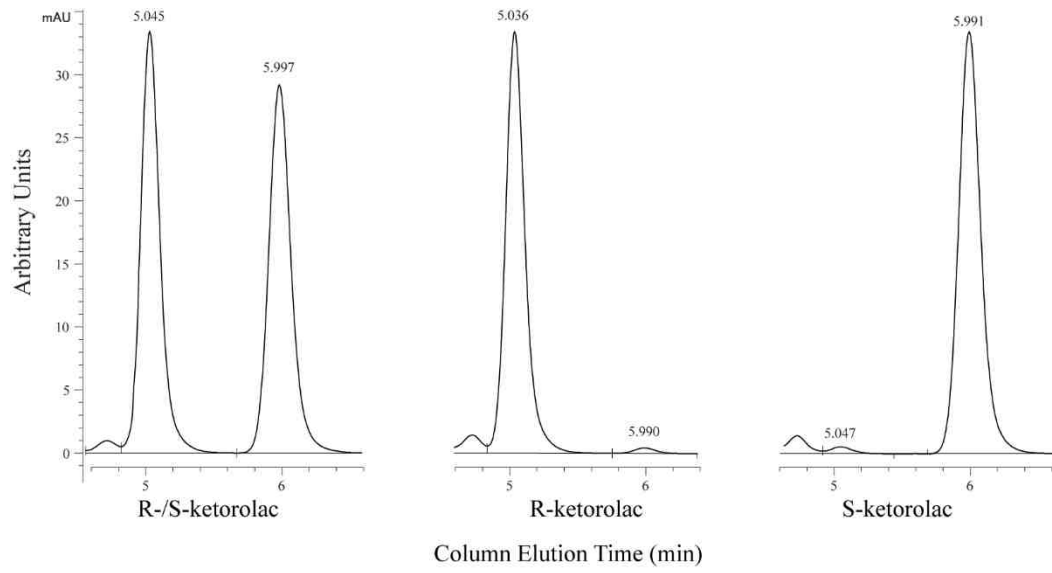


Figure 2.4

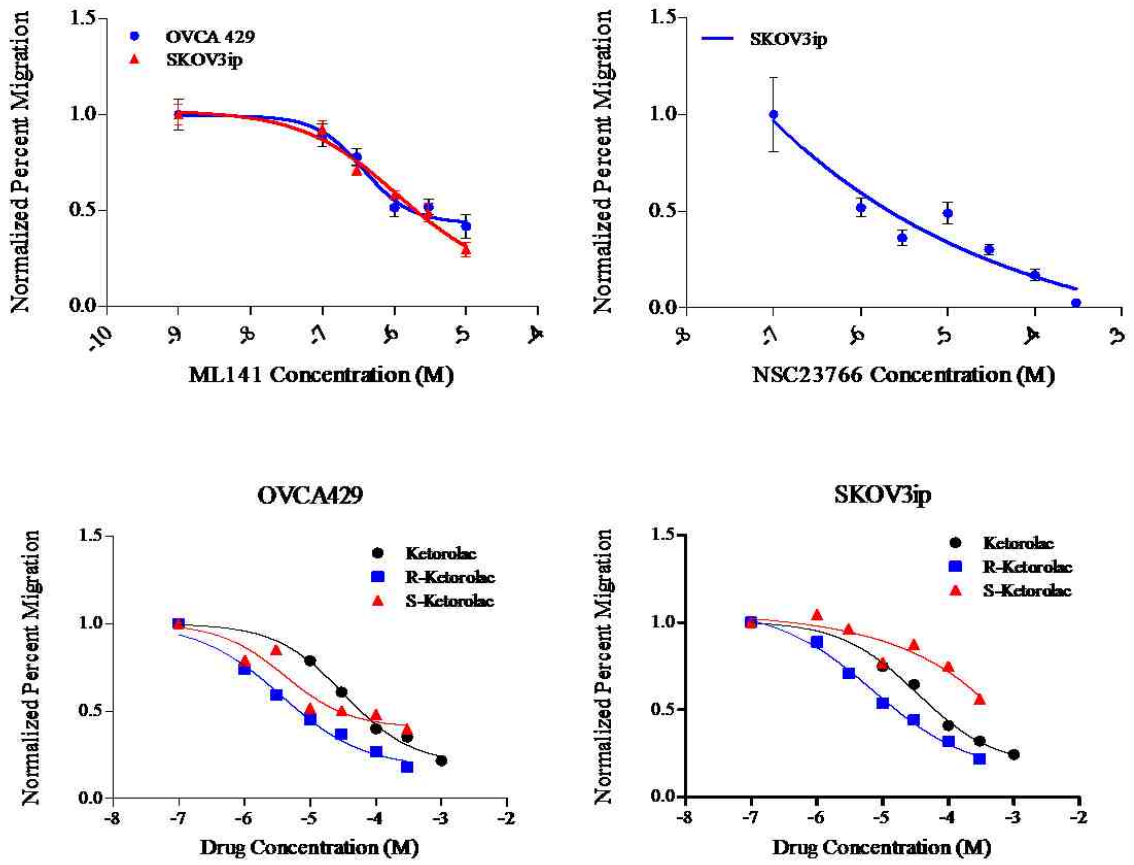


Figure 2.5

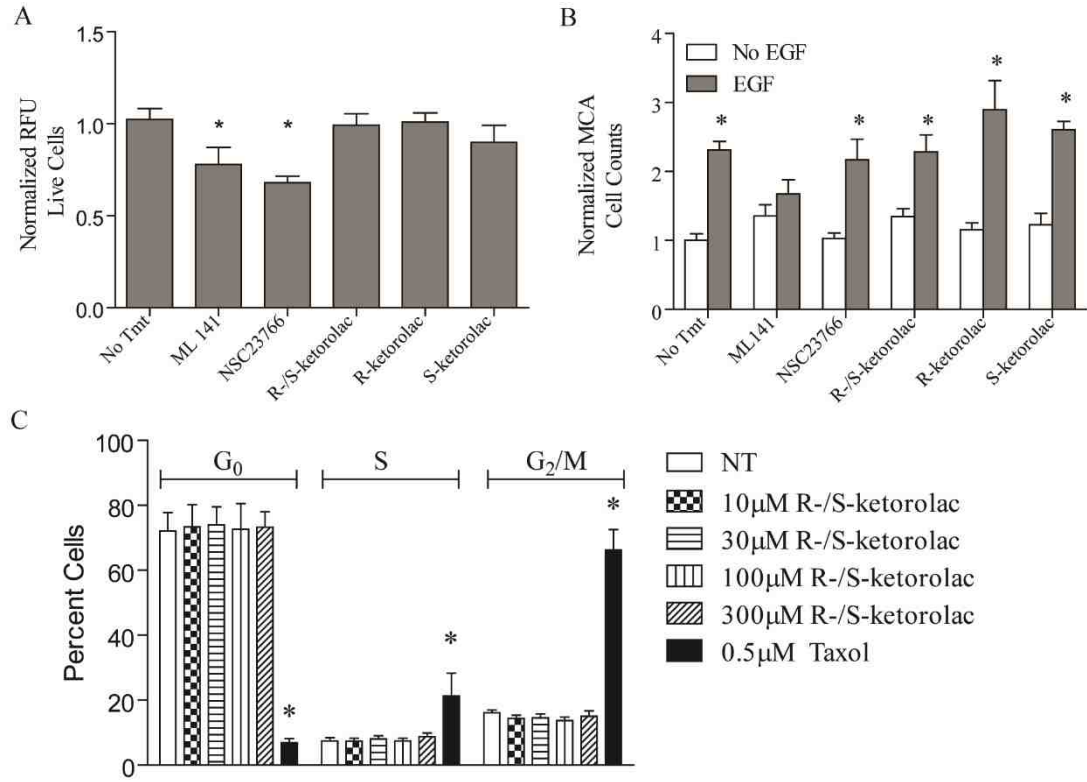


Figure 2.6

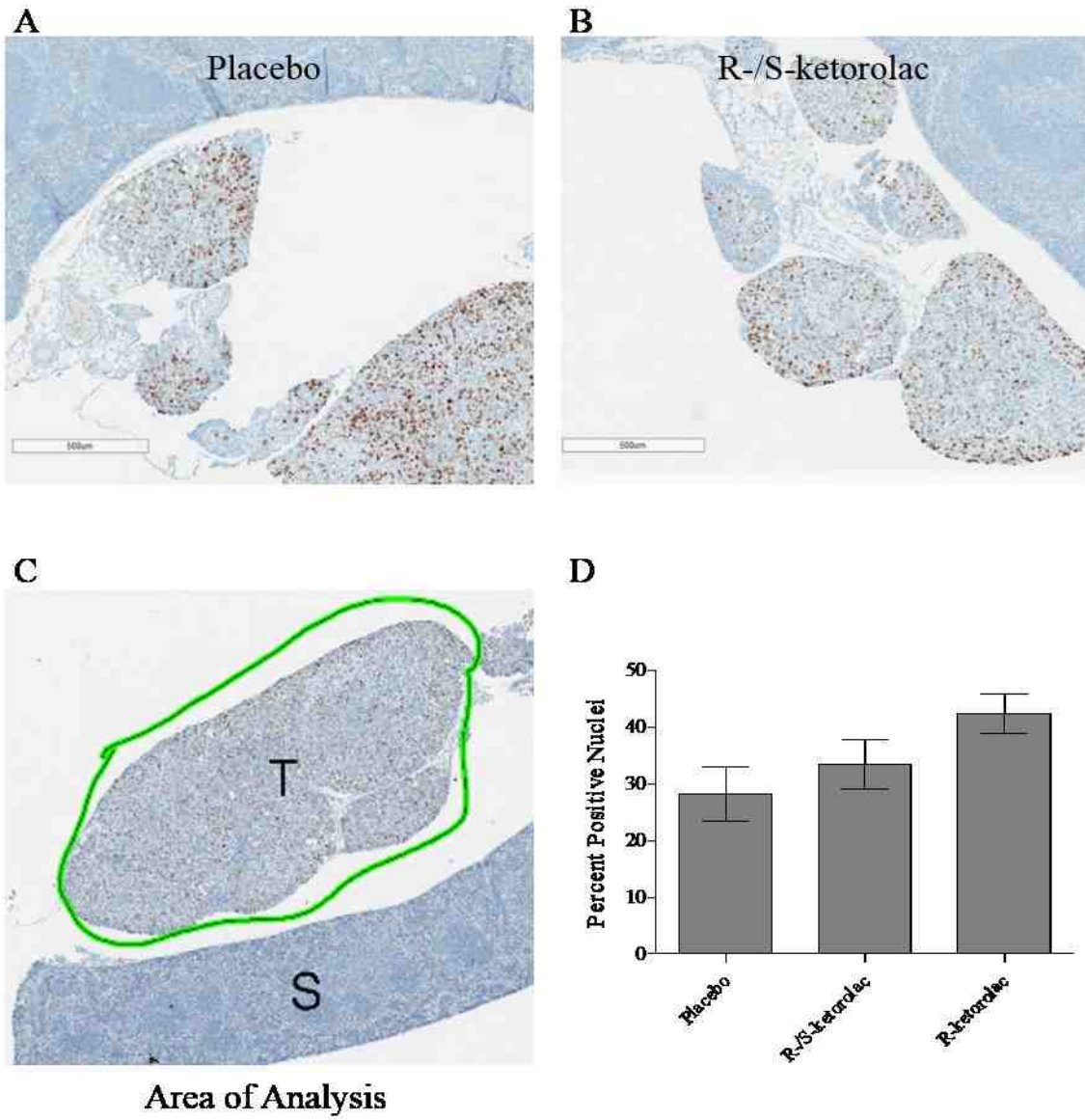


Figure 2.7

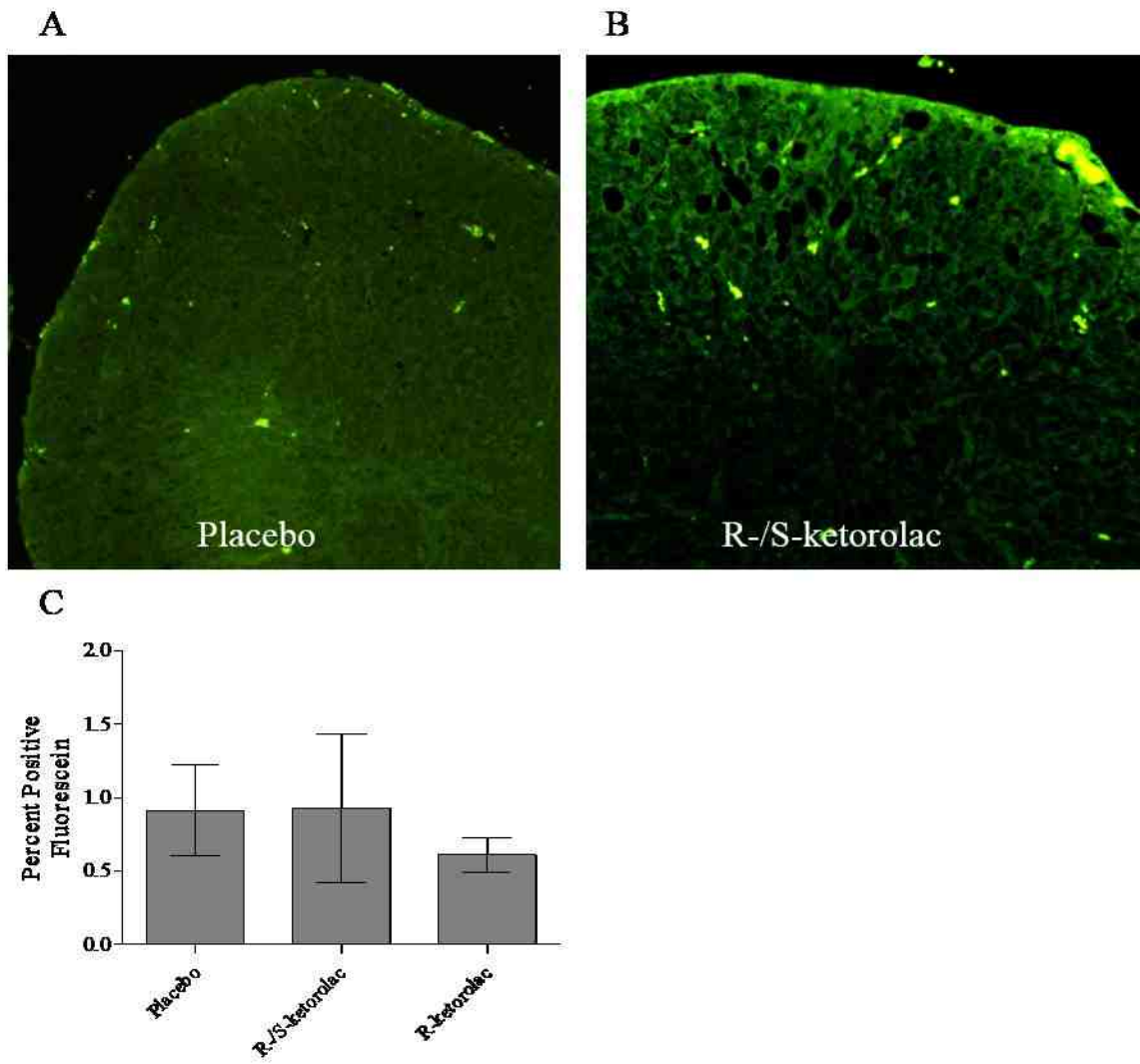


Figure 2.8

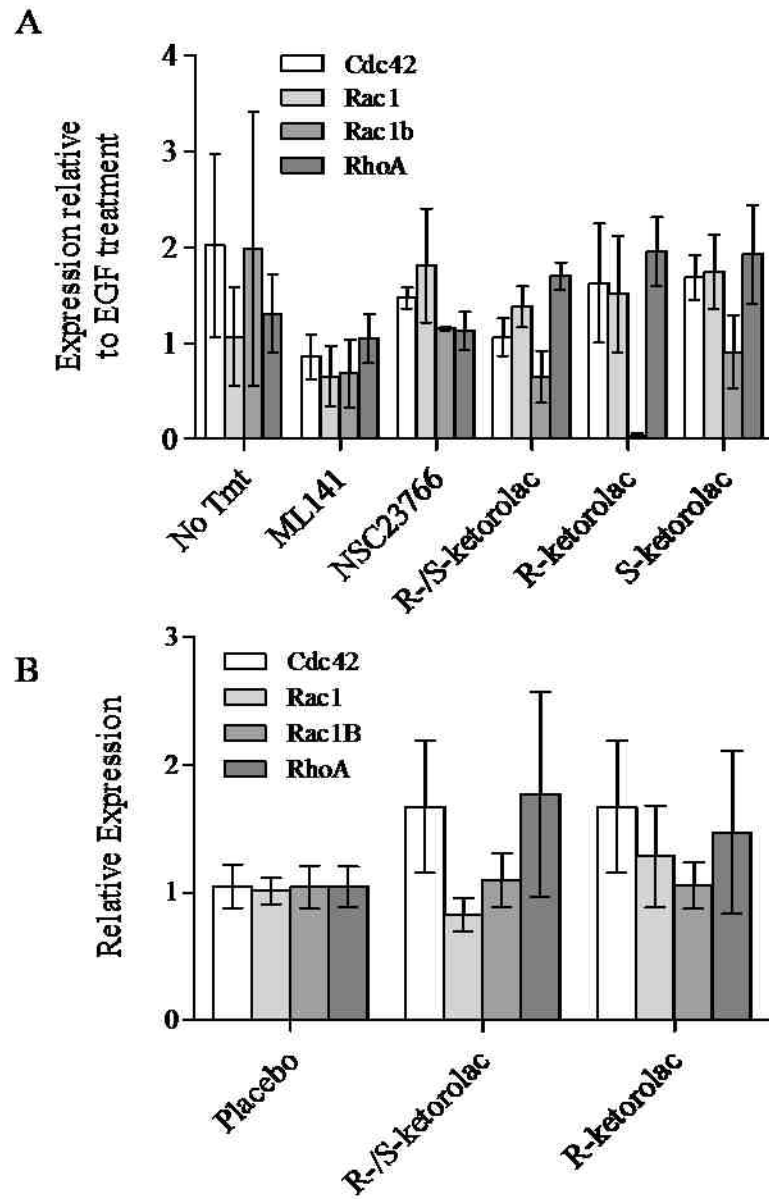


Figure 2.9

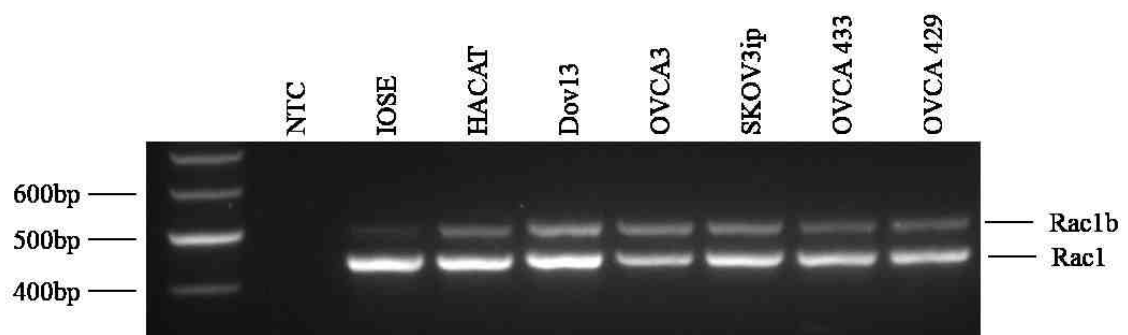
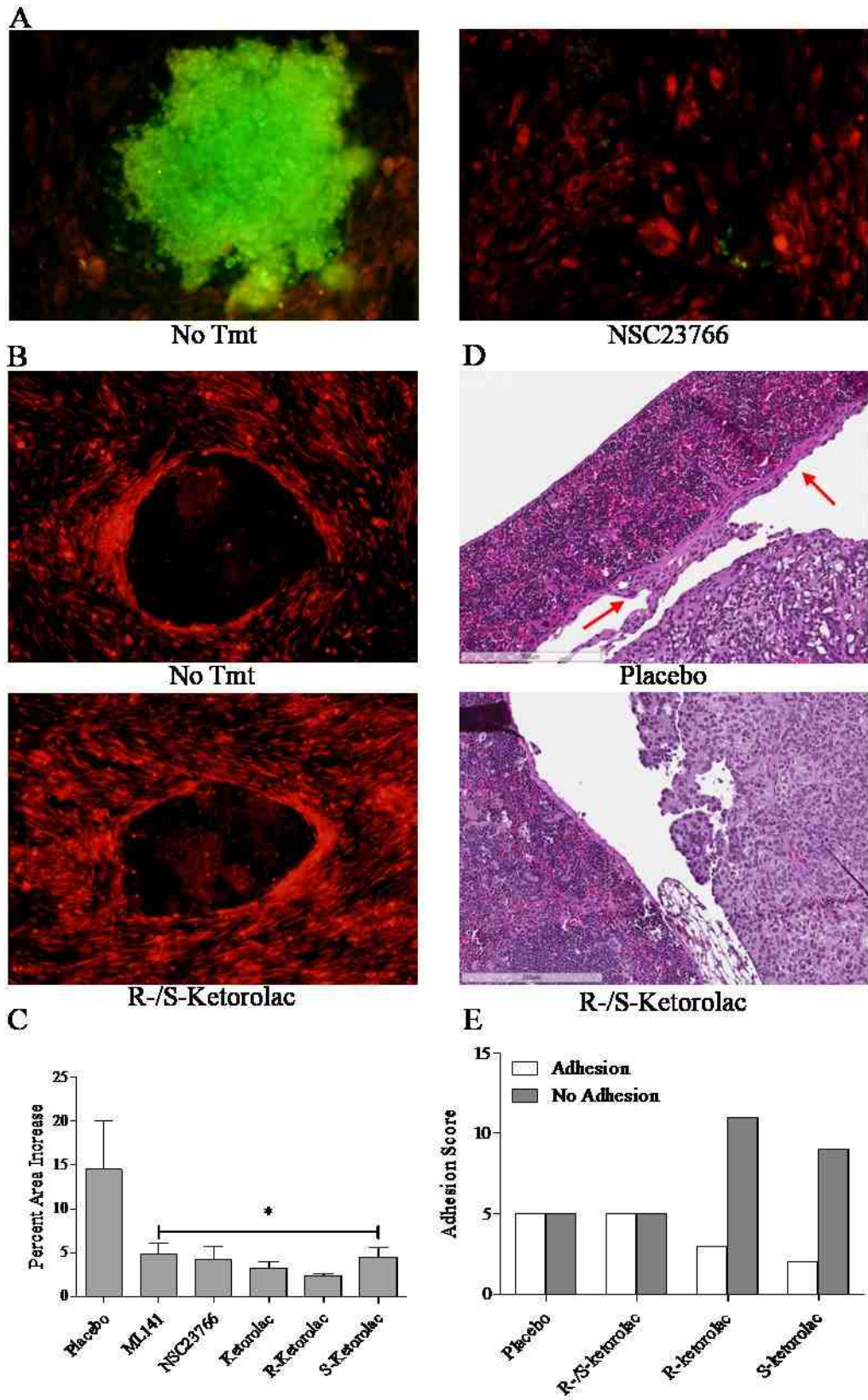


Figure 2.10



**A novel pharmacologic activity of ketorolac
for therapeutic benefit in ovarian cancer patients**

Introduction

Ovarian cancer is the leading cause of death from gynecologic malignancies and the second most common gynecologic cancer (2). Five year patient survival remains less than 50% and the mortality rate has not changed appreciably in two decades (2). The majority of women are diagnosed with metastatic disease, and although a substantial proportion of women respond to initial treatment, recurrence is common (161). Despite concerted efforts, identification of effective targeted therapies has remained elusive in this disease (162). There remains a great need to identify new strategies to treat and manage ovarian cancer.

The Ras-homologous (Rho) family of small GTPases (Rac, Cdc42 and Rho) are key regulators of cancer-relevant cellular functions including actin reorganization, cell motility, cell-cell and cell-extracellular matrix (ECM) adhesion and invasion (66,76,163,164). In many human tumors (including colon and breast), there is clinical and experimental evidence that aberrant Rho-family signaling contributes to tumor growth, survival, invasion and metastasis (76,96,162,165). Based on these functions, Rac1 and Cdc42 have been recognized as attractive therapeutic targets (96,103) and inhibitors are effective in experimental systems (112–114,120,166,167) but specific inhibitors of Rac1 or Cdc42 have not been translated to clinical use.

A Cdc42 selective inhibitor effectively blocked migration of two ovarian tumor cell lines (112,120) suggesting that Rho-family GTPases may be potential therapeutic

targets in ovarian cancer. Using findings obtained from a high throughput screen of the Prestwick library of off patent, FDA-approved drugs and cheminformatics approaches, we identified the R-enantiomers of a limited number of non-steroidal anti-inflammatory drugs (NSAIDs) as inhibitors of Rac1 and Cdc42. The corresponding S-enantiomers are considered the active component in racemic drug formulations acting as NSAIDs with selective activity against cyclooxygenases (COX). One candidate, R-ketorolac, inhibited ovarian tumor cell migration and adhesion without causing cytotoxicity (150,168). Our data indicate that the clinically administered racemic ketorolac (Toradol®) has two distinct pharmacologic activities; the well-established inhibition of COX 1 and 2 by S-ketorolac serving as the basis of the FDA-approved indication for pain management, and a previously unrecognized property of Rac1 and Cdc42 inhibition conferred by the R-enantiomer. Cell based measurement of GTPase activity demonstrated that R-ketorolac specifically inhibits epidermal growth factor stimulated Rac1 and Cdc42 activation at low micromolar concentrations. The GTPase inhibitory effects of R-ketorolac in cells mimic those of established Rac1 (NSC23766) and Cdc42 (CID2950007/ML141) specific inhibitors (150).

In this study we report that R-ketorolac achieved an effective concentration in peritoneal fluids and inhibited Rac1 and Cdc42 activity in cells retrieved from the peritoneal compartment of post-surgical ovarian cancer patients following administration of the racemic drug for postoperative pain management. A medical record review to compare the ovarian cancer-specific survival of ovarian cancer patients who did or did not receive ketorolac for post-operative analgesia revealed increased survival of patients receiving ketorolac. This observation is in keeping with reports for improved clinical

outcomes associated with ketorolac usage, as compared to other NSAIDs, in breast cancer patients (126,143,150,160). Although it has been long recognized that R-enantiomers of NSAIDs are poor inhibitors of cyclooxygenase activity (133,134,151), potential pharmacologic activities or benefits of the R-enantiomers has remained largely unexplored. Our findings show that Rac1 and Cdc42 are unrealized therapeutic targets in ovarian cancer and use of ketorolac may benefit ovarian cancer patients.

Results

Expression of Rac1 and Cdc42 in ovarian cancer

Based on the established functions of Rho-family GTPases, ovarian cancer metastasis is predicted to be strongly dependent on Rac1/Cdc42-regulated pathways for exfoliation, formation of multicellular aggregates, mesothelial adhesion, and localized invasion into the interstitial collagen-rich submesothelial matrix (32,162,169). To test if these GTPases are dysregulated in ovarian cancer, we examined grade dependent expression of Cdc42 and Rac1 protein by immunohistochemical staining of human tumor samples (Fig 3.1) and GTPase mRNA using quantitative PCR analysis of ovarian cancer tissue cDNA arrays (Fig 3.2, 3.3). Cdc42 protein overexpression levels were highly significant for malignant, high grade tumors ($p < 0.001$) compared to lower grade tumors without an apparent increase in mRNA levels. In contrast, there was little evidence of increased expression of Rac1 protein with increasing grade (Fig 3.1). However, significantly elevated expression of a constitutively active splice variant *Rac1b* (170–172), was detected in ovarian tumors (Fig 3.2). These findings provide evidence for

aberrant expression of Rac1 and Cdc42 in ovarian cancer and suggest that they may represent therapeutic targets for this disease.

Study design and patient population

In previous work, we identified R-ketorolac as an inhibitor of Rac1 and Cdc42 at low micromolar concentrations (123,150). R-ketorolac is inactive against the enzyme targets of S-ketorolac, COX-1 and COX-2 (133,134,151), and the inhibitory concentration IC₅₀ values for inhibition of Rac1 and Cdc42 by S-ketorolac were more than 100-fold greater than R-ketorolac (123). Thus, the racemic R-/S-ketorolac possesses two distinct pharmacologic activities and our findings identify R-ketorolac as a novel inhibitor of Rac1 and Cdc42.

In this “Phase 0” feasibility study, ketorolac was administered for its FDA-approved indication for post-operative pain management. Eligible patients had suspected advanced stage ovarian, fallopian tube or primary peritoneal cancer with planned optimal cytoreductive efforts. Secondary eligibility was met if the patient had confirmed ovarian cancer, was optimally cytoreduced and had an intraperitoneal (IP) port placed for planned peritoneal chemotherapy. The patients had no active post-operative bleeding, did not require therapeutic anticoagulation and had good post-operative organ function. Forty-two patients met primary eligibility, and considering secondary eligibility requirements, twenty patient samples were collected at surgery. Samples of blood and peritoneal fluids after ketorolac administration were obtained from thirteen patients. Pathologic analysis of the twenty surgical samples confirmed fifteen patients (75%) had stage III or IV disease. Histologically, 100% had high-grade carcinoma; one was a carcinosarcoma, 16/19 were

pure serous carcinomas, one was primary peritoneal and one fallopian tube primary, and the rest ovarian primary tumors. The average age was 60.8 (Range 33-81), race and ethnic distribution was 85% Caucasian (29.4% Hispanic), 5% American Indian and 10% Black or African American. Ketorolac dosages administered based on clinical indications were 15 mg (33% of patients) or 30 mg (77% of patients). As illustrated in Fig 3.4A, blood and peritoneal fluid were obtained at T=0, 1 h, 6 h and 24 h after administration of the recommended dose of ketorolac.

Distribution of R- and S-ketorolac in peritoneal fluids.

Serum and peritoneal fluid samples were analyzed by HPLC to resolve and quantify R- and S-ketorolac enantiomers in order to determine enantiomeric ratios and distribution over time (Fig 3.4B,C). Clinical-grade ketorolac tromethamine is a 1:1 mixture of R- and S-enantiomers (Fig 3.5); however, the racemic distribution favors the R-form in both serum and peritoneal fluids at each time point in keeping with the established shorter half-life of S-ketorolac in human serum based on differences in pharmacokinetic parameters for each enantiomer (134,151,173). Ketorolac distributes to the peritoneum within 1h after IV administration, and ketorolac levels in the peritoneal fluids are nearly equivalent to those present in the serum at 6 h and decline dramatically by 24 h in both serum and peritoneal fluids. Our results represent the first evidence of ketorolac distribution to peritoneal fluids. The half-maximal inhibitory concentration IC_{50} for Rac1 and Cdc42 by R-ketorolac are 0.57 and 1.07 μ M, respectively whereas the IC_{50} values for S-ketorolac for these targets was >100 μ M (123). The concentrations of R- and S-ketorolac in the peritoneal fluids were 0.98 μ M and 0.32 μ M respectively, 6 h after IV

ketorolac administration. Thus, R-ketorolac achieved concentrations in the peritoneal fluids at or above the IC₅₀ values for Rac1 and Cdc42 and is predicted to inhibit these GTPase targets in cells obtained from this compartment.

Analysis of patient-derived cells.

Tumor cell enriched fractions were prepared from ascites samples obtained at the time of cytoreductive surgery from ovarian cancer patients and post-surgery immediately prior and 1 h, 6 h, and 24 h post IV ketorolac administration (Fig 3.4A). Both Rac1 and Cdc42 were highly activated in freshly isolated tumor cells from ascites and the activity level declined within 48 h in culture medium (Fig 3.6A) suggesting that the ovarian tumor environment fosters Rac1 and Cdc42 GTPase activation. Post-surgery, we observed a statistically significant decrease in Rac1 and Cdc42 activity with time after ketorolac administration (Fig 3.6B,C). In contrast, RhoA activity was insensitive to ketorolac (Fig 3.8), further affirming the selectivity of the drug. R-ketorolac predominates in the peritoneal fluids at the S-enantiomer is virtually undetectable at 24 h (Fig 3.4C) indicating that the R-enantiomer is bioactive and accounts for the observed inhibition of the GTPases *in vivo*.

Retrospective patient outcomes review

Peri-operative ketorolac was used in 14% of the 123 women in the study. Younger women (<50 years) were more likely than older women to receive peri-operative ketorolac ($p < 0.05$); all other clinical and treatment characteristics were similar between the two groups. At 60 months of follow-up, 3/17 ketorolac treated patients (18%) and 40/92 non-treated patients (43%) had died of ovarian cancer. Stratified log-rank tests for categorical factors such as age group, AJCC stage, completion of chemotherapy as planned, and receipt of neo-adjuvant chemotherapy as coded in Table 3.1, showed a consistent ketorolac survival benefit in each strata (Figs 3.10-3.13). The better survival in women treated with ketorolac consistently found in the stratified analysis was also evident in the proportional hazards analysis when we adjusted for age at diagnosis, AJCC stage, completion of chemotherapy as planned, and receipt of neo-adjuvant chemotherapy: the adjusted hazard ratio for ovarian cancer-specific mortality associated with perioperative ketorolac (yes vs. no) was 0.30 (95% CI 0.11-0.88) (Table 3.1). On the basis of the proportional hazards model, an example survival plot is shown in Fig 3.9 for women who had AJCC stage III cancer, were 50-60 years at diagnosis, did not receive neoadjuvant therapy, and completed post-surgery chemotherapy as planned. Other survival plots are shown in Figs 3.10-3.13 and while these plots highlight the results for women who completed their post-surgery chemotherapy as planned, all combinations of women defined by stage of disease, age at diagnosis, neoadjuvant therapy, and post-surgery chemotherapy showed a consistently better survival with ketorolac versus without. These preliminary findings suggest that perioperative ketorolac reduces ovarian cancer-specific mortality.

Discussion

In many human cancers, aberrant Rho-family GTPase activity or downstream signaling pathways are associated with increased aggressiveness and poor patient prognosis (54,67,76,103,173). The specific mechanisms by which Rho-family GTPases modulate tumor development and progression remain under investigation (54,76,162,163,165,174); however, experimental evidence places Rac1 and Cdc42 within the metastatic cascade. Little is known regarding Rac1 and Cdc42 expression in ovarian cancer. We demonstrated elevated expression of Rac1 and Cdc42 in human ovarian cancer specimens and high activity of these GTPases in freshly isolated tumor cells from ascites obtained at surgery (Figs 3.1 and 3.6). In a recent study, high Rac1 protein expression in ovarian cancer was associated with early recurrence and poor prognosis (59). Furthermore, partial silencing of Rac1 by shRNA decreased tumor cell proliferation, migration and invasion in culture, and decreased growth of subcutaneous ovarian cancer xenografts *in vivo* (59). We find that R-ketorolac inhibits adhesion and invasion of primary human ovarian tumor cells from patient ascites (150) thereby indicating that pharmacologic inhibition of Rac1 and Cdc42 also blocks these tumor-relevant functions. The cumulative observations in conjunction with inhibition of ovarian tumor cell migration by a Cdc42 specific inhibitor (112) indicate the potential value of targeting Rac1 and Cdc42 in ovarian cancer.

In the present study, we show evidence that Rac1 and Cdc42 inhibition can be achieved in ovarian cancer patients following administration of racemic ketorolac (Toradol®). Ketorolac is a 1:1 racemic mix of the R- and S-enantiomers. The S-form inhibits COX enzymes which confers the drug's anti-inflammatory activities. The COX

inhibitory action of S-ketorolac supports its indication for post-operative pain management, but also limits its long term use due to COX-related toxicity (133,134,151). R-ketorolac has little activity against COX (133,134,151) and therefore is not functional as an NSAID, but is bioactive and inhibits Rac1 and Cdc42 (150). Importantly, the levels of R-ketorolac within the peritoneal fluids were sufficient to inhibit Rac1 and Cdc42 activity in cells obtained from the peritoneal cavity following ketorolac administration. The innovative Phase 0 clinical trial design enabled real time sampling of fluids and cells from the peritoneal cavity. Direct demonstration of the difference in racemic distribution of ketorolac enantiomers illustrates the value of a study design that allows direct testing of drug and cell activities within peritoneal fluids rather than extrapolation from serum drug levels.

Furthermore, the peritoneal bioactivity of ketorolac is shown to have benefit for ovarian cancer patient outcomes. We found that perioperative use of ketorolac reduces ovarian cancer specific mortality (Fig 3.9). There is precedence in the literature that ketorolac usage in the perioperative period is associated with improved cancer outcomes. The first observation was made for breast cancer patients in 2010 (143). In this study, ketorolac use was associated with a decrease risk of breast cancer relapse (HR=0.37, 95%CI=0.0-0.79). Follow-up papers noted that this relapse reduction was most pronounced in the first 24 months post-surgery (126, 143). No change in breast cancer recurrence was noted in patients who received sufentanil, clonidine, ketamine, or other intraoperative analgesics. Lung cancer patients receiving ketorolac displayed improved overall survival as well (175). The authors hypothesize that the benefit is due to the anti-inflammatory actions of ketorolac, particularly on the extravasation of circulating tumor

cells in the transient inflammatory environment stimulated by surgery (126). Ketorolac appears to have more pronounced positive outcomes than other NSAIDs (126), and this may be based on the combined impact of anti-inflammatory activity by the S-enantiomer and R-enantiomer effects on Rac1 and Cdc42 leading to decreased adhesion and implantation of circulating or residual tumor cells. Ketorolac is not cytotoxic to ovarian tumor cells (150), but predicted decreases in establishment or further development of micrometastases due to Rac1 and Cdc42 inhibition would be expected to improve response to subsequent chemotherapy, which cannot be initiated until patients have recovered from cytoreductive surgery.

Collectively, our findings support the potential repositioning of ketorolac as an addition to current ovarian cancer therapy. Our work demonstrates that the R-enantiomer of ketorolac acts as a first-in-class drug for inhibition of the cancer-relevant targets Rac1 and Cdc42 (123,150) and provides the first evidence that these therapeutic targets can be inhibited in humans using an approved drug. There is precedence for pharmacologic activities dictated by R-enantiomers of specific NSAIDs against novel (non-COX) targets (145,159,176). For example, R-etodolac and its analogs SDX-301 and SDX-308 display anti-tumor activity in chronic lymphocytic leukemia and activity against multiple myeloma in cell and animal models (145,159,160,176–178). R-etodolac also significantly suppressed tumors in a colitis-related mouse model colon cancer (145) and retarded tumor development and metastasis in a transgenic mouse model of prostate cancer (176). These examples and others demonstrate that R-enantiomers of NSAIDs can possess unanticipated anticancer activities based on interactions with non-COX targets. Further evidence that targeting Rac1 may provide therapeutic benefit in ovarian cancer was

recently reported (64). Zoledronic acid is a nitrogen containing bisphosphonate that inhibits prenylation of small GTPases.

Administration of this drug decreased growth of ovarian cancer peritoneal xenografts through inhibition of angiogenesis driven by a Rac1 mediated pathway (64). Collectively, our results suggest that racemic ketorolac may provide a survival benefit to ovarian cancer patients through inhibition of COX enzymes by the S-enantiomer and inhibition of the small GTPases Rac1 and Cdc42 by the R-enantiomer. Additional studies to determine whether clinical benefit can be observed in ovarian cancer patients through perioperative administration of ketorolac in a placebo-controlled clinical trial are in process.

Patients and Methods

Immunohistochemical analysis of GTPase targets

Immunohistochemical staining was performed using standard procedures. Rac1 was stained with mAb (clone 102, BD Biosciences, 10155-1-AP) and Cdc42 was stained with rabbit pAb (Protein Tech Group). A Vectastain Ready-to-Use (RTU) ABCperoxidase kit and ImmPact DAB (SK-4105) were used to visualize primary antibody labeling with hematoxylin nuclear counterstain (H-3401) for tissue staining and samples were mounted in VectaMount (H-5000); (all from Vector Laboratories).

For large scale ovarian tumor profiling, tissue microarrays were purchased from US BioMax, Inc. (Rockville, MD, cat# OV1005 061 and OV8010 009). In total 180 unique tissue samples were included in the evaluation; ranging from stage I-IV and grades 1-3 (Table 3.2). All tumor types were validated and staining was scored by a

pathologist with gynecologic pathology specialty (Dr. Lesley Lomo) and evaluated for location (nuclear and cytoplasmic), as well as intensity of positive staining. Scoring was based on the product of the percentage of cells stained and the intensity of the staining in each localization (3+: strong, 2+: intermediate, 1+: weak and 0: no staining), resulting in a minimum of 0 (100% cells x 0) and a maximum of 300 (100% cells x 3+).

Specimens were deparaffinized and hydrated using xylene and graded ethanol solutions finishing with phosphate buffered saline. Epitopes were retrieved using a Tissue Tek decloaking chamber (Biocare Medical) at 120.5°C for 15 min and allowed to cool slowly to room temperature. Pretreatment with hydrogen peroxide (3%) in phosphate buffered saline was used to reduce background.

To optimize staining conditions, selected cases representing residual, deidentified specimens from patients who had undergone diagnostic and therapeutic surgery for malignant (primary ovarian cancer, or prostate, breast or colorectal cancer as case controls) and non-malignant diseases (benign ovarian neoplasms, or benign prostate, breast or colorectal neoplasms as case controls) were obtained through the UNM Human Tissue Repository under an approved IRB protocol (SRC001-10). Colon cancers overexpressing Rac1 and Cdc42 served as a positive control and ovarian tumor tissue was comparatively evaluated against benign ovarian tissue.

Quantitative PCR (qPCR) of ovarian cancer cDNA arrays

qPCR analysis of Rho family GTPases was performed using Tissuescan Ovarian Cancer cDNA microarrays from Origene (Rockville, MD, cat# HORT301, HORT302, HORT303) and standard techniques (Table 3.3). qPCR was performed using Origene SYBR Green I master mix solution diluted to a final concentration of 1X with primers at a concentration of 0.33 μ M. PCR mix was added to each well of the microarray plate and incubated on ice for 15m to dissolve the cDNA. qPCR was conducted using a Bio-Rad iCycler (Hercules, CA) under the following conditions; 95° for 5m, 30 cycles of (95° for 15s, 60° for 30s, 72° for 1m), followed by melt curve analysis, hold at 4°. CT values obtained using iCycler software. Relative expression levels were determined using $\Delta\Delta$ CT values. Amplification utilized Qiagen Quantitect primers for *Cdc42* (Valencia, CA, QT01674442), *Rac1* (QT00065856), *RhoA* (QT00044723), and β -*actin* (Origene), and custom *Rac1b* forward primer, 5'-TCCGCAAACAGTTGGAGA-3', was coupled with *Rac1* reverse primer, 5'CTACATGTTTGCGGATAGGATAGGG-3', synthesized by Invitrogen (Carlsbad, CA). The identity of the PCR product as *Rac1b* was confirmed by sequence analysis.

Patients, study design and treatment

A Phase 0 trial investigating the use of postoperative ketorolac was reviewed and approved by the University of New Mexico Health Sciences Center Human Research Review Committee (clinicaltrials.gov - NCT01670799). Patients presenting with a new diagnosis of ovarian, fallopian tube or primary peritoneal cancer were screened for eligibility. Eligible women were at least 18 years old, an ECOG Performance Status <2

and had consented to a planned debulking surgery- Consent was obtained prior to surgery if primary eligibility was met. Secondary eligibility after surgery included confirmed histologic diagnosis of epithelial ovarian, fallopian tube or primary peritoneal cancer; optimal cytoreduction and placement of an intraperitoneal port for planned chemotherapy; adequate renal function and no postoperative complications prohibiting ketorolac use. Patients with known bleeding disorders or other contraindications to NSAID use were excluded.

Subjects received a single IV dose of Toradol® (15 or 30 mg based on the patient age and creatinine clearance) within the first 72 hours of surgery when all clinical safety parameters were met. Use of other NSAIDs during the trial were not permitted; however narcotic regimens were allowed for postoperative pain management. All study protocols were reviewed by an independent data and safety monitoring board. Baseline ascites samples were obtained at surgery. Subsequent peritoneal fluid samples were collected from the intraperitoneal port prior to dosing and at 1, 6, and 24 h after single dose ketorolac administration. Peripheral blood was collected at the same time points. Serum and peritoneal fluid were separated from cellular material via low speed centrifugation. Tumor cells were further purified on Ficoll gradients to remove red blood cells and negative selection with anti-CD45 beads to remove lymphocytes. The resulting tumor cell fractions were analyzed by flow cytometry for EpCAM and MUC16/CA125 (Fig 3.7).

High performance liquid chromatography

R- and S-enantiomers of ketorolac were analyzed by high performance liquid chromatography (HPLC) using published procedures (179). HPLC performed with a

50mm long 5 μ m silica guard column (Phenomenex, 03B-4053-N0) attached to a Partisil® 5 μ m ODS(3) 85 Å LC Column 150 x 4.6 mm (Phenomenex, 00F-0120-E0) followed by a Lux 5 μ m Cellulose-3 50 x 4.6mm in reverse phase (Phenomenex, 00G-4493-E0). The columns are equilibrated with acetonitrile/0.1% Formic acid in water (25:75) at a flow rate of 2ml/min. A standard curve of racemic ketorolac in water was generated based on an injection volume of 10 μ l and ketorolac was detected on a UV310 detector. 500 μ l serum (or ascites) samples were mixed with 200 μ l of 600mM sulfuric acid then diluted and mixed in 3ml diethyl ether. The organic layer was separated by centrifugation at 2500 rpm for 5 min using a Hermle Z440K. The organic layer was removed and evaporated to dryness, then reconstituted in 200 μ l mobile phase. Retention times for R-ketorolac and S-ketorolac were 5.1 min and 6.1 min respectively, and were validated against each individual enantiomer. The R-value for the standard curve of total ketorolac was 0.9997 and represented a concentration range that spanned established human serum concentrations (0.092 μ g/ml to 6.0 μ g/ml).

Analysis of GTPase activity

Two methods were used to assess GTPase activity in cells based on effector binding. Commercial GLISA kits from Cytoskeleton, Inc., analyzed Rac1 (Denver, CO, cat# BK-128), Cdc42 (BK-127) or RhoA (BK-124) per manufacturer instructions. Alternatively, Rac1, Cdc42 and RhoA activities were measured using a flow cytometric effector binding assay (123,180). Briefly, active Rac1 and Cdc42 GTPases in prepared cell lysates were quantified individually based on binding to GST-PAK1-PBD from Millipore (Bellerica, MA, cat#14-864) immobilized on GSH beads and use of specific

antibodies for bound GTPase detection. Antibodies used to quantify the amount of active (GTP-bound) GTPases captured on the beads are listed in Supplemental Methods. Fluorescence intensity (mean channel fluorescence, MCF) was measured by flow cytometry (Accuri C6). GTPase activity was calculated by $(\text{MCF of sample group} - \text{MCF of unstimulated group}) / \text{MCF of stimulated group}$. Equal amounts of protein were used for each assay.

Isolation of patient derived cells

To purify ovarian cancer cells from ascites, cells were recovered from ascites samples by low speed centrifugation at 1000 rpm. The cell pellets were gently resuspended and overlaid on a Ficoll (density 1.077 ± 0.001 g/ml; GE Healthcare 17-5442-02) to separate red blood cells from lymphocytes and tumor cells per manufacturer's instructions. Anti-CD45 beads (Life Technologies) were used to deplete lymphocytes and the resulting tumor cell fraction was analyzed visually and by flow cytometry. For flow cytometric analysis, cells suspended in phosphate buffered saline (PBS) were fixed with formaldehyde (2-4% final concentration) for 10 min, chilled for 20 min and then processed for immunostaining as described by Cell Signaling Technology {[http://www.cellsignal.com/contents/resources-protocols/flow-cytometry-protocol\(flow\)/flow](http://www.cellsignal.com/contents/resources-protocols/flow-cytometry-protocol(flow)/flow); webpage Accessed July 22, 2014}. Briefly, non-specific mAb binding to human Fc receptor was blocked by pretreatment for 10 min at room temperature with human Fc receptor binding inhibitor (14-916, Affymetrix eBioscience). Antibody staining was performed in PBS containing 0.5% BSA using $0.5-1 \times 10^6$ cells/assay for one hour at room temperature.

Tumor cell fractions were positive for EpCAM (detected with mAb against EpCAM clone BerEP4, Dako) and MUC16/CA125 (detected with a Cy5-labeled rabbit pAb directed against human MUC16/CA125; bs-0091R-Cy5, Bioss Antibodies) and negative for CD45 (detected with a PE-labeled rabbit pAb directed against human CD45/LCA, 12-9459, Affymetrix eBioscience) (Fig 3.7).

For analysis of GTPase activity in patient-derived cells, active RhoA was quantified based on binding to GST-Rhotekin (RT01, Cytoskeleton, Inc.). Antibodies specific for Cdc42 (sc-8401, Santa Cruz Biotechnology, Inc.), Rac1 (610650, BD Transduction Labs) or RhoA (26C4, sc-418, Santa Cruz Biotechnology, Inc.) and Alexa Fluor 488 donkey anti-mouse IgG (A21202, Life Technologies) were also used.

Retrospective patient outcomes review

A medical record review was conducted under institutional review board approval with a waiver of patient consent. Ovarian cancer patients were identified from the New Mexico Tumor Registry [NMTR] a member of the population-based Surveillance, Epidemiology, and End Results [SEER] Program of the National Cancer Institute (2). Inclusion criteria were as follows: invasive, epithelial ovarian cancer (any histology), age 40-79 years at diagnosis, years of diagnosis 2004–2006, and receipt of surgery at an Albuquerque, NM hospital (only three hospitals in the metropolitan area provide this level of surgery). Diagnosis years of 2004-2006 ensured at least 6 years follow-up (mortality followed through Dec 31, 2012) for each patient. We abstracted the surgical medical records for all analgesics and anesthesia medications used before hospital admission, during surgery and hospital stay, and given at discharge. Of the 138 potential

cases, 6 women did not undergo surgery because of advanced disease/severe comorbidities or desired palliative care only, 1 woman had her surgery in another state, 2 women died before surgery, and medical records were not located for 6 women, leaving 123 women in the final analysis.

Statistical analysis

qPCR findings for GTPase expression levels were analyzed using one-way ANOVA followed by Dunnett's multiple comparisons test to determine differences between ovarian cancer grade. IHC data was analyzed using one-way ANOVA followed by Tukey's post test to determine significant differences between groups. Data obtained from patient fluid and cell samples was analyzed as a repeated measure ANOVA followed by Dunnett's multiple comparisons test to determine significant differences between groups. For the retrospective medical record review, information from the medical record was merged with information from the NMTR for final analysis. Clinical and treatment characteristics of patients who did and did not receive peri-operative ketorolac were compared with chi-square tests and t-tests. In a preliminary, crude analysis the Kaplan-Meier method was used to estimate the survival probabilities. The difference in survival based on receipt of peri-operative ketorolac was examined using the stratified log-rank test to adjust the effect of a single categorical factor such as age group, AJCC stage, etc. Because this was an observational study and not a randomized controlled trial, the final analysis was based on a Cox proportional hazards model to adjust for clinical and treatment characteristics that may have differed between those who did and did not receive peri-operative ketorolac. We estimated the hazard ratio (HR) for

ovarian cancer-specific mortality comparing those who did and did not receive peri-operative ketorolac while adjusting for age at diagnosis (<50, 50-64, ≥65) AJCC stage (I, II, III, IV), completion of chemotherapy as planned (yes, no), and receipt of neoadjuvant chemotherapy (yes, no). Based on the Cox proportional hazards regression, an example survival plots are presented in Figs 3.9-3.13.

Table 3.1

Table 3.1. Hazard ratios (HRs) for ovarian cancer specific mortality for each characteristic adjusted for the other characteristics in the table.			
Characteristic	Number	Hazard Ratio (95% Confidence Interval)	p-value**
Peri-operative ketorolac			.013
No	106	1.00 (referent)	
Yes	17	0.32 (0.11 – 0.90)	
AJCC* stage			.048
I	26	1.00 (referent)	
II	11	0.50 (0.11 – 2.39)	
III	57	2.14 (0.96 – 4.80)	
IV	29	1.60 (0.67 – 3.80)	
Age (years)			.054
< 50	36	1.00 (referent)	
50 – 60	55	2.39 (1.13 – 5.01)	
60 +	32	1.74 (0.77 – 3.93)	
Neoadjuvant chemotherapy			.040
No	101	1.00 (referent)	
Yes	22	1.99 (1.07 – 3.73)	
*: AJCC = American Joint Committee on Cancer			
**: Likelihood Ratio Test p-value			

Table 3.2

Table 3.2. Patient Characteristics for IHC Microarrays OV1005 and OV8010		
Age [#]	46.6 +/- 13.7 (std. dev)	
Stage I [#]		12
	A	5
	B	5
	C	4
Stage II [#]		21
	A	13
	B	6
	C	3
Stage III [#]		1
	C	31
Stage IV [#]		11
Stage undetermined [#]		51
Normal stroma		20
Benign/borderline		25
Grade - Low* (1 [#])		13
Grade - Intermediate* (1-2, 2 [#])		7
Grade - High* (2, 2-3, 3 [#])		98
<p>*Diagnoses by board certified pathologist with gynecologic pathology specialization were as follows: Clear cell carcinoma (4); endometrioid carcinoma (13); endometrioid neoplasm (5); mucinous carcinoma (4); mucinous neoplasm (9); mucinous cystadenoma (5); normal stroma only-no epithelia (20); papillary serous carcinoma (78); serous neoplasm (5); serous cystadenoma (4); undifferentiated carcinoma (16). There was 77% agreement with [#]BioMax specification sheet, differences were confined to ID of rarer subtypes (endometrioid, clear cell, mucinous, transitional and serous). Samples included in analysis: 163 of 180 total (9% were excluded due to poor staining at edge of slide or no neoplasm in the section).</p>		

Table 3.3

Table 3.3 - Patient Characteristics for cDNA Microarray		
Age	57.26 +/- 14.85 (st. dev)	
Stage I	A	20
	B	8
	C	10
Stage II	A	4
	B	9
	C	4
Stage III	A	15
	B	17
	C	26
Stage IV	A	10
Grade Not Reported		10
Grade I		9
Grade II		32
Grade III		60
Grade IV		9
<p>Diagnoses were as follows: Carcinoma of Ovary (2); Carcinoma of ovary, endometrioid (6); Carcinoma of ovary, papillary serous (8); Carcinoma of ovary, clear cell (1); Adenocarcinoma of ovary, endometrioid (23); Adenocarcinoma of ovary, papillary serous (32); Adenocarcinoma of ovary, serous (28); Adenocarcinoma of ovary, metastatic (2); Adenocarcinoma of ovary, mucinous (4); Adenocarcinoma of ovary, clear cell (5); Tumor of ovary, borderline (2); Tumor of ovary, papillary serous, borderline (2); Tumor of ovary, serous, borderline (5). These microarray plates consisted of 19 normal, 9 Grade I, 32 Grade II, 60 Grade III, 9 Grade IV, and 10 grade not reported patients. Patients with grade not reported were not included in grade analysis.</p>		

Table 3.4

Table 3.4 - Ketorolac enantiomer concentration in serum or peritoneal fluids.		
Sample	[R] μM	[S] μM
Serum 1h	3.97	1.65
Serum 6h	1.44	0.33
Serum 24h	0.40	0.02
Ascites 1h	0.5	0.33
Ascites 6h	0.98	0.32
Ascites 24h	0.27	0.03

Figure Legends

Figure 3.1 – Overexpression of Rac1 and Cdc42 protein in ovarian cancer

specimens. A-C Representative images of ovarian serous cancer tissue are shown. Clinical characteristics of the samples in the array are provided in Supplemental Table S1. Magnification 200X. Scale bar 20 μ m. **A** Hematoxylin/Eosin staining of normal ovarian tissue (H&E). **B-C** Samples were stained with antibodies against Rac1 or Cdc42 and avidin/biotin horse radish peroxidase enzyme complex. Controls and tissue samples were developed for identical times. **D-E** Tissue pathology and staining evaluated by board certified pathologist with gynecologic pathology specialization (Dr. Lesley Lomo, Dept of Pathology, UNM) and statistical analyses by statistician (Dr. Ed Bedrick, Dept of Biostatistics, University of Colorado). For Rac1 one way non-parametric ANOVA ($p=0.0087$) and Tukey's post-test shows normal stroma vs. intermediate to high grade carcinoma $p<0.05$ with all other comparisons non-significant. For Cdc42 one way non-parametric ANOVA ($p=0.0001$) and Tukey's post-test shows normal stroma and benign to borderline tumor vs. intermediate to high grade carcinoma $p<0.05$ with all other comparisons non-significant.

Figure 3.2 – Expression of constitutively active Rac1b mRNA is elevated in ovarian

cancer specimens. Tissuescan ovarian cancer cDNA microarrays (Origene) were amplified using primers against *Rac1*, *Rac1b*, *Cdc42*, *RhoA*, and β -actin as described in methods. As per the manufacturer's description, patients with endometriosis, leiomyoma of myometrium, follicular cysts, abscesses, or secretory endometrium, but otherwise healthy ovarian tissue, were considered normal ($n=19$). Tissues defined as low grade have

a FIGO score of 1 (n=19) or 2 (n=32). Tissues considered high grade have a FIGO score of 3 (n=60) or 4 (n=9). The cDNAs of 10 patients were excluded due to a lack of grade information. Clinical characteristics of the samples in the array are provided in Supplemental Table S2. Groups were compared to normal using a two-tailed t-test, and significant increase in *Rac1b* was detected. * indicates significance is $p \leq 0.05$. Serous only, analysis by grade is reported in Supplemental Figure S1.

Figure 3.3 – Expression of Rho-family GTPases in primary patient cDNA samples

analyzed by grade for serous cancer only. Tissuescan ovarian cancer cDNA microarrays (Origene) were amplified using primers against *Rac1*, *Rac1b*, *Cdc42*, *RhoA*, and β -actin as described in methods. This analysis does not include endometrioid tissue. As per the manufacturer description, patients with leiomyoma of myometrium, follicular cysts, abscesses, or secretory endometrium, but otherwise healthy ovarian tissue, were considered normal (n=11). Data from two normal patients were not included due to Grade 3 carcinomas of adjacent tissues. Tissues are grade I (n=2), grade II (n=24), grade III (n=48), or grade IV (n=9). The cDNA of 10 patients were excluded due to a lack of grade information. Groups were compared to normal cDNA using a two-tailed t-test, * indicates significance is $p \leq 0.05$.

Figure 3.4 – Ketorolac distributes to peritoneal fluids and is enriched in the R-

enantiomer. A Ascites samples were obtained at cytoreductive surgery and one to three days after surgery patients received a single dose of either 15 mg or 30 mg of clinical racemic ketorolac. Blood and peritoneal fluid from patients were collected prior to dosing

(T=0), and at 1 hour, 6 hours, and 24 hours after dosing as depicted by the arrows. **B-C** Ketorolac enantiomers (R and S) were measured in blood and peritoneal fluids using HPLC. **B** Total ketorolac levels in sera and peritoneal fluids. **C** The levels of each ketorolac enantiomer (R or S) at each time point in sera and peritoneal fluids were measured. Concentration conversion to micromolar in serum and peritoneal fluids is provided in Table 3.3. Administered drug is a 1:1 ratio of R to S (Fig 3.5), but S-ketorolac is eliminated more rapidly than R-ketorolac leading to a ratio favoring the R-enantiomer in both serum and peritoneal fluids. The R-value for the standard curve used to calculate the ketorolac concentrations was 0.9997 and represented a concentration range that spanned established human serum concentrations [0.092 µg/ml to 4.0 µg/ml; 3.0 µg/ml= 10 µM).

Figure 3.5 – Racemic distribution of clinical drug. To confirm that this apparent shift in racemic ratio was not due to either 1) unequal distribution of the racemates in the administered drug or 2) differential extraction of each racemate from serum proteins, we conducted control experiments. **A** Racemic distribution of ketorolac enantiomers of the clinically administered drug was confirmed by HPLC. **B** Clinical grade ketorolac incubated with human serum (shown) and ascites fluid (not shown, but identical results) at 37°C for 1 hr and the samples were then processed as for samples obtained from patients. The equal distribution of R- and S-ketorolac in the extracted control sample indicates that the difference in enantiomer composition in patient samples is not due to differential extraction from serum proteins during sample processing and more likely

represents a pharmacokinetic parameter such as preferential binding of S-ketorolac to tissue proteins.

Figure 3.6 – GTPases are activated in patient ascites and inhibited by ketorolac

administration *in vivo*. A GTPase activity and target inhibition in patient derived cells.

GLISA PAK-effector binding was used to individually detect activated Rac1-GTP or Cdc42GTP in tumor cells isolated from ovarian cancer patient ascites. Purified GTP-loaded GTPases were used to calculate ng GTP-bound GTPase in the patient sample.

Unpaired, two-tailed t-tests showed samples in culture for 48 h were statistically different from fresh ascites samples for both Rac1 and Cdc42 ($p=0.0109$). The levels of active

GTPase declined sharply with 48 h in culture indicating that soluble factors in the ascites serve to upregulate Rac1 and Cdc42 GTPase activities. **B-C** Rac1 GTPase target

inhibition following administration of racemic ketorolac to ovarian cancer patients post-surgery. Cells isolated from patient ascites samples post-surgery were assayed for active

Rac1 or Cdc42 using a flow based effector binding assay. Patient diagnoses were all stage III, high grade ovarian serous or papillary serous carcinoma, with one mixed serous

endometrioid carcinoma and one suspected primary peritoneal carcinoma (Pt 20, 24, 35,

39, 43). Fluorescence readings were normalized to the 0 h time point drawn immediately prior to ketorolac administration. For Rac1, one way non-parametric ANOVA ($p=0.0009$)

and Bonferroni multiple comparisons test *indicates $p\leq 0.05$, ** indicates $p\leq 0.01$ for: 0 h vs 6 h (**); 0 h vs 24 h (**); 1 h vs 6 h (*); 1 h vs 24 h (**). Differences between 0 h vs.

1 h and 6 h vs. 24 h were non-significant. For Cdc42, one way non-parametric ANOVA ($p=0.0250$) and Bonferroni multiple comparison test $p<0.05$ for 0 h vs 24 h (*) was

significant and all others were non-significant. RhoA was not responsive to ketorolac (Fig 3.8).

Figure 3.7 – Purified Ovarian Tumor Cells Express EpCam and MUC16/CA125.

Ovarian tumor cell identification by flow cytometry using patient ascites samples from three individuals (designated 29, 30, and 35). Tumor cells were purified from ascites using Ficoll gradients to remove red blood cells and CD45 microbead negative selection to remove leukocytes. The resulting cells (gated as R3) were negative for CD45 and positive for EpCAM and MUC16/CA125. Marker analyses were tracked by flow cytometry on a Becton Dickinson FACScalibur Flow Cytometer.

Figure 3.8 – RhoA activity is insensitive to ketorolac treatment.

A-B RhoA GTPase target inhibition assayed by quantification of active RhoA using a flow based Rhotekin effector binding assay. **A** Patient derived tumor cells purified from ascites fluids at the time of debulking surgery were treated *in vitro* for 1 h with 10 μ M R-ketorolac, S-ketorolac or CID2950007—a Cdc42 selective inhibitor (19, 20). Tumor cells incubated with 0.1% DMSO served as a negative control. **B** Results of administration of racemic ketorolac to ovarian cancer patients post-surgery. Cells isolated from patient ascites samples post-surgery were assayed as in (A). Patient diagnoses were stage II-III, high grade ovarian serous or papillary serous carcinoma, with one suspected primary peritoneal carcinoma (Pt 20, 21, 43). Fluorescence readings were normalized to 0.1% DMSO control or the 0 h time point drawn immediately prior to ketorolac administration.

One way non-parametric ANOVA and Bonferroni multiple comparison test showed no statistically significant differences between either the *ex vivo* or the *in vivo* samples.

Figure 3.9 – Example Survival among ovarian cancer patients with and without perioperative ketorolac. Cox proportional hazards regression was used to estimate ovarian cancer specific survival probabilities for women who did (dashed line, 17 women) and did not (solid line, 92 women) receive ketorolac among ovarian cancer cases with AJCC Stage III cancer, 5060 years of age at diagnosis, no neoadjuvant chemotherapy and completed chemotherapy as planned (overall adjusted Hazard Ratio = 0.30, 95%CI = 0.11 – 0.88, likelihood ratio test p-value = 0.013).

Figure 3.10 – Survival estimates based on Cox-regression for Stage I (AJCC) with completion of chemotherapy. Cox proportional hazards regression was used to estimate ovarian cancer specific survival probabilities for women who did (dashed line) and did not (solid line) receive ketorolac among ovarian cancer cases with AJCC Stage I cancer, sorted by age group and +/- neoadjuvant chemotherapy.

Figure 3.11 – Survival estimates based on Cox-regression for Stage II (AJCC) with completion of chemotherapy. Cox proportional hazards regression was used to estimate ovarian cancer specific survival probabilities for women who did (dashed line) and did not (solid line) receive ketorolac among ovarian cancer cases with AJCC Stage II cancer, sorted by age group and +/- neoadjuvant chemotherapy.

Figure 3.12 – Survival estimates based on Cox-regression for Stage III (AJCC) with completion of chemotherapy. Cox proportional hazards regression was used to estimate ovarian cancer specific survival probabilities for women who did (dashed line) and did not (solid line) receive ketorolac among ovarian cancer cases with AJCC Stage III cancer, sorted by age group and +/- neoadjuvant chemotherapy.

Figure 3.13 – Survival estimates based on Cox-regression for Stage IV (AJCC) with completion of chemotherapy. Cox proportional hazards regression was used to estimate ovarian cancer specific survival probabilities for women who did (dashed line) and did not (solid line) receive ketorolac among ovarian cancer cases with AJCC Stage IV cancer, sorted by age group and +/- neoadjuvant chemotherapy.

Figure 3.1

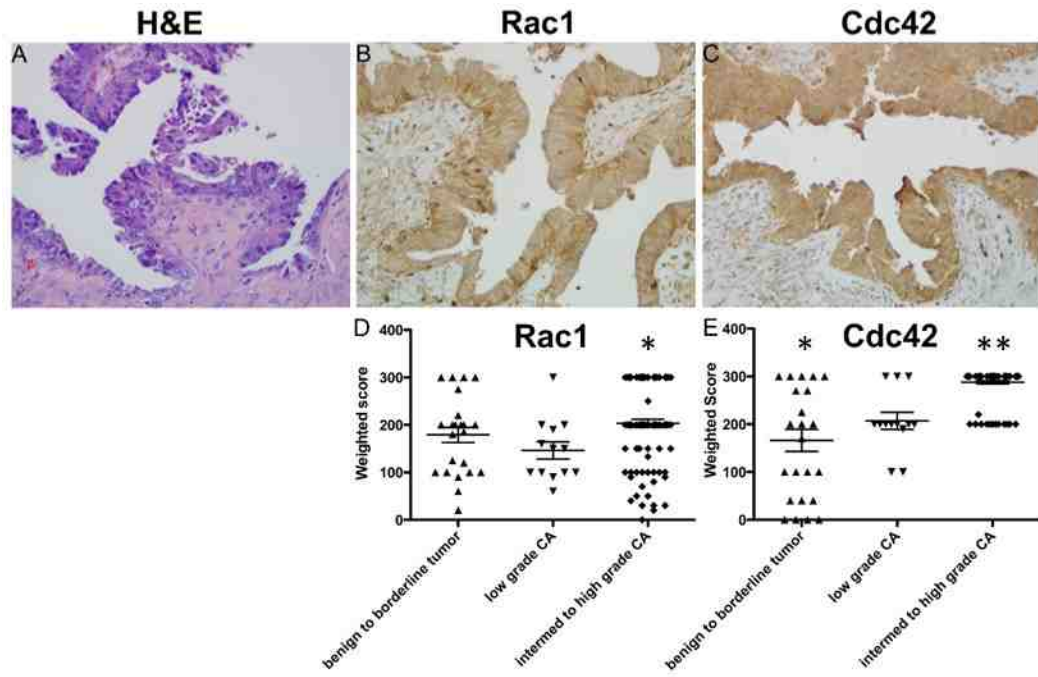


Figure 3.2

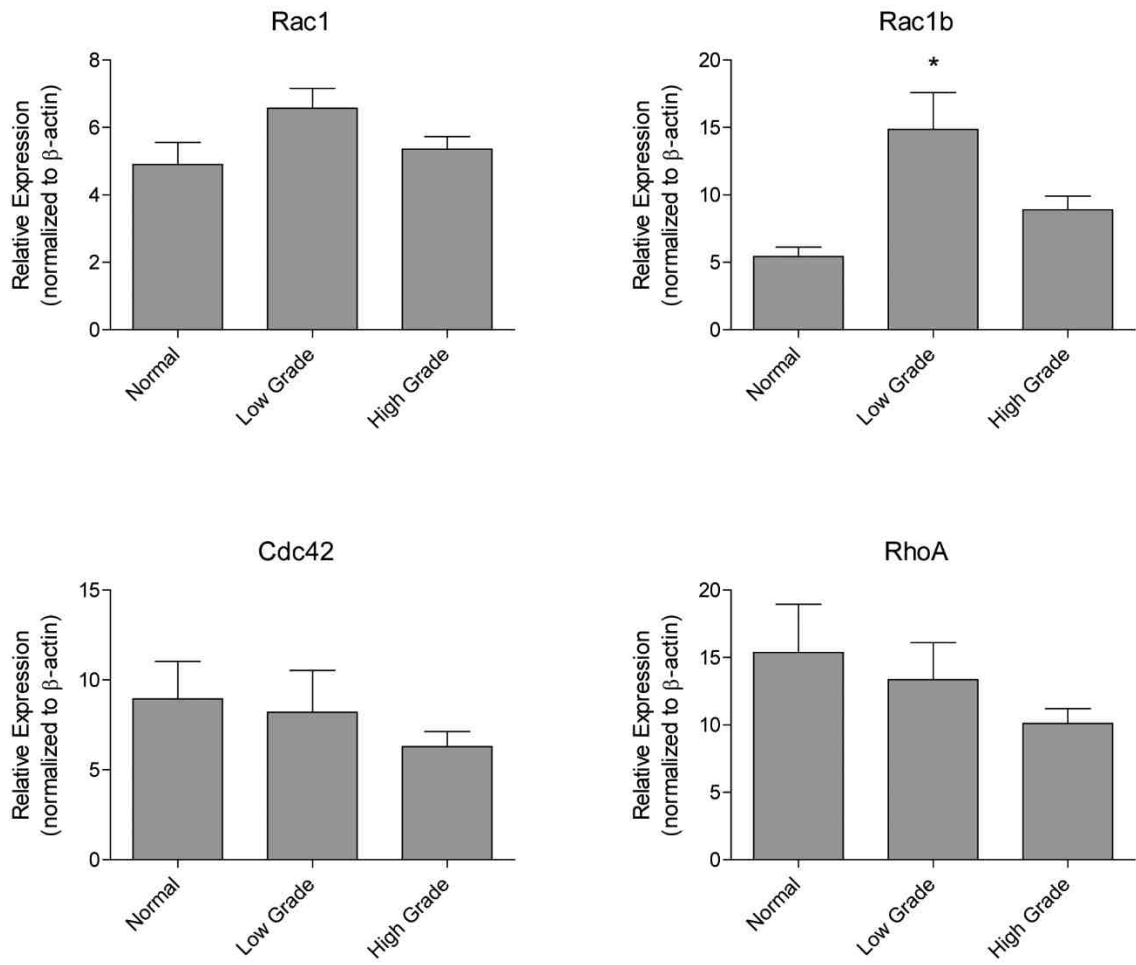


Figure 3.3

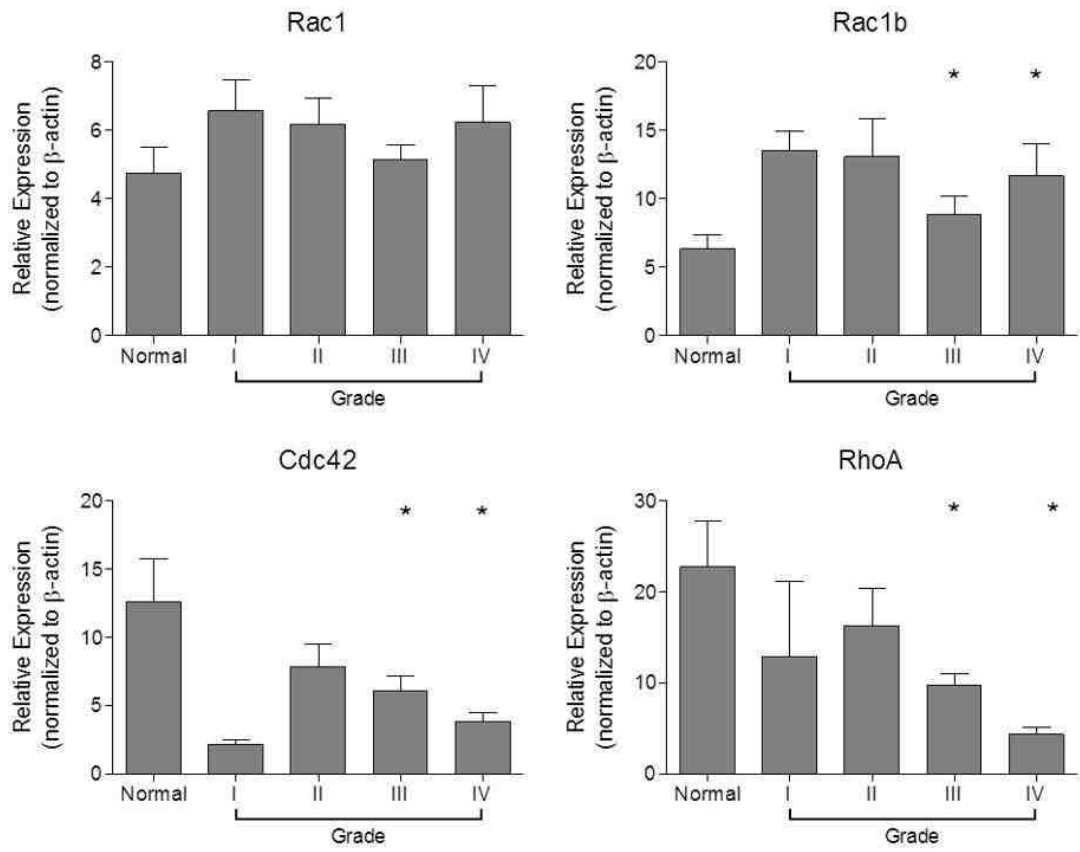


Figure 3.4

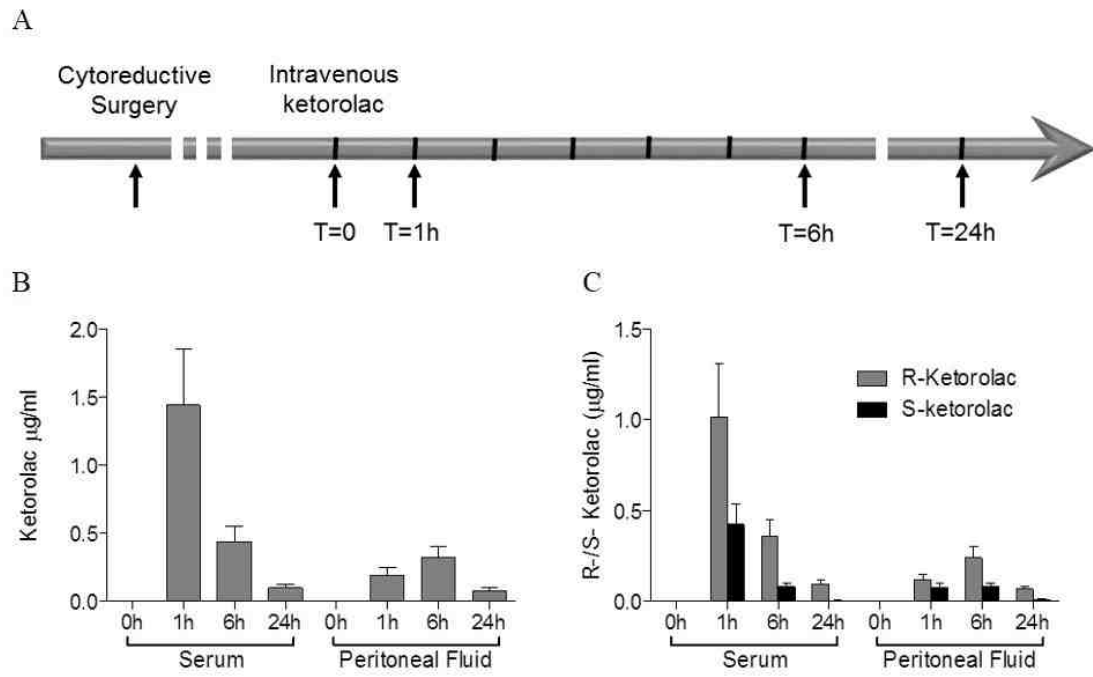


Figure 3.5

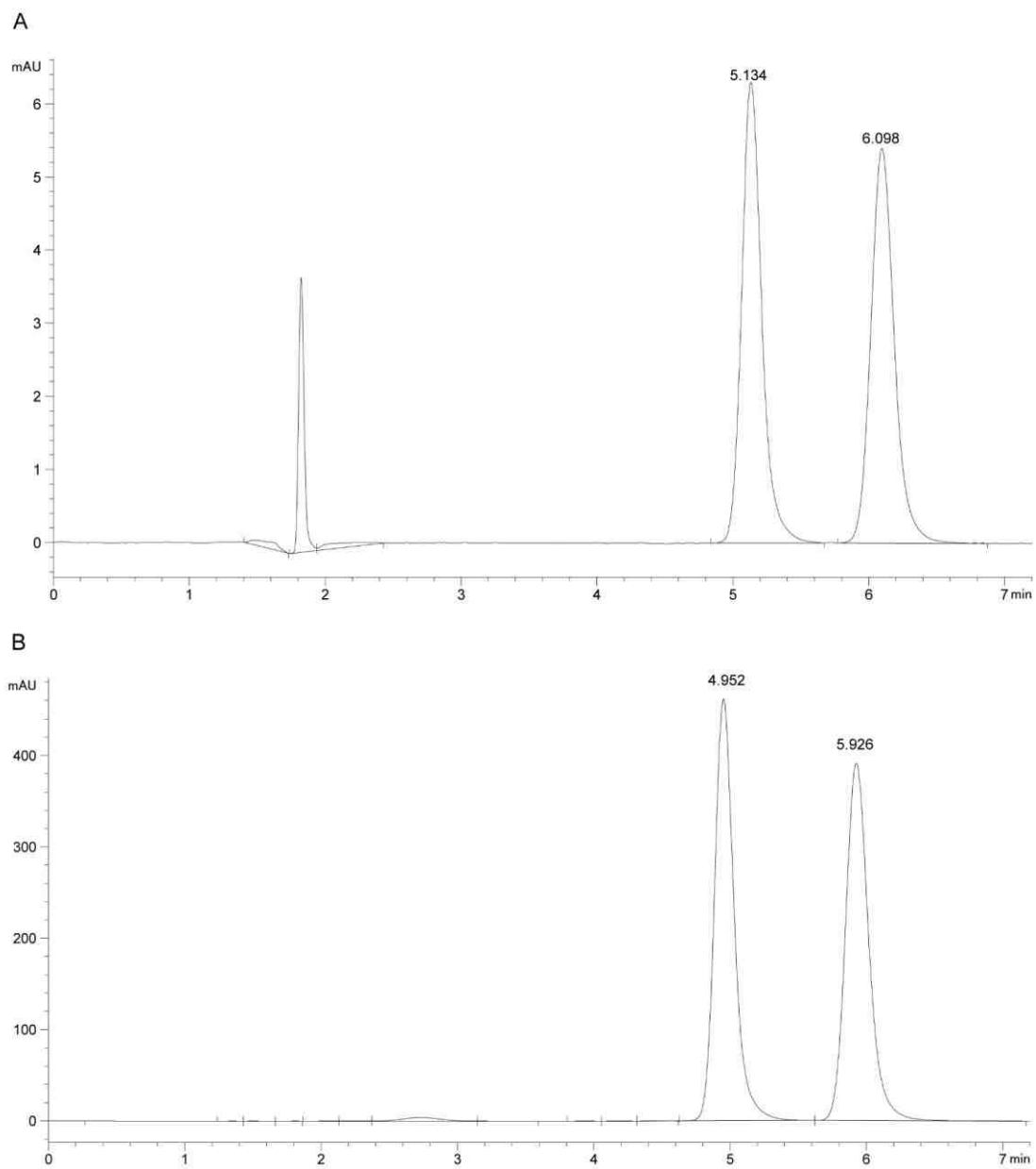


Figure 3.6

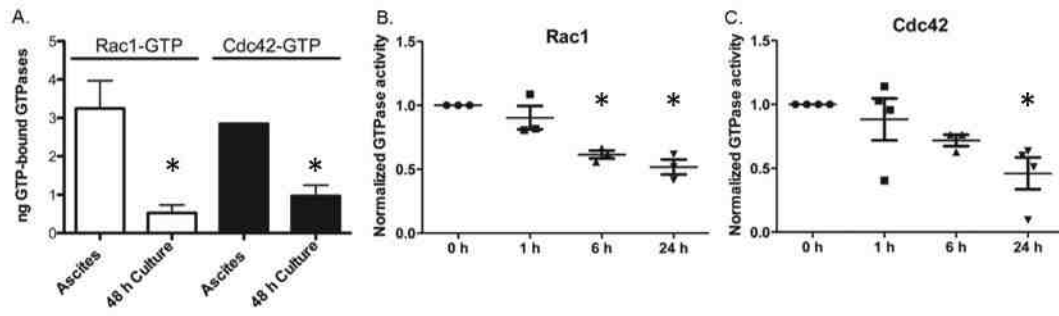


Figure 3.7

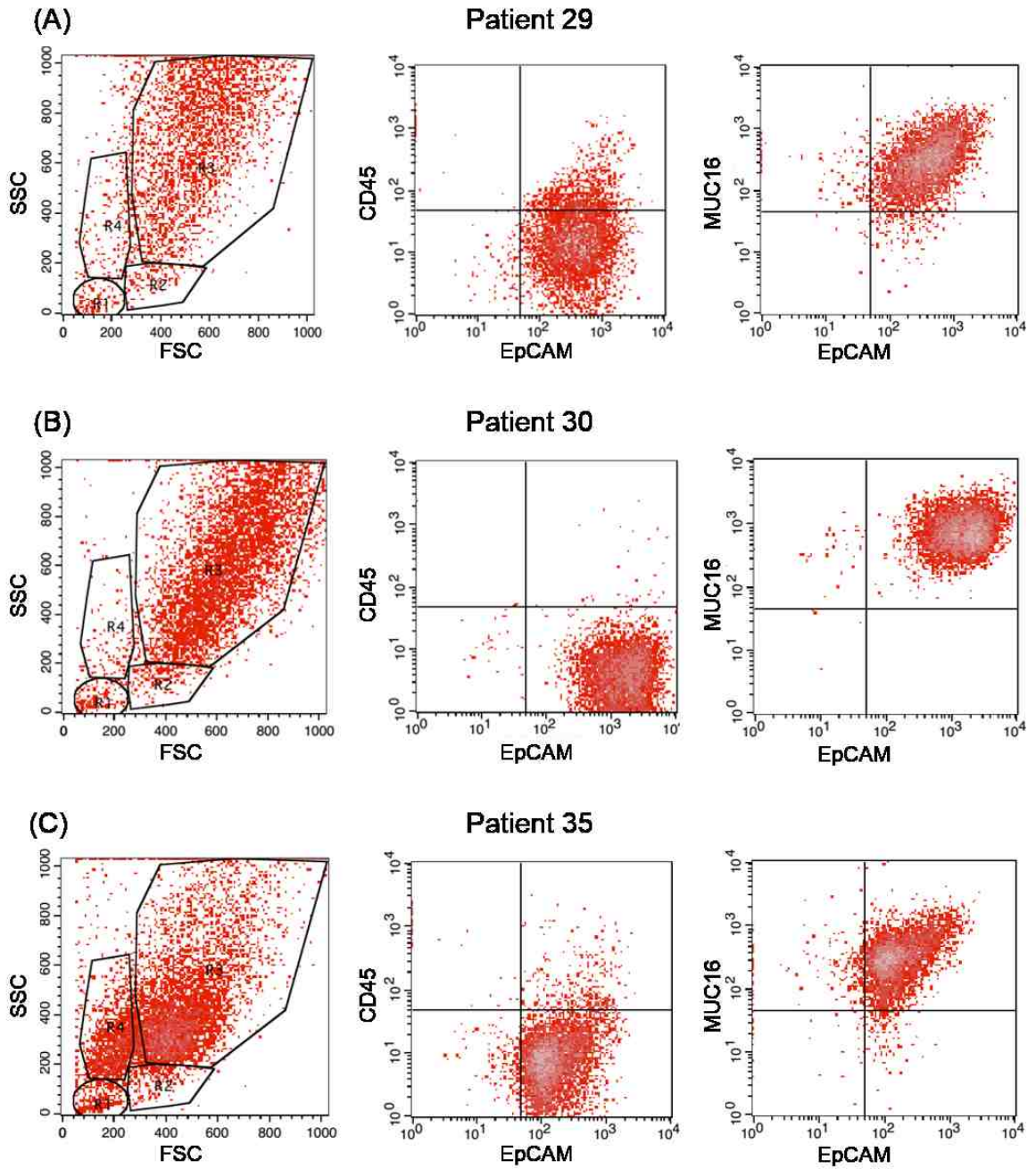


Figure 3.8

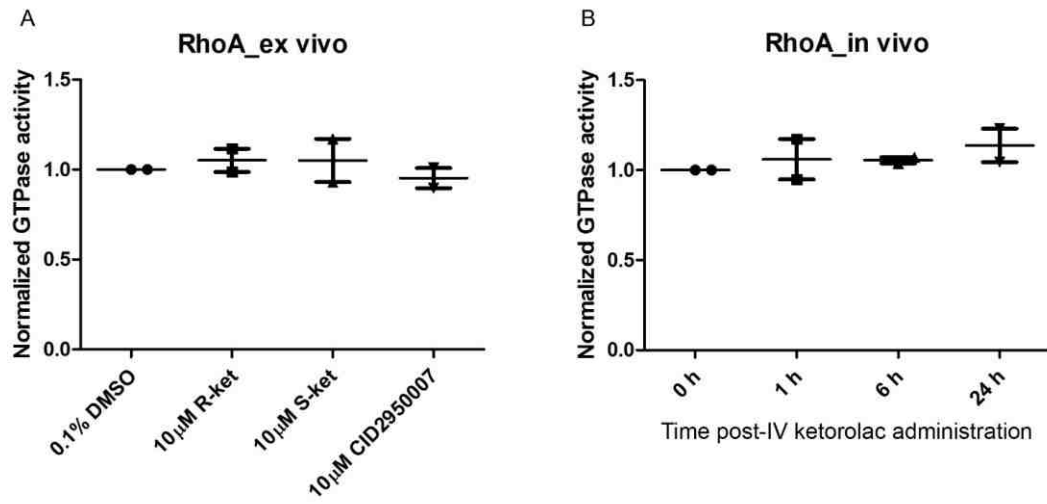


Figure 3.9

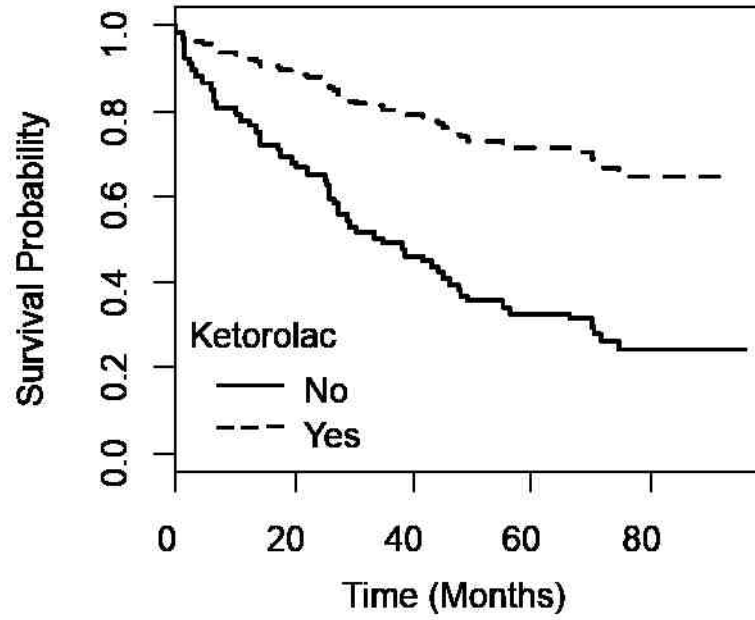


Figure 3.10

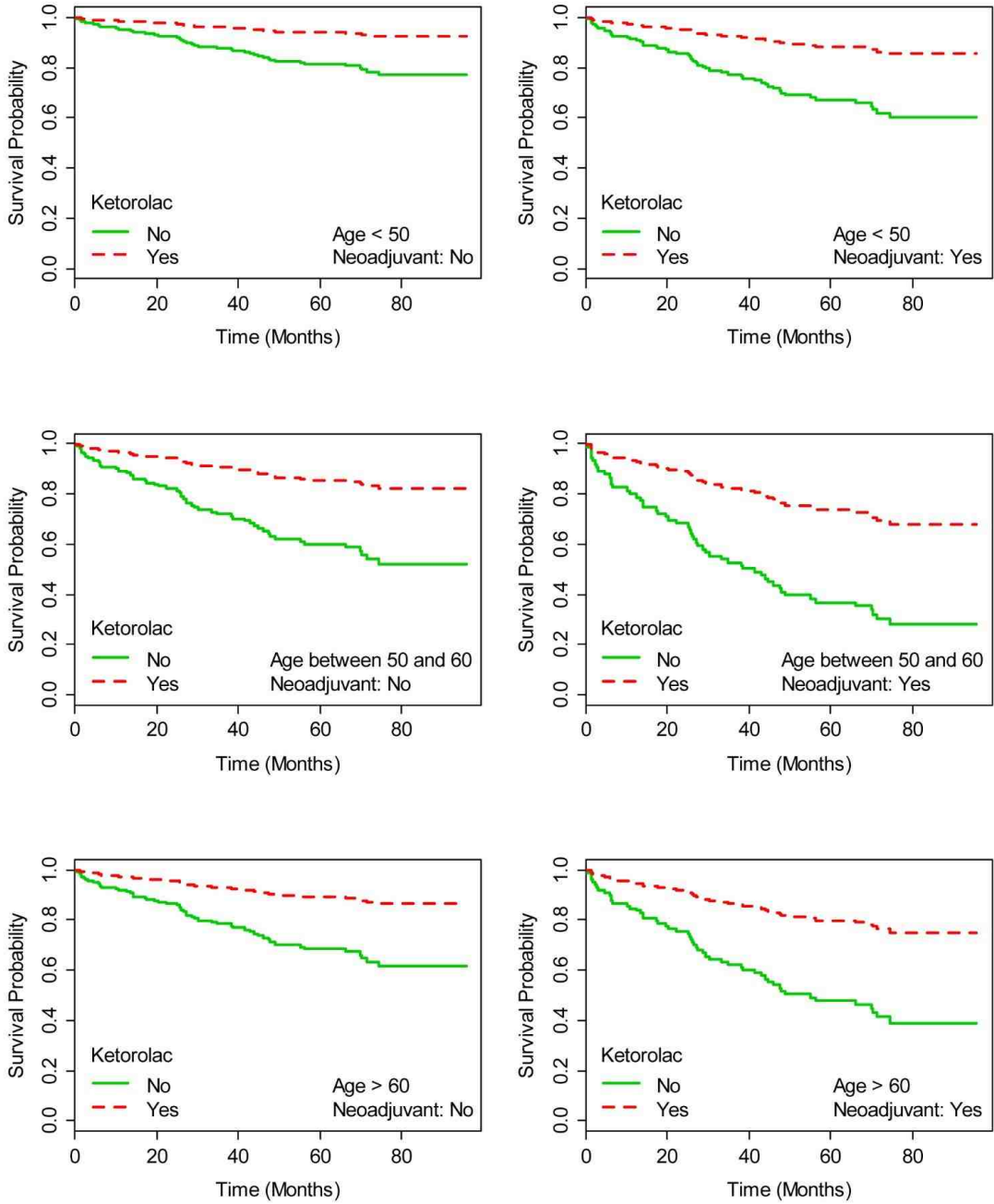


Figure 3.11

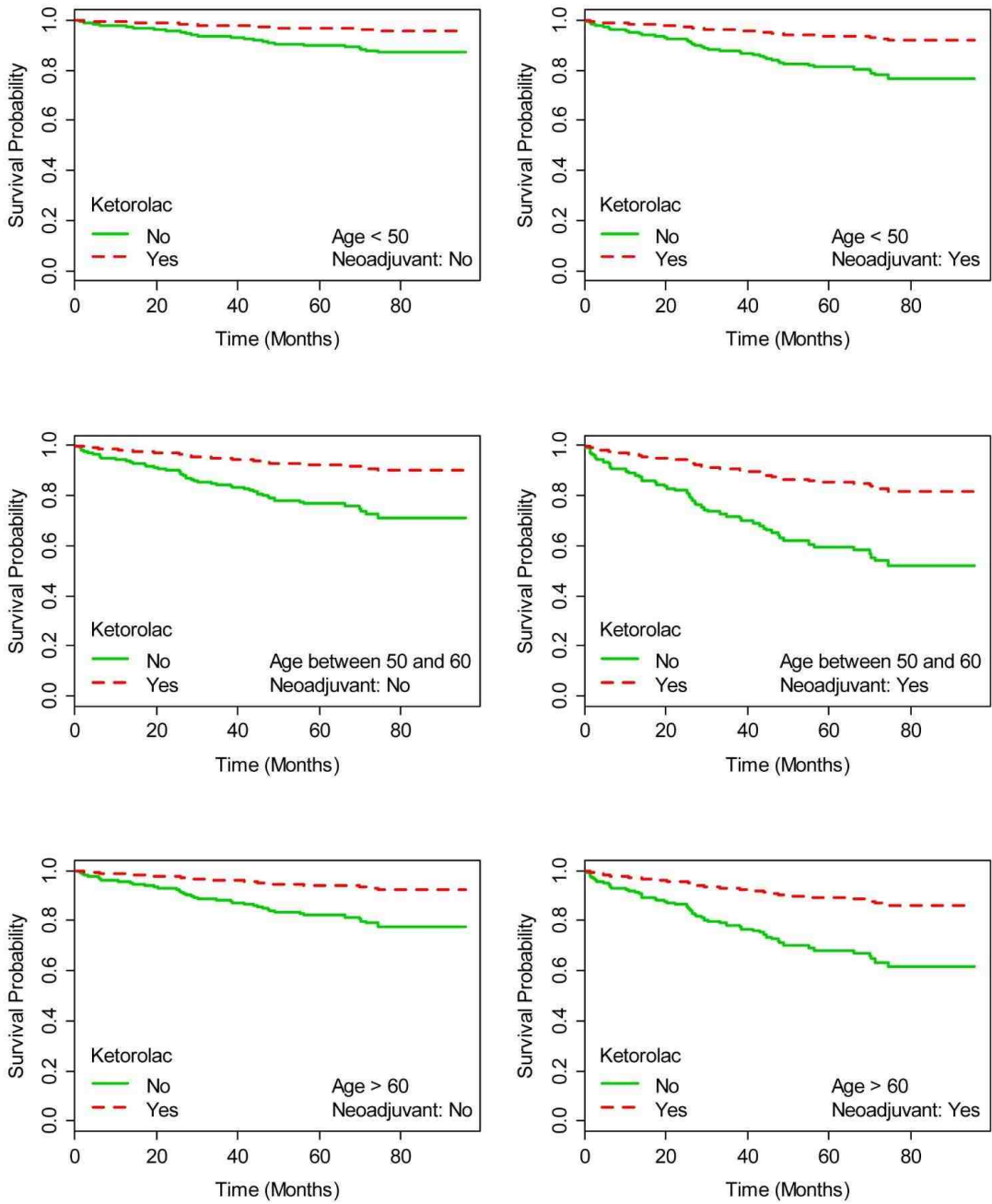


Figure 3.12

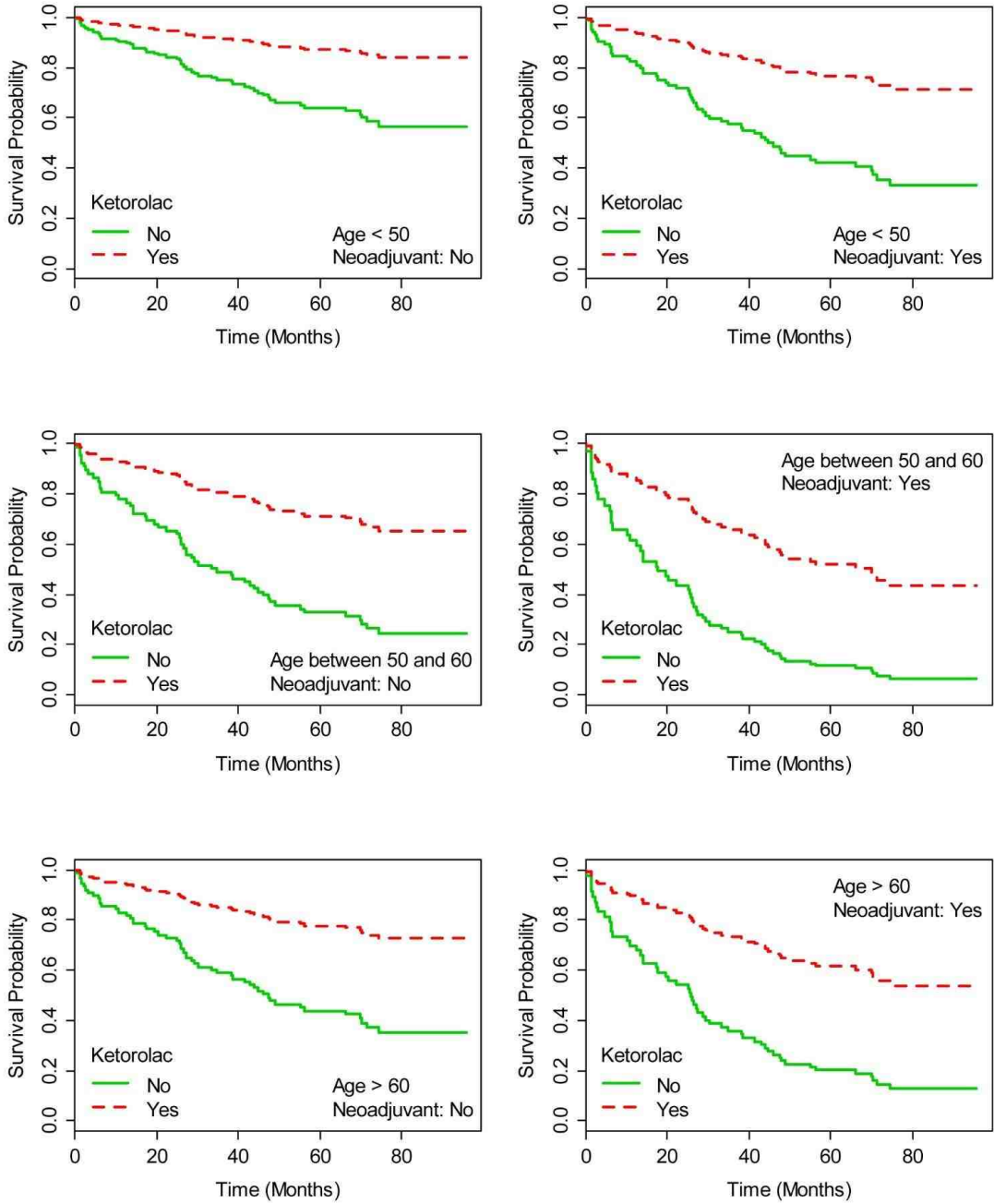
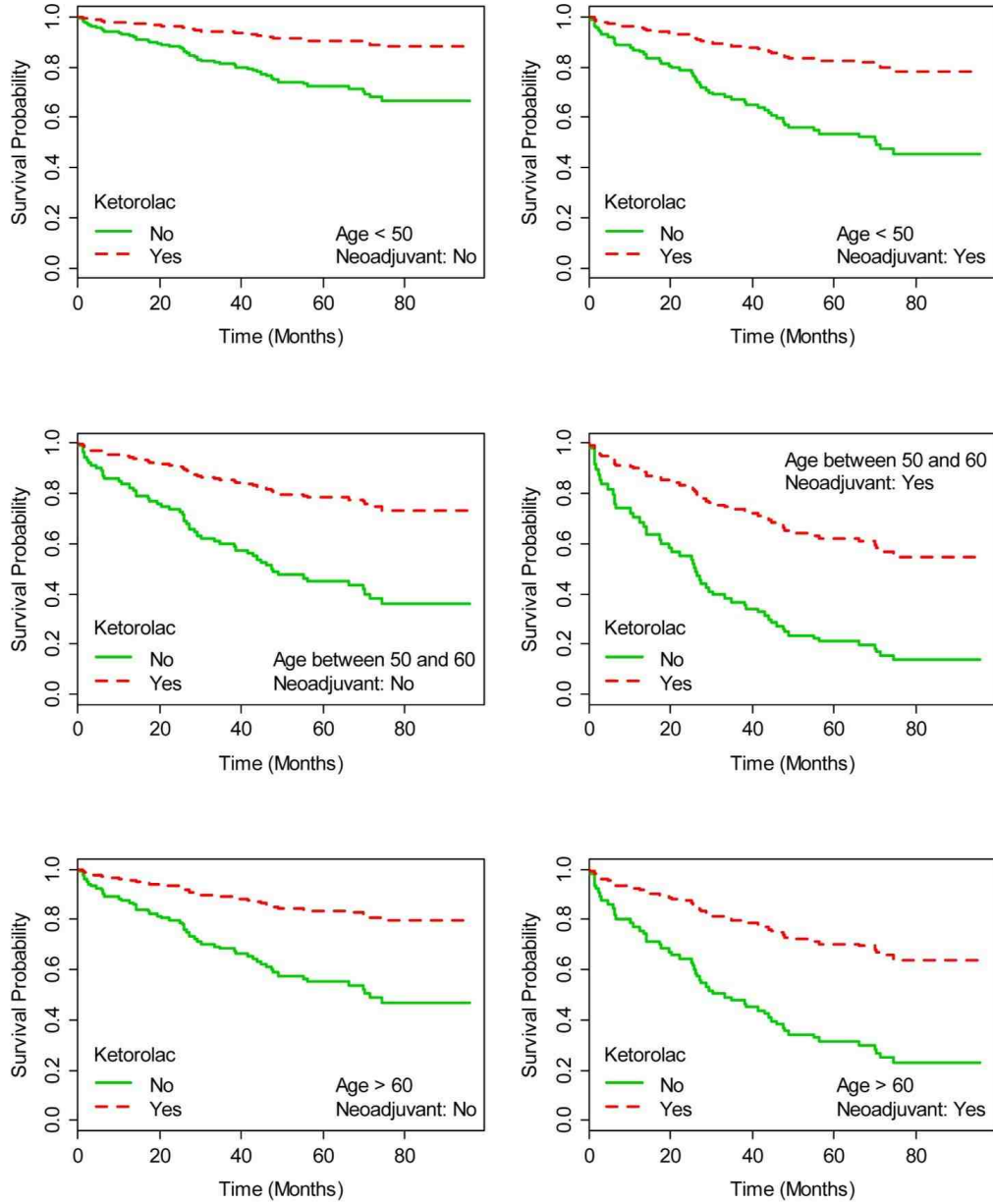


Figure 3.13



Chapter 4

Project Summary

4.1 Overview

As the leading cause of death due to gynecological malignancy, ovarian cancer is a significant health problem in the United States (1-3). Advanced stage diagnosis, limited treatment options, high rates of recurrence, and refractory disease contribute to the high mortality rate, which has remained constant since the 1970s (2,3). Treatment for ovarian cancer involves cytoreductive surgery and a recovery period followed by chemotherapy to combat any residual disease. Chemotherapeutic drugs for the first-line treatment of ovarian cancer are limited to platinum based compounds and taxane derivatives. While these treatments are beneficial to the patients initially, recurrence is common (2,3,5) With these challenges in mind, there is a need to develop therapies that will improve patient survival.

Recently, collaborative work between Drs. Angela Wandinger-Ness and Larry Sklar (UNM) identified a single R-enantiomer of the chiral NSAID naproxen as having activity against the Rho family GTPases Cdc42 and Rac1 (123). Further *in silico* modeling performed by Dr. Oleg Ursu (UNM) predicted that the single R-enantiomer of the chiral NSAID ketorolac would have similar activity against Cdc42 and Rac1 (123). There is evidence that the use of NSAIDs can provide survival benefit in colon and breast cancer patients (126, 143) and that ketorolac specifically improves 5 year survival rates in breast cancer patients (126, 143). Therefore, ketorolac was pursued as a candidate option for ovarian cancer patients.

In this project, I demonstrated that the Rho family GTPases Cdc42 and Rac1 are viable therapeutic targets in the treatment of ovarian cancer. Additionally, I was able to show that the use of the R-enantiomer of the NSAID ketorolac inhibits cellular adhesion and migration events regulated by Cdc42 and Rac1. Finally, in a small phase 0 clinical study, I was able to determine that the NSAID ketorolac is distributed to the peritoneal cavity in sufficient concentrations to inhibit Cdc42 and Rac1.

4.2 Ras GTPases in Cancer

Perhaps the most well studied GTPases in cancer are mutations of the Ras family of proto-oncogenes (79). Because Ras GTPases function as nodes in a number of different cell signaling pathways involved in tumorigenesis, they make promising targets for therapeutics. In addition to Ras, aberrant signaling of a number of other Ras family GTPases have been identified in cancer (58,76). Cdc42 is reported to be overexpressed in multiple cancer types, and levels of expression appear to drive disease progression (58,76). Similarly, Rac1 has been reported to be overexpressed in multiple cancer types, and has been linked to a number of cellular events related to cancer metastasis (58,76). Additionally, the constitutively active splice variant Rac1b has been reported in breast, colon, and lung cancer (59,61,68). Due to these findings, it was important to examine these GTPases in the context of ovarian cancer.

IHC performed by Elsa Romero and Dr. Lesley Lomo determined that Cdc42 and Rac1 are overexpressed at the protein level in ovarian cancer (Fig 3.1). The increasing overexpression of Cdc42 with advanced disease is consistent with findings in testicular (53) and breast (74) cancers. Cdc42 is necessary for directed migration (87) and is known

to be involved in collective cell migration (87,88). Rac1 overexpression is well documented in cancer (76,163,164). While there was no change in the levels of *Cdc42* or *Rac1* mRNA, I identified mRNA expression of the splice variant *Rac1b* in low grade tumors when compared to normal tissue (Fig 3.2). *Rac1b* levels could not be determined in tissue sections as there are no validated antibodies available. *Rac1b* has increased nucleotide exchange ability, decreased GTPase activity, increased affinity for GTP, reduced interaction with regulators and enhanced binding to effectors. It has also been reported to have preferential binding to NF- κ B (181). With preferential binding to NF- κ B, it is possible that *Rac1b* is driving gene transcription contributing to EMT, increasing cell migration, and cell adhesion. Because *Rac1b* is largely tumor specific, it is likely that ascites formed during early tumor development contains growth factors that lead to the expression of *Rac1b*. The expression of *Rac1b* mRNA in the low grade ovarian cancer suggests that it is contributing to tumor development and leads to metastatic events characteristic of advanced disease (5). These data support the hypothesis that *Cdc42* and *Rac1* are required for metastatic spread and are valid therapeutic targets, as they facilitate cell adhesion and migration to distant secondary sites within the peritoneal cavity.

4.3 Effect of Ketorolac on Ovarian Cancer Cells in Culture

The initial objective of this project was to examine the cellular effects of ketorolac on ovarian cancer cells in culture (Table 4.1) and *in vivo* (Table 4.2). It has been reported that ketorolac can induce apoptosis, inhibit proliferation or induce cell cycle arrest in osteoblasts and chondrocytes (155,156). I observed that neither R-/S-

Table 4.1

Table 4.1 – Summary of the effect of Cdc42 and Rac1 inhibition on SKOV3ip ovarian cancer cells					
	ML141	NSC23766	R-/S-ketorolac	R-ketorolac	S-ketorolac
Cytotoxicity	NC	NC	NC	NC	NC
Proliferation	↓	↓	NC	NC	NC
Migration	↓	↓	↓	↓	↓
GTPase expression	NC	NC	↓	↓	NC
Organotypic Adhesion	↓↓	↓↓			
Organotypic Spreading	↓	↓	↓	↓	↓

NC = No Change, ↓ = decrease, number of arrows indicates level of change

ketorolac nor single enantiomer ketorolac is cytotoxic to SKOV3ip cells at concentrations approximating therapeutic serum concentrations (data not shown). Similarly, R-/S-ketorolac did not impair proliferation of SKOV3ip cells after 96h treatment (Fig 2.5A-B). Cells treated with 300 μ M S-ketorolac show a slight but not significant decrease in cell proliferation, consistent with observations of COX-1/-2 inhibition in other cell types (155,156). However, this concentration of S-ketorolac exceeded a normal therapeutic dose. These findings suggest that ketorolac improves survival benefit through a mechanism not related to cell apoptosis or proliferation.

Cellular adhesion is partially regulated by Cdc42 and Rac1 and is required for metastasis (76,163). We utilized MCAs cultured in the presence of EGF and an organotypic cell culture model (158) to mimic the specific adhesive environments (9,10,31) seen *in vivo*. This provides a preferred substrate for adhesion, migration, and invasion studies using single cells or MCAs. As early as 4h, MCAs were able to adhere to the organotypic layer and begin disaggregation (Fig 2.10A). Specific inhibition of Cdc42 and Rac1 with ML141 or NSC23766 inhibited MCA adhesion and spreading at 4h. It has been proposed that MCAs dislodged from tumors during surgery contribute to recurrence (23). Consistent with other reports (146), I observe that MCA adhesion occurs rapidly, but can be blocked through specific inhibition of Cdc42 and Rac1. It has been reported that ketorolac treatment of ovarian cancer cells can reduce Cdc42 and Rac1 activity in as little as 15 minutes (150). These data suggest that early administration of ketorolac can reduce the number of metastatic implants that may occur in a patient, thereby improving patient outcome.

MCAs cultured in the presence of specific inhibitors, R-/S-ketorolac, or a single ketorolac enantiomer did not spread on the organotypic layer as extensively as control MCAs (Fig 2.10C) consistent with an inhibition of migration (Fig 2.4). Cdc42 serves as an environmental sensor to the cell to initiate filopodia formation, causing nascent adhesions (76). Coordination with Rac1 allows maturation of the lamellipodia and migration to occur (76). Through selective inhibition of both Cdc42 and Rac1, I observed a decrease in overall migration. Because the formation of metastatic tumors necessitates adhesion, migration, and invasion, these data further support the idea that inhibition of Cdc42 and Rac1 conferred by R-ketorolac could benefit ovarian cancer patients. Taken together, these data suggest that inhibition of adhesion and spreading of MCAs is a possible mechanism for the reported improved survival in patients (Fig 2.10) (65).

4.4 Effect of Ketorolac on Ovarian Cancer Cells *in vivo*

Human ovarian cancer metastases implant in a predictable manner (5,9). I used an intraperitoneal xenograft mouse model of recurrent ovarian cancer to assess the effect of ketorolac *in vivo*. Tumor deposition within the mouse peritoneal cavity is similar to what is seen in advanced stage human ovarian cancer (Fig 2.1A). Specifically, the omentum has a high level of cancer cell engraftment, with smaller metastases throughout the peritoneal cavity. We assessed overall tumor burden through the quantification of tumors within the peritoneal cavity. We found that R-/S-ketorolac and R-ketorolac treated animals had a significant decrease of approximately 30% and 20%, respectively, in tumor burden compared to placebo treated animals. S-ketorolac treated animals had slightly less

Table 4.2

Table 4.2 – Summary of the effect of Cdc42 and Rac1 inhibition on SKOV3ip ovarian cancer cells <i>in vivo</i>			
	R-/S-ketorolac	R-ketorolac	S-ketorolac
Tumor Burden	↓↓↓	↓↓	↓
Proliferation	NC	NC	NC
Apoptosis	NC	NC	NC
GTPase expression	NC	NC	NC
Splenic Adhesion	NC	NC, p=0.052	NC, p=0.052

NC = No Change, ↓ = decrease, number of arrows indicates level of change

than 20% decrease in tumor burden, which did not reach significance. Administration and dosage of R-/S-ketorolac to the mice was similar to that administered to patients (132). The decrease in tumor burden observed in the animals The data collected from the animals reflects the survival data that have been reported following treatment with ketorolac for breast (126,143) and ovarian (65) cancers.

Serum collected from the animals indicated that the single enantiomer doses were not significantly different than R-/S-ketorolac (Fig 2.1C). Despite being more than 99% pure as stock solutions, serum recovered from the animals treated with single enantiomers did not contain the expected enantiomer ratio (Fig 2.1C). Serum from R-ketorolac treated animals contained slightly elevated levels of S-ketorolac, while serum from S-ketorolac treated animals contained over 50% R-ketorolac. The predominance of the R-enantiomer in serum was not simply due to the recovery process favoring the R-enantiomer over the S-enantiomer. In order to further investigate this finding, pooled normal human plasma samples were spiked with stock ketorolac solutions and submitted to the recovery protocol, and chromatograms from spiked plasma resembled stock solutions, suggesting an interconversion in the mouse. The interconversion from S- to R-enantiomers is a species specific response that has been well documented (151). The mouse model allows researchers to assess the effect R-ketorolac alone on tumor cell engraftment. However, other investigators have suggested that the mechanism by which ketorolac improves 5 year survival is COX-dependent (126,143). I believe that Cdc42 and Rac1 inhibition by R-ketorolac contributes as well. Due to interconversion of S-ketorolac to R-ketorolac by mice (Fig 2.1)(134), we are unable to fully assess the contribution of COX inhibition by S-ketorolac. However, the use of a COX knockout

mouse to mimic S-ketorolac function or an alternate COX inhibitor without GTPase inhibitory activity may allow us to evaluate the anti-inflammatory effects of NSAIDs on tumor burden.

To assess cellular effects of ketorolac, omental tumors were removed, along with adjacent tissue. These tissues were paraffin embedded and sectioned. Apoptosis and proliferation within the tumors were examined using TUNEL and Ki-67 staining. Similar to what was seen in culture, treatment with ketorolac had no significant effect on apoptosis (Fig 2.8B) or proliferation (Fig 2.7D). Cellular architecture and distribution of SKOV3ip cells within the animals was visually assessed via H&E staining. R-ketorolac and S-ketorolac treated animals showed a reduction of adherent SKVO3ip cells to the exterior of the splenic capsule. However, there was no change in adhesion in animals treated with R-/S-ketorolac.

My cellular adhesion data indicates that treatment with R-/S-ketorolac or single enantiomers decreases adhesion of MCAs. When adhesion of SKOV3ip cells to the splenic capsule was examined, I observe that R-ketorolac or S-ketorolac decreases levels of adhesion while the racemic mix does not (Fig 2.10E). If we examine this in context of serum concentrations, it indicates that R-ketorolac treated animals had a higher serum concentration of R-ketorolac ($4.85\mu\text{M} \pm 1.2\mu\text{M}$) than either R-/S-ketorolac ($2.38\mu\text{M} \pm 0.78\mu\text{M}$) or S-ketorolac ($2.70\mu\text{M} \pm 0.82\mu\text{M}$) alone. This indicates that the effect is not due to saturation effect seen by higher concentrations of S-ketorolac exhibiting an effect on Cdc42 and Rac1 (150). Because S-ketorolac interconverts to R-ketorolac and a longer exposure to R-ketorolac between doses. A partial exposure to R-ketorolac may explains why S-ketorolac treatment group did not have a significant reduction in tumor burden.

COX-1/2 inhibition has been reported to inhibit some cell-cell adhesions (129). It is possible COX inhibition by the S-ketorolac, coupled with Cdc42 and Rac1 inhibition by R-ketorolac, was sufficient to inhibit some early SKOV3ip adhesion, thus slowing tumor development.

4.5 Limitations of the Mouse Model

Although useful, this tumor model does have some limitations. Images of these animals were captured using the Light Tools small animal imager, which allowed us to look at gross morphology and visualize tumors. However, this instrument is mostly qualitative, and we experienced difficulties with quantification of tumor foci. The omental tumor was resected prior to imaging and was imaged separately. While generally a solid tumor, in some instances it appears as a loose bundle of tumors. These differences in structure change how the omental tumor was quantified and may be blunting the response of ketorolac on tumor burden. There may be additional data to be collected if we analyze the number of tumor foci in the omental tumor alone. One method to improve quantification was to measure overall fluorescence. However, post image processing on multiple platforms indicated there was no difference in levels of fluorescence. This was largely due to image saturation, or autofluorescence from the mice. As a result, we were unable to use the current images for fluorescence analysis. However, Dr. Mara Steinkamp at UNM Dept of Pathology has developed a far red fluorescing SKOV3ip cell line we can use for future studies. It would allow us to use the Perkin-Elmer IVIS platform, which can directly measure levels of fluorescence or bioluminescence. This would allow us to eliminate the majority of autofluorescence from mice, and allow for longitudinal studies.

The use of the omental tumor also provides interesting alternatives to measure early tumor formation events. Preliminary work identified the NSAID R-naproxen was an inhibitor of Cdc42 and Rac1 (123). In an early animal study using naproxen, I observed that R-naproxen reduced tumor burden (Fig 2.7A). For this experiment, I was able to weigh the omental tumor prior to tissue preservation. I observed a trend to lower tumor weights with R-naproxen treated animals, and a significant decrease in tumor weight in R-/S-ketorolac and R-ketorolac treated animals (Fig 2.7B). However this analysis was not performed in subsequent animal studies. Additionally, a recent study describes an intraperitoneal injection of a large number of ovarian cancer cells, which are allowed to adhere for a short period of time (158). The omentum, bearing adherent ovarian cancer cells, is then collected. This method would allow us to recapitulate the early adhesion we see with MCAs in culture. We would be able to measure fluorescence of the omentum to obtain a quantitative measurement of the effect of ketorolac on early implantation within the omentum.

4.6 Ketorolac in Ovarian Cancer Patients

It has been reported that ketorolac provides early survival benefit to breast cancer patients (126, 143) and the proposed mechanism is through COX-1/-2 inhibition of COX-dependent events. It has been postulated that ketorolac would have the same effect on ovarian cancer patients. However, I have been able to show there are COX-independent effects caused by R-ketorolac. As ketorolac is an approved analgesic treatment in patients undergoing gynecological surgery (65), a small phase 0 study to examine the effects of a single dose of ketorolac used perioperatively in ovarian cancer patients was undertaken.

In our Phase 0 study, patients received a single dose of intravenous R-/S-ketorolac, Toradol®, following cytoreductive surgery. Serum and peritoneal fluid were collected from patients to monitor ketorolac concentrations, determine distribution to the peritoneal cavity, and to isolate cells for GTPase activity assays. Toradol® at the time of administration, is a 50:50 mix of R-/S-ketorolac as measured by HPLC (Fig 3.8). Previous research shows no interconversion of ketorolac occurs in humans and there is a preferential elimination of S-ketorolac over R-ketorolac (133,134,151). Ketorolac in serum was detectable immediately following administration and was still present at 24h (Fig 3.3). Ketorolac was detectable in the peritoneal fluid at 1h after administration and persisted until 24h. In serum and peritoneal fluid, R-ketorolac was predominant over S-ketorolac, indicating that S-ketorolac is preferentially eliminated before R-ketorolac. This is the first documented evidence of ketorolac distribution within the peritoneal cavity, indicating that it is possible to affect cancer cells directly within the peritoneal cavity, not just the surrounding tissue.

Work done by Yun Guo looked at GTPase activity in cells isolated from the peritoneal fluid (Fig 3.6). Cdc42 and Rac1 activity decreased in primary patient cells that had been in culture for 48h, compared to freshly isolated cells (Fig 3.6). Following administration of ketorolac, Cdc42 and Rac1 activity in cells collected from the peritoneal fluid decreased over 24h (Fig 3.4) but there was no effect on RhoA (Fig 3.13). These data indicate that the environment within the peritoneal cavity activates Cdc42 and Rac1 and following administration of ketorolac, peritoneal concentrations are sufficient to inhibit GTPase activity (Table 3.3). Taken together, these data suggest a potential mechanism by which ketorolac provides survival benefit to patients. Dr. Linda Cook

(UNM) performed a retrospective analysis of patients treated for ovarian cancer at the UNM Cancer Center, those patients who received ketorolac had reduced risk of cancer-specific mortality within 5 years of treatment (Fig 3.5). Although more work is required to follow up on these findings, this study highlights the importance ketorolac may play in the treatment of ovarian cancer. Recently, it has been demonstrated that inhibition of Rac1 in angiogenesis reduces tumor burden in peritoneal xenografts (117). Additionally, inhibition of Cdc42 and Rac1 has improved outcome in animal models of colon and prostate cancer (113,114). Not all NSAIDs improve patient outcomes, indicating that there are likely non-COX targets that are being affected. The work presented here suggests that Toradol®, administered as R/S-ketorolac may have dual targets. S-ketorolac inhibition of COX-1/2 reduces pain and inflammation, while R-ketorolac inhibition of Cdc42 and Rac1 reduces adhesion related events. Used in conjunction with current cytoreductive surgery, chemotherapy, and other treatment strategies, I believe that the use of ketorolac may provide benefit to ovarian cancer patients through S-ketorolac inhibition of COX targets and R-ketorolac interaction with non-COX targets.

4.7 Future directions

The use of NSAIDs as potential therapeutics in the treatment of cancer has been gaining support in recent years (129,131,154). When first examined, it was believed that an inhibition of COX-1/2, and COX-dependent events, was the main driver for the early success of NSAIDs. Work has gone into determining the molecular events responsible for NSAIDs improving clinical outcome (131,154). Ketorolac is an NSAID used to alleviate pain during surgery, including gynecological surgery. Our group and

others have established that ketorolac can provide survival benefit to cancer patients. I have demonstrated that R-ketorolac has COX independent effects that may be beneficial to the treatment of ovarian cancer. Although we have shown that R-ketorolac inhibits Cdc42 and Rac1 related events in ovarian cancer cells, the exact mechanism at work *in vivo* is still unclear.

Cdc42 and Rac1 regulate a number of different adhesion molecules, including integrins and cadherins. While we have been able to show that there are cellular effects when ovarian cancer cells are treated with ketorolac, we have not yet identified the cellular events *in vivo* that contribute to decreased tumor burden. Cdc42 and Rac1 both interact with integrins to form nascent adhesions during cell migration. It would be beneficial to know if these adhesions are disrupted. β -catenin is one protein that helps to regulate cell-cell adhesions. Rac1 interacts with β -catenin through IQGAP, although the exact interaction is not well understood. Examining these adhesive events, especially in the context of MCA formation and stability, may help elucidate the role R-ketorolac is playing in improving patient survival.

Thus far, animal work has only used R-ketorolac as a single compound. However, in the treatment of ovarian cancer patients, it would most likely be used in combination with traditional chemotherapies. Studying a synergistic response between ketorolac and typical chemotherapeutics will likely lead to improved outcomes in the animal model. It is known that the formation of MCAs leads to chemoresistance (25) and it has been postulated that the compact structure creates a gradient that protects the inner cells. It is known that R-ketorolac decreases adhesion, which will likely result in less compact

MCAs. If adhesion in MCAs can be sufficiently reduced, then it may be possible able to resensitize MCAs to chemotherapeutics.

The survival curves generated by Dr. Linda Cook (Fig 3.9-3.13) show as much as a 40% improved chance of survival based on the use of ketorolac. In an effort to explain this effect, this project has explored how R-ketorolac may confer survival benefit through inhibition of Cdc42 and Rac1 related cellular events required for metastasis. While the animal data is promising, it is not as robust as we would expect to see based on the survival data, suggesting there are other factors we have not accounted for. What remains unclear is the extent to which Cdc42 and Rac1/1b are required for ovarian cancer metastasis and recurrence. Is one more important than the other or is the synergy between the two required? If it is the cooperation between these GTPases that is important, then using a selective drug, such as R-ketorolac, to target both would be ideal. Identifying which is more essential to driving recurrence will dictate how to design derivatives for future drug development. It has recently been suggested that the perioperative environment plays a major role in determining cancer outcomes (perioperative paper). The effect of R-ketorolac on the peritoneal environment is currently unknown. It is clear ketorolac affects the perioperative environment of the peritoneal cavity enough to reduce recurrence, but the extent of that effect needs to be explored. My work has demonstrated a mechanism to account for the observed improved survival of breast and ovarian cancer patients following administration of ketorolac. Cdc42 and Rac1 inhibition by R-ketorolac decreases adhesion and migration events related to recurrence. Further work is required to optimize the animal model and fully explain the interaction between Cdc42 and Rac1 as they relate to ovarian cancer recurrence.

Literature Cited

1. Heintz APM, Odicino F, Maisonneuve P, Quinn MA, Benedet JL, Creasman WT, et al. Carcinoma of the ovary. *Int J Gynecol Obstet*. 2006;95:S161–92.
2. Howlander N, Noone A, Krapcho M, Garshell J, Miller D, Altekruse S, et al. SEER Cancer Statistics Review, 1975-2012. 2015 Apr 5;
3. Siegel R, Ma J, Zou Z, Jemal A. Cancer statistics, 2014: Cancer Statistics, 2014. *CA Cancer J Clin*. 2014 Jan;64(1):9–29.
4. Serov S, Scully R, Sobin L. Histological Typing of Tumours. World Health Organ. 1973;9.
5. Lengyel E. Ovarian Cancer Development and Metastasis. *Am J Pathol*. 2010 Sep;177(3):1053–64.
6. Auersperg N, Woo MMM, Gilks CB. The origin of ovarian carcinomas: a developmental view. *Gynecol Oncol*. 2008 Sep;110(3):452–4.
7. Kurman RJ, Shih I-M. Molecular pathogenesis and extraovarian origin of epithelial ovarian cancer—Shifting the paradigm. *Hum Pathol*. 2011 Jul;42(7):918–31.
8. Naora H. The heterogeneity of epithelial ovarian cancers: reconciling old and new paradigms. *Expert Rev Mol Med*. 2007;9(13):1–12.
9. Shield K, Ackland ML, Ahmed N, Rice GE. Multicellular spheroids in ovarian cancer metastases: Biology and pathology. *Gynecol Oncol*. 2009 Apr;113(1):143–8.
10. Nieman KM, Romero IL, Van Houten B, Lengyel E. Adipose tissue and adipocytes support tumorigenesis and metastasis. *Biochim Biophys Acta BBA - Mol Cell Biol Lipids*. 2013 Oct;1831(10):1533–41.
11. Kenny HA, Kaur S, Coussens LM, Lengyel E. The initial steps of ovarian cancer cell metastasis are mediated by MMP-2 cleavage of vitronectin and fibronectin. *J*

Clin Invest. 2008 Apr 1;118(4):1367–79.

12. Steinkamp MP, Kanigel-Winner K, Davies S, Muller CY, Zhang Y, Hoffman RM, et al. Ovarian tumor attachment, invasion, and vascularization reflect unique microenvironments in the peritoneum: insights from xenograft and mathematical models. *Mol Cell Oncol*. 2013;3:97.
13. Burleson KM, Boente MP, Pambuccian SE, Skubitz AP. Disaggregation and invasion of ovarian carcinoma ascites spheroids. *J Transl Med*. 2006 Jan 24;4(1):6.
14. Kim A, Ueda Y, Naka T, Enomoto T. Therapeutic strategies in epithelial ovarian cancer. *J Exp Clin Cancer Res CR*. 2012;31:14.
15. Busschots S, O'Toole S, O'Leary JJ, Stordal B. Carboplatin and taxol resistance develops more rapidly in functional BRCA1 compared to dysfunctional BRCA1 ovarian cancer cells. *Exp Cell Res*. 2015 Aug 1;336(1):1–14.
16. Cannistra SA. Cancer of the ovary. *N Engl J Med*. 2004;351(24):2519–29.
17. Scarabelli C, Gallo A, Zarrelli A, Visentin C, Campagnutta E. Systematic pelvic and para-aortic lymphadenectomy during cytoreductive surgery in advanced ovarian cancer: potential benefit on survival. *Gynecol Oncol*. 1995 Mar;56(3):328–37.
18. Dauplat J, Hacker NF, Nieberg RK, Berek JS, Rose TP, Sagae S. Distant metastases in epithelial ovarian carcinoma. *Cancer*. 1987 Oct 1;60(7):1561–6.
19. Naora H, Montell DJ. Ovarian Cancer Metastasis: Integrating insights from disparate model organisms. *Nat Rev Cancer*. 2005 May;5(5):355–66.
20. Ahmed N, Stenvers KL. Getting to Know Ovarian Cancer Ascites: Opportunities for Targeted Therapy-Based Translational Research. *Front Oncol* [Internet]. 2013 [cited 2015 Jul 16];3. Available from: <http://journal.frontiersin.org/article/10.3389/fonc.2013.00256/abstract>
21. Pradeep S, Kim SW, Wu SY, Nishimura M, Chaluvally-Raghavan P, Miyake T, et al. Hematogenous metastasis of ovarian cancer: rethinking mode of spread. *Cancer Cell*. 2014 Jul 14;26(1):77–91.

22. Ahmed N, Thompson EW, Quinn MA. Epithelial–mesenchymal interconversions in normal ovarian surface epithelium and ovarian carcinomas: An exception to the norm. *J Cell Physiol.* 2007 Dec;213(3):581–8.
23. Shield K, Riley C, Quinn MA, Rice GE, Ackland ML, Ahmed N. Alpha2beta1 integrin affects metastatic potential of ovarian carcinoma spheroids by supporting disaggregation and proteolysis. *J Carcinog.* 2007;6:11.
24. Filippovich IV, Sorokina NI, Robillard N, Chatal JF. Radiation-induced apoptosis in human ovarian carcinoma cells growing as a monolayer and as multicell spheroids. *Int J Cancer J Int Cancer.* 1997 Sep 4;72(5):851–9.
25. Makhija S, Taylor DD, Gibb RK, Gerçel-Taylor C. Taxol-induced bcl-2 phosphorylation in ovarian cancer cell monolayer and spheroids. *Int J Oncol.* 1999 Mar;14(3):515–21.
26. Bates RC, Edwards NS, Yates JD. Spheroids and cell survival. *Crit Rev Oncol Hematol.* 2000 Dec;36(2-3).
27. Kobayashi H, Man S, Graham CH, Kapitain SJ, Teicher BA, Kerbel RS. Acquired multicellular-mediated resistance to alkylating agents in cancer. *Proc Natl Acad Sci U S A.* 1993 Apr 15;90(8):3294–8.
28. Desoize B, Jardillier J. Multicellular resistance: a paradigm for clinical resistance? *Crit Rev Oncol Hematol.* 2000 Dec;36(2-3):193–207.
29. Hensley HH, Roder NA, O'Brien SW, Bickel LE, Xiao F, Litwin S, et al. Combined In Vivo Molecular and Anatomic Imaging for Detection of Ovarian Carcinoma-Associated Protease Activity and Integrin Expression in Mice. *Neoplasia.* 2012 Jun;14(6):451–IN2.
30. Burleson KM, Hansen LK, Skubitz APN. Ovarian carcinoma spheroids disaggregate on type I collagen and invade live human mesothelial cell monolayers. *Clin Exp Metastasis.* 2005 Jun;21(8):685–97.
31. Kenny HA, Chiang C-Y, White EA, Schryver EM, Habis M, Romero IL, et al. Mesothelial cells promote early ovarian cancer metastasis through fibronectin secretion. *J Clin Invest.* 2014 Oct 1;124(10):4614–28.

32. Vaughan S, Coward JI, Bast RC, Berchuck A, Berek JS, Brenton JD, et al. Rethinking ovarian cancer: recommendations for improving outcomes. *Nat Rev Cancer*. 2011;11(10):719–25.
33. Greene MH, Boice JD, Greer BE, Blessing JA, Dembo AJ. Acute nonlymphocytic leukemia after therapy with alkylating agents for ovarian cancer: a study of five randomized clinical trials. *N Engl J Med*. 1982 Dec 2;307(23):1416–21.
34. Travis LB, Holowaty EJ, Bergfeldt K, Lynch CF, Kohler BA, Wiklund T, et al. Risk of leukemia after platinum-based chemotherapy for ovarian cancer. *N Engl J Med*. 1999 Feb 4;340(5):351–7.
35. Rose PG, Nerenstone S, Brady MF, Clarke-Pearson D, Olt G, Rubin SC, et al. Secondary surgical cytoreduction for advanced ovarian carcinoma. *N Engl J Med*. 2004 Dec 9;351(24):2489–97.
36. Nehate C, Jain S, Saneja A, Khare V, Alam N, Dubey RD, et al. Paclitaxel formulations: challenges and novel delivery options. *Curr Drug Deliv*. 2014;11(6):666–86.
37. Press JZ, De Luca A, Boyd N, Young S, Troussard A, Ridge Y, et al. Ovarian carcinomas with genetic and epigenetic BRCA1 loss have distinct molecular abnormalities. *BMC Cancer*. 2008;8:17.
38. Banerjee S, Kaye SB, Ashworth A. Making the best of PARP inhibitors in ovarian cancer. *Nat Rev Clin Oncol*. 2010 Sep;7(9):508–19.
39. Windbichler GH, Hausmaninger H, Stummvoll W, Graf AH, Kainz C, Lahodny J, et al. Interferon-gamma in the first-line therapy of ovarian cancer: a randomized phase III trial. *Br J Cancer*. 2000 Mar;82(6):1138–44.
40. Alberts DS, Marth C, Alvarez RD, Johnson G, Bidzinski M, Kardatzke DR, et al. Randomized phase 3 trial of interferon gamma-1b plus standard carboplatin/paclitaxel versus carboplatin/paclitaxel alone for first-line treatment of advanced ovarian and primary peritoneal carcinomas: results from a prospectively designed analysis of progression-free survival. *Gynecol Oncol*. 2008 May;109(2):174–81.

41. Shu CA, Konner JA. Breaking down the evidence for bevacizumab in ovarian cancer. *The Oncologist*. 2015 Feb;20(2):91–3.
42. Paley PJ, Staskus KA, Gebhard K, Mohanraj D, Twiggs LB, Carson LF, et al. Vascular Endothelial Growth Factor Expression in Early Stage Ovarian Carcinoma. *Cancer*. 1997 Jul 1;80(1):98–106.
43. Jubb AM, Harris AL. Biomarkers to predict the clinical efficacy of bevacizumab in cancer. *Lancet Oncol*. 2010 Dec;11(12):1172–83.
44. Wennerberg K. The Ras superfamily at a glance. *J Cell Sci*. 2005 Mar 1;118(5):843–6.
45. Bar-Sagi D, Hall A. Ras and Rho GTPases: a family reunion. *Cell*. 2000 Oct 13;103(2):227–38.
46. Mitin N, Rossman KL, Der CJ. Signaling interplay in Ras superfamily function. *Curr Biol CB*. 2005 Jul 26;15(14):R563–74.
47. Jaffe AB, Hall A. Rho GTPases: biochemistry and biology. *Annu Rev Cell Dev Biol*. 2005;21:247–69.
48. Vang R, Shih I-M, Kurman RJ. Ovarian Low-grade and High-grade Serous Carcinoma: Pathogenesis, Clinicopathologic and Molecular Biologic Features, and Diagnostic Problems. *Adv Anat Pathol*. 2009 Sep;16(5):267–82.
49. Vereczkey I, Serester O, Dobos J, Gallai M, Szakács O, Szentirmay Z, et al. Molecular Characterization of 103 Ovarian Serous and Mucinous Tumors. *Pathol Oncol Res*. 2011 Sep;17(3):551–9.
50. Milojkovic Kerklaan B, Kerklaan BM, Diéras V, Le Tourneau C, Mergui-Roelvink M, Huitema ADR, et al. Phase I study of lonafarnib (SCH66336) in combination with trastuzumab plus paclitaxel in Her2/neu overexpressing breast cancer: EORTC study 16023. *Cancer Chemother Pharmacol*. 2013 Jan;71(1):53–62.
51. Sun J, Blaskovich MA, Knowles D, Qian Y, Ohkanda J, Bailey RD, et al. Antitumor Efficacy of a Novel Class of Non-thiol-containing Peptidomimetic Inhibitors of Farnesyltransferase and Geranylgeranyltransferase I Combination Therapy with the

- Cytotoxic Agents Cisplatin, Taxol, and Gemcitabine. *Cancer Res.* 1999;59(19):4919–26.
52. Meier W, Bois A du, Rau J, Gropp-Meier M, Baumann K, Huober J, et al. Randomized phase II trial of carboplatin and paclitaxel with or without lonafarnib in first-line treatment of epithelial ovarian cancer stage IIB-IV. *Gynecol Oncol.* 2012 Aug;126(2):236–40.
 53. Kamai T, Yamanishi T, Shirataki H, Takagi K, Asami H, Ito Y, et al. Overexpression of RhoA, Rac1, and Cdc42 GTPases is associated with progression in testicular cancer. *Clin Cancer Res Off J Am Assoc Cancer Res.* 2004 Jul 15;10(14):4799–805.
 54. Fritz G, Kaina B. Rho GTPases: promising cellular targets for novel anticancer drugs. *Curr Cancer Drug Targets.* 2006;6(1):1–14.
 55. Vasioukhin V, Bauer C, Yin M, Fuchs E. Directed Actin Polymerization Is the Driving Force for Epithelial Cell–Cell Adhesion. *Cell.* 2000 Jan 21;100(2):209–19.
 56. Noritake J, Fukata M, Sato K, Nakagawa M, Watanabe T, Izumi N, et al. Positive Role of IQGAP1, an Effector of Rac1, in Actin-Meshwork Formation at Sites of Cell-Cell Contact. *Mol Biol Cell.* 2004 Mar 1;15(3):1065–76.
 57. Kuroda S, Fukata M, Nakagawa M, Kaibuchi K. Cdc42, Rac1, and Their Effector IQGAP1 as Molecular Switches for Cadherin-Mediated Cell–Cell Adhesion. *Biochem Biophys Res Commun.* 1999 Aug 19;262(1):1–6.
 58. Ellenbroek SIJ, Collard JG. Rho GTPases: functions and association with cancer. *Clin Exp Metastasis.* 2007 Nov;24(8):657–72.
 59. Schnelzer A, Prechtel D, Knaus U, Dehne K, Gerhard M, Graeff H, et al. Rac1 in human breast cancer: overexpression, mutation analysis, and characterization of a new isoform, Rac1b. *Oncogene.* 2000 Jun 15;19(26):3013–20.
 60. Bid HK, Roberts RD, Manchanda PK, Houghton PJ. RAC1: An Emerging Therapeutic Option for Targeting Cancer Angiogenesis and Metastasis. *Mol Cancer Ther.* 2013 Oct 1;12(10):1925–34.

61. Matos P, Jordan P. Increased Rac1b expression sustains colorectal tumor cell survival. *Mol Cancer Res MCR*. 2008 Jul;6(7):1178–84.
62. Pan Y, Bi F, Liu N, Xue Y, Yao X, Zheng Y, et al. Expression of seven main Rho family members in gastric carcinoma. *Biochem Biophys Res Commun*. 2004 Mar 12;315(3):686–91.
63. Liu S-Y, Yen C-Y, Yang S-C, Chiang W-F, Chang K-W. Overexpression of Rac-1 small GTPase binding protein in oral squamous cell carcinoma. *J Oral Maxillofac Surg*. 2004 Jun;62(6):702–7.
64. Leng R, Liao G, Wang H, Kuang J, Tang L. Rac1 expression in epithelial ovarian cancer: effect on cell EMT and clinical outcome. *Med Oncol [Internet]*. 2015 Feb [cited 2015 Jul 16];32(2). Available from: <http://link.springer.com/10.1007/s12032-014-0329-5>
65. Guo Y, Kenney SR, Cook LS, Adams SF, Rutledge T, Romero E, et al. A novel pharmacologic activity of ketorolac for therapeutic benefit in ovarian cancer patients. *Clin Cancer Res*. 2015 Jun 12;clincanres.0461.2015.
66. Gonzalez-Villasana V, Fuentes-Mattei E, Ivan C, Dalton HJ, Rodriguez-Aguayo C, Fernandez-de Thomas RJ, et al. Rac1/Pak1/p38/MMP-2 Axis Regulates Angiogenesis in Ovarian Cancer. *Clin Cancer Res*. 2015 May 1;21(9):2127–37.
67. Malosio ML, Gilardelli D, Paris S, Albertinazzi C, Curtis I de. Differential Expression of Distinct Members of Rho Family GTP-Binding Proteins during Neuronal Development: Identification of Rac1B, a New Neural-Specific Member of the Family. *J Neurosci*. 1997 Sep 1;17(17):6717–28.
68. Zhou C, Licciulli S, Avila JL, Cho M, Troutman S, Jiang P, et al. The Rac1 splice form Rac1b promotes K-ras-induced lung tumorigenesis. *Oncogene*. 2013 Feb 14;32(7):903–9.
69. Singh A, Karnoub AE, Palmby TR, Lengyel E, Sondek J, Der CJ. Rac1b, a tumor associated, constitutively active Rac1 splice variant, promotes cellular transformation. *Oncogene*. 2004 Dec 16;23(58):9369–80.

70. Matos P, Jordan P. Expression of Rac1b stimulates NF-kappaB-mediated cell survival and G1/S progression. *Exp Cell Res.* 2005 May 1;305(2):292–9.
71. Radisky DC, Levy DD, Littlepage LE, Liu H, Nelson CM, Fata JE, et al. Rac1b and reactive oxygen species mediate MMP-3-induced EMT and genomic instability. *Nature.* 2005 Jul 7;436(7047):123–7.
72. Nowell PC, Hungerford DA. Chromosome studies on normal and leukemic human leukocytes. *J Natl Cancer Inst.* 1960 Jul;25:85–109.
73. Farmer H, McCabe N, Lord CJ, Tutt ANJ, Johnson DA, Richardson TB, et al. Targeting the DNA repair defect in BRCA mutant cells as a therapeutic strategy. *Nature.* 2005 Apr 14;434(7035):917–21.
74. Fritz G, Brachetti C, Bahlmann F, Schmidt M, Kaina B. Rho GTPases in human breast tumours: expression and mutation analyses and correlation with clinical parameters. *Br J Cancer.* 2002 Sep 9;87(6):635–44.
75. Jones MB, Krutzsch H, Shu H, Zhao Y, Liotta LA, Kohn EC, et al. Proteomic analysis and identification of new biomarkers and therapeutic targets for invasive ovarian cancer. *Proteomics.* 2002 Jan;2(1):76–84.
76. Hall A. Rho family GTPases. *Biochem Soc Trans.* 2012 Dec 1;40(6):1378–82.
77. Didsbury J, Weber RF, Bokoch GM, Evans T, Snyderman R. rac, a novel ras-related family of proteins that are botulinum toxin substrates. *J Biol Chem.* 1989 Oct 5;264(28):16378–82.
78. Ridley AJ. Rho GTPases and actin dynamics in membrane protrusions and vesicle trafficking. *Trends Cell Biol.* 2006;16(10):522–9.
79. Nobes C, Marsh M. Dendritic cells: new roles for Cdc42 and Rac in antigen uptake? *Curr Biol CB.* 2000 Oct 19;10(20):R739–41.
80. Joneson T, Bar-Sagi D. A Rac1 effector site controlling mitogenesis through superoxide production. *J Biol Chem.* 1998 Jul 17;273(29):17991–4.

81. Caron E, Hall A. Identification of two distinct mechanisms of phagocytosis controlled by different Rho GTPases. *Science*. 1998 Nov 27;282(5394):1717–21.
82. Adamson P, Marshall CJ, Hall A, Tilbrook PA. Post-translational modifications of p21rho proteins. *J Biol Chem*. 1992 Oct 5;267(28):20033–8.
83. Zhang FL, Casey PJ. Protein prenylation: molecular mechanisms and functional consequences. *Annu Rev Biochem*. 1996;65:241–69.
84. Parsons JT, Horwitz AR, Schwartz MA. Cell adhesion: integrating cytoskeletal dynamics and cellular tension. *Nat Rev Mol Cell Biol*. 2010 Sep;11(9):633–43.
85. Kraynov VS, Chamberlain C, Bokoch GM, Schwartz MA, Slabaugh S, Hahn KM. Localized Rac activation dynamics visualized in living cells. *Science*. 2000 Oct 13;290(5490):333–7.
86. Heasman SJ, Ridley AJ. Mammalian Rho GTPases: new insights into their functions from in vivo studies. *Nat Rev Mol Cell Biol*. 2008 Sep;9(9):690–701.
87. Cau J, Hall A. Cdc42 controls the polarity of the actin and microtubule cytoskeletons through two distinct signal transduction pathways. *J Cell Sci*. 2005 Jun 15;118(Pt 12):2579–87.
88. Etienne-Manneville S, Hall A. Cdc42 regulates GSK-3beta and adenomatous polyposis coli to control cell polarity. *Nature*. 2003 Feb 13;421(6924):753–6.
89. Nayal A, Webb DJ, Brown CM, Schaefer EM, Vicente-Manzanares M, Horwitz AR. Paxillin phosphorylation at Ser273 localizes a GIT1–PIX–PAK complex and regulates adhesion and protrusion dynamics. *J Cell Biol*. 2006 May 22;173(4):587–9.
90. Gardiner EM, Pestonjamas KN, Bohl BP, Chamberlain C, Hahn KM, Bokoch GM. Spatial and temporal analysis of Rac activation during live neutrophil chemotaxis. *Curr Biol CB*. 2002 Dec 10;12(23):2029–34.
91. Pollard TD, Blanchoin L, Mullins RD. Molecular mechanisms controlling actin filament dynamics in nonmuscle cells. *Annu Rev Biophys Biomol Struct*.

2000;29:545–76.

92. Allen WE, Zicha D, Ridley AJ, Jones GE. A role for Cdc42 in macrophage chemotaxis. *J Cell Biol.* 1998 Jun 1;141(5):1147–57.
93. Kiosses WB, Shattil SJ, Pampori N, Schwartz MA. Rac recruits high-affinity integrin α v β 3 to lamellipodia in endothelial cell migration. *Nat Cell Biol.* 2001 Mar;3(3):316–20.
94. Hotulainen P, Lappalainen P. Stress fibers are generated by two distinct actin assembly mechanisms in motile cells. *J Cell Biol.* 2006 May 8;173(3):383–94.
95. Eswaran J, Li D-Q, Shah A, Kumar R. Molecular Pathways: Targeting P21-Activated Kinase 1 Signaling in Cancer—Opportunities, Challenges, and Limitations. *Clin Cancer Res.* 2012 Jul 15;18(14):3743–9.
96. Baker NM, Chow HY, Chernoff J, Der CJ. Molecular Pathways: Targeting RAC–p21-Activated Serine–Threonine Kinase Signaling in RAS-Driven Cancers. *Clin Cancer Res.* 2014 Sep 15;20(18):4740–6.
97. Gurzu S. Epithelial-mesenchymal, mesenchymal-epithelial, and endothelial-mesenchymal transitions in malignant tumors: An update. *World J Clin Cases.* 2015;3(5):393.
98. Hudson LG, Zeineldin R, Stack MS. Phenotypic plasticity of neoplastic ovarian epithelium: unique cadherin profiles in tumor progression. *Clin Exp Metastasis.* 2008 Oct;25(6):643–55.
99. Kassim SK, El-Salahy EM, Fayed ST, Helal SA, Helal T, Azzam EE, et al. Vascular endothelial growth factor and interleukin-8 are associated with poor prognosis in epithelial ovarian cancer patients. *Clin Biochem.* 2004 May;37(5):363–9.
100. Goncharenko-Khaider N, Matte I, Lane D, Rancourt C, Piché A. Ovarian cancer ascites increase Mcl-1 expression in tumor cells through ERK1/2-Elk-1 signaling to attenuate TRAIL-induced apoptosis. *Mol Cancer.* 2012;11:84.
101. Lane D, Matte I, Rancourt C, Piché A. Osteoprotegerin (OPG) protects ovarian cancer cells from TRAIL-induced apoptosis but does not contribute to malignant

- ascites-mediated attenuation of TRAIL-induced apoptosis. *J Ovarian Res.* 2012;5(1):34.
102. Marcoux N, Vuori K. EGF receptor mediates adhesion-dependent activation of the Rac GTPase: a role for phosphatidylinositol 3-kinase and Vav2. *Oncogene.* 2003;22(38):6100–6.
103. Mardilovich K, Olson MF, Baugh M. Targeting Rho GTPase signaling for cancer therapy. *Future Oncol.* 2012 Feb 1;8(2):165–77.
104. Gao Y, Dickerson JB, Guo F, Zheng J, Zheng Y. Rational design and characterization of a Rac GTPase-specific small molecule inhibitor. *Proc Natl Acad Sci U S A.* 2004 May 18;101(20):7618–23.
105. Ishizaki T, Uehata M, Tamechika I, Keel J, Nonomura K, Maekawa M, et al. Pharmacological Properties of Y-27632, a Specific Inhibitor of Rho-Associated Kinases. *Mol Pharmacol.* 2000 May 1;57(5):976–83.
106. Strumane K, Rygiel T, van der Valk M, Collard JG. Tiam1-deficiency impairs mammary tumor formation in MMTV-c-neu but not in MMTV-c-myc mice. *J Cancer Res Clin Oncol.* 2008 Jul 1;135(1):69–80.
107. Tobert JA. Lovastatin and beyond: the history of the HMG-CoA reductase inhibitors. *Nat Rev Drug Discov.* 2003 Jul;2(7):517–26.
108. Cordle A, Koenigsnecht-Talboo J, Wilkinson B, Limpert A, Landreth G. Mechanisms of Statin-mediated Inhibition of Small G-protein Function. *J Biol Chem.* 2005 Oct 7;280(40):34202–9.
109. Cardwell CR, Hicks BM, Hughes C, Murray LJ. Statin Use After Colorectal Cancer Diagnosis and Survival: A Population-Based Cohort Study. *J Clin Oncol.* 2014 Oct 1;32(28):3177–83.
110. Walker EJ, Ko AH, Holly EA, Bracci PM. Statin use and risk of pancreatic cancer: Results from a large, clinic-based case-control study. *Cancer.* 2015 Apr 15;121(8):1287–94.

111. Habis M, Wroblewski K, Bradaric M, Ismail N, Yamada SD, Litchfield L, et al. Statin Therapy Is Associated with Improved Survival in Patients with Non-Serous-Papillary Epithelial Ovarian Cancer: A Retrospective Cohort Analysis. *PLoS ONE*. 2014 Aug 13;9(8):e104521.
112. Hong L, Kenney SR, Phillips GK, Simpson D, Schroeder CE, Nöth J, et al. Characterization of a Cdc42 Protein Inhibitor and Its Use as a Molecular Probe. *J Biol Chem*. 2013 Mar 22;288(12):8531–43.
113. Zins K, Lucas T, Reichl P, Abraham D, Aharinejad S. A Rac1/Cdc42 GTPase-Specific Small Molecule Inhibitor Suppresses Growth of Primary Human Prostate Cancer Xenografts and Prolongs Survival in Mice. *PLoS ONE*. 2013 Sep 11;8(9):e74924.
114. Zins K, Gunawardhana S, Lucas T, Abraham D, Aharinejad S. Targeting Cdc42 with the small molecule drug AZA197 suppresses primary colon cancer growth and prolongs survival in a preclinical mouse xenograft model by downregulation of PAK1 activity. *J Transl Med*. 2013 Nov 27;11(1):295.
115. Shutes A, Onesto C, Picard V, Leblond B, Schweighoffer F, Der CJ. Specificity and Mechanism of Action of EHT 1864, a Novel Small Molecule Inhibitor of Rac Family Small GTPases. *J Biol Chem*. 2007 Dec 7;282(49):35666–78.
116. Rosenblatt AE, Garcia MI, Lyons L, Xie Y, Maiorino C, Désiré L, et al. Inhibition of the Rho GTPase, Rac1, decreases estrogen receptor levels and is a novel therapeutic strategy in breast cancer. *Endocr Relat Cancer*. 2011 Apr 1;18(2):207–19.
117. Fehlings MG, Theodore N, Harrop J, Maurais G, Kuntz C, Shaffrey CI, et al. A Phase I/IIa Clinical Trial of a Recombinant Rho Protein Antagonist in Acute Spinal Cord Injury. *J Neurotrauma*. 2011 Mar 8;28(5):787–96.
118. Inglese J, Johnson RL, Simeonov A, Xia M, Zheng W, Austin CP, et al. High-throughput screening assays for the identification of chemical probes. *Nat Chem Biol*. 2007 Aug;3(8):466–79.
119. Wermuth CG. Selective Optimization of Side Activities: Another Way for Drug Discovery. *J Med Chem*. 2004 Mar 1;47(6):1303–14.

120. Surviladze Z, Waller A, Wu Y, Romero E, Edwards BS, Wandinger-Ness A, et al. Identification of a Small GTPase Inhibitor Using a High-Throughput Flow Cytometry Bead-Based Multiplex Assay. *J Biomol Screen*. 2010 Jan 1;15(1):10–20.
121. Tessema M, Simons PC, Cimino DF, Sanchez L, Waller A, Posner RG, et al. Glutathione-S-transferase-green fluorescent protein fusion protein reveals slow dissociation from high site density beads and measures free GSH. *Cytometry A*. 2006 May 1;69A(5):326–34.
122. Schwartz SL, Tessema M, Buranda T, Pylypenko O, Rak A, Simons PC, et al. Flow cytometry for real-time measurement of guanine nucleotide binding and exchange by Ras-like GTPases. *Anal Biochem*. 2008 Oct 15;381(2):258–66.
123. Oprea TI, Sklar LA, Agola JO, Guo Y, Silberberg M, Roxby J, et al. Novel activities of select NSAID R-enantiomers against Rac1 and Cdc42 GTPases. *PLoS ONE*.
124. Roszkowski AP, Rooks WH, Tomolonis AJ, Miller LM. ANTI-INFLAMMATORY AND ANALGETIC PROPERTIES OF d-2-(6'-METHOXY-2'-NAPHTHYL)-PROPIONIC ACID (NAPROXEN). *J Pharmacol Exp Ther*. 1971 Oct 1;179(1):114–23.
125. Pedro M de, Baeza S, Escudero M-T, Dierssen-Sotos T, Gómez-Acebo I, Pollán M, et al. Effect of COX-2 inhibitors and other non-steroidal inflammatory drugs on breast cancer risk: a meta-analysis. *Breast Cancer Res Treat*. 2015 Jan 15;149(2):525–36.
126. Retsky M, Demicheli R, Hrushesky W, Forget P, Kock M, Gukas I, et al. Reduction of Breast Cancer Relapses with Perioperative Non-Steroidal Anti-Inflammatory Drugs: New Findings and a Review. *Curr Med Chem*. 2013 Sep 1;20(33):4163–76.
127. Harris RE, Beebe-Donk J, Alshafie GA. Similar reductions in the risk of human colon cancer by selective and nonselective cyclooxygenase-2 (COX-2) inhibitors. *BMC Cancer*. 2008 Aug 14;8(1):237.
128. Botting RM. Inhibitors of cyclooxygenases: mechanisms, selectivity and uses. *J Physiol Pharmacol Off J Pol Physiol Soc*. 2006 Nov;57 Suppl 5:113–24.

129. Díaz-González F, Sánchez-Madrid F. NSAIDs: Learning new tricks from old drugs. *Eur J Immunol.* 2015 Mar 1;45(3):679–86.
130. FitzGerald GA, Patrono C. The Coxibs, Selective Inhibitors of Cyclooxygenase-2. *N Engl J Med.* 2001 Aug 9;345(6):433–42.
131. Thun MJ, Henley SJ, Patrono C. Nonsteroidal Anti-inflammatory Drugs as Anticancer Agents: Mechanistic, Pharmacologic, and Clinical Issues. *J Natl Cancer Inst.* 2002 Feb 20;94(4):252–66.
132. Sinha V, Kumar R, Singh G. Ketorolac tromethamine formulations: an overview. *Expert Opin Drug Deliv.* 2009 Aug 11;6(9):961–75.
133. Jett M-F, Ramesha CS, Brown CD, Chiu S, Emmett C, Voronin T, et al. Characterization of the Analgesic and Anti-Inflammatory Activities of Ketorolac and Its Enantiomers in the Rat. *J Pharmacol Exp Ther.* 1999 Mar 1;288(3):1288–97.
134. Handley DA, Cervoni P, McCray JE, McCullough JR. Preclinical Enantioselective Pharmacology of (R)- and (S)- Ketorolac. *J Clin Pharmacol.* 1998 Feb 1;38(2S):25S – 35S.
135. Brune, Patrignani P. New insights into the use of currently available non-steroidal anti-inflammatory drugs. *J Pain Res.* 2015 Feb;105.
136. Hinz B, Cheremina O, Besz D, Zlotnick S, Brune K. Impact of naproxen sodium at over-the-counter doses on cyclooxygenase isoforms in human volunteers. *Int J Clin Pharmacol Ther.* 2008 Apr;46(4):180–6.
137. Sawyer GA, Anderson BC, Raukar NP, Fadale PD. Intramuscular Ketorolac Injections in the Athlete. *Sports Health Multidiscip Approach.* 2012 Jul 1;4(4):319–27.
138. Suh N, Reddy BS, DeCastro A, Paul S, Lee HJ, Smolarek AK, et al. Combination of Atorvastatin with Sulindac or Naproxen Profoundly Inhibits Colonic Adenocarcinomas by Suppressing the p65/ β -Catenin/Cyclin D1 Signaling Pathway in Rats. *Cancer Prev Res (Phila Pa).* 2011 Nov 1;4(11):1895–902.

139. Fischer SM, Hawk ET, Lubet RA. Coxibs and Other Nonsteroidal Anti-Inflammatory Drugs in Animal Models of Cancer Chemoprevention. *Cancer Prev Res (Phila Pa)*. 2011 Nov 1;4(11):1728–35.
140. Lubet RA, Steele VE, Juliana MM, Grubbs CJ. Screening Agents for Preventive Efficacy in a Bladder Cancer Model: Study Design, End Points, and Gefitinib and Naproxen Efficacy. *J Urol*. 2010 Apr;183(4):1598–603.
141. Wilson JC, Murray LJ, Hughes CM, Black A, Anderson LA. Non-steroidal anti-inflammatory drug and aspirin use and the risk of head and neck cancer. *Br J Cancer*. 2013 Mar 19;108(5):1178–81.
142. Ranger GS. Current concepts in colorectal cancer prevention with cyclooxygenase inhibitors. *Anticancer Res*. 2014 Nov;34(11):6277–82.
143. Forget P, Vandenhende J, Berliere M, Machiels J-P, Nussbaum B, Legrand C, et al. Do Intraoperative Analgesics Influence Breast Cancer Recurrence After Mastectomy? A Retrospective Analysis: *Anesth Analg*. 2010 Jun;110(6):1630–5.
144. Legge F, Paglia A, Asta M D', Fuoco G, Scambia G, Ferrandina G. Phase II study of the combination carboplatin plus celecoxib in heavily pre-treated recurrent ovarian cancer patients. *BMC Cancer*. 2011 May 31;11(1):214.
145. Lindhagen E, Nissle S, Leoni L, Elliott G, Chao Q, Larsson R, et al. R-etodolac (SDX-101) and the related indole–pyran analogues SDX-308 and SDX-309 potentiate the antileukemic activity of standard cytotoxic agents in primary chronic lymphocytic leukaemia cells. *Cancer Chemother Pharmacol*. 2006 Dec 22;60(4):545–53.
146. Iwanicki MP, Davidowitz RA, Ng MR, Besser A, Muranen T, Merritt M, et al. Ovarian Cancer Spheroids Use Myosin-Generated Force to Clear the Mesothelium. *Cancer Discov*. 2011 Jul 1;1(2):144–57.
147. Muranen T, Selfors LM, Worster DT, Iwanicki MP, Song L, Morales FC, et al. Inhibition of PI3K/mTOR Leads to Adaptive Resistance in Matrix-Attached Cancer Cells. *Cancer Cell*. 2012 Feb 14;21(2):227–39.
148. Casey RC, Burleson KM, Skubitz KM, Pambuccian SE, Oegema Jr. TR, Ruff LE, et al. β 1-Integrins Regulate the Formation and Adhesion of Ovarian Carcinoma

Multicellular Spheroids. *Am J Pathol.* 2001 Dec;159(6):2071–80.

149. Allen HJ, Porter C, Gamarra M, Piver MS, Johnson EA. Isolation and morphologic characterization of human ovarian carcinoma cell clusters present in effusions. *Exp Cell Biol.* 1987;55(4):194–208.
150. Guo Y, Kenney SR, Muller CY, Adams SF, Rutledge T, Murray-Krezaan C, et al. R-Ketorolac targets Cdc42 and rac1 and alters ovarian cancer cell behaviors critical for invasion and metastasis. *Mol Cancer Ther.*
151. Mrosczak E, Combs D, Chaplin M, Tsina I, Tarnowski T, Rocha C, et al. Chiral Kinetics and Dynamics of Ketorolac. *J Clin Pharmacol.* 1996 Jun 1;36(6):521–39.
152. Vaish V, Piplani H, Rana C, Vaiphei K, Sanyal SN. NSAIDs may regulate EGR-1-mediated induction of reactive oxygen species and non-steroidal anti-inflammatory drug-induced gene (NAG)-1 to initiate intrinsic pathway of apoptosis for the chemoprevention of colorectal cancer. *Mol Cell Biochem.* 2013 Feb 23;378(1-2):47–64.
153. Lin C, Crawford DR, Lin S, Hwang J, Sebuyira A, Meng R, et al. Inducible COX-2-dependent apoptosis in human ovarian cancer cells. *Carcinogenesis.* 2011 Jan 1;32(1):19–26.
154. Duncan K, Uwimpuhwe H, Czibere A, Sarkar D, Libermann TA, Fisher PB, et al. NSAIDs induce apoptosis in nonproliferating ovarian cancer cells and inhibit tumor growth in vivo. *IUBMB Life.* 2012 Jul 1;64(7):636–43.
155. García-Martínez O, De Luna-Bertos E, Ramos-Torrecillas J, Manzano-Moreno FJ, Ruiz C. Repercussions of NSAIDS drugs on bone tissue: The osteoblast. *Life Sci.* 2015 Feb 15;123:72–7.
156. Beitzel K, McCarthy MB, Cote MP, Apostolakos J, Russell RP, Bradley J, et al. The Effect of Ketorolac Tromethamine, Methylprednisolone, and Platelet-Rich Plasma on Human Chondrocyte and Tenocyte Viability. *Arthrosc J Arthrosc Relat Surg.* 2013 Jul;29(7):1164–74.
157. Kenny HA, Dogan S, Zillhardt M, K. Mitra A, Yamada SD, Krausz T, et al. Organotypic Models of Metastasis: A Three-dimensional Culture Mimicking the Human Peritoneum and Omentum for the Study of the Early Steps of Ovarian

- Cancer Metastasis. In: Stack MS, Fishman DA, editors. Ovarian Cancer [Internet]. Boston, MA: Springer US; 2009 [cited 2015 Jul 16]. p. 335–51. Available from: http://link.springer.com/10.1007/978-0-387-98094-2_16
158. Kenny HA, Lal-Nag M, White EA, Shen M, Chiang C-Y, Mitra AK, et al. Quantitative high throughput screening using a primary human three-dimensional organotypic culture predicts in vivo efficacy. *Nat Commun* [Internet]. 2015 Feb 5 [cited 2015 Jul 16];6. Available from: <http://www.nature.com/ncomms/2015/150205/ncomms7220/full/ncomms7220.html>
159. Yasui H, Hideshima T, Ikeda H, Ocio EM, Kiziltepe T, Vallet S, et al. Novel etodolac analog SDX-308 (CEP-18082) induces cytotoxicity in multiple myeloma cells associated with inhibition of β -catenin/TCF pathway. *Leukemia*. 2007 Feb 1;21(3):535–40.
160. Yasui H, Hideshima T, Hamasaki M, Roccaro AM, Shiraishi N, Kumar S, et al. SDX-101, the R-enantiomer of etodolac, induces cytotoxicity, overcomes drug resistance, and enhances the activity of dexamethasone in multiple myeloma. *Blood*. 2005 Jul 15;106(2):706–12.
161. Kopf PG, Scott JA, Agbor LN, Boberg JR, Elased KM, Huwe JK, et al. Cytochrome P4501A1 Is Required for Vascular Dysfunction and Hypertension Induced by 2,3,7,8-Tetrachlorodibenzo-p-Dioxin. *Toxicol Sci*. 2010 Oct 1;117(2):537–46.
162. Jayson GC, Kohn EC, Kitchener HC, Ledermann JA. Ovarian cancer. *The Lancet*. 2014 Oct 17;384(9951):1376–88.
163. Lawson CD, Burridge K. The on-off relationship of Rho and Rac during integrin-mediated adhesion and cell migration. *Small GTPases*. 2014 Jan 1;5(1):e27958.
164. Karlsson R, Pedersen ED, Wang Z, Brakebusch C. Rho GTPase function in tumorigenesis. *Biochim Biophys Acta BBA - Rev Cancer*. 2009 Dec;1796(2):91–8.
165. Leve F, Morgado-Díaz JA. Rho GTPase signaling in the development of colorectal cancer. *J Cell Biochem*. 2012 Aug 1;113(8):2549–59.
166. Friesland A, Zhao Y, Chen Y-H, Wang L, Zhou H, Lu Q. Small molecule targeting Cdc42–intersectin interaction disrupts Golgi organization and suppresses cell

- motility. *Proc Natl Acad Sci*. 2013 Jan 22;110(4):1261–6.
167. Montalvo-Ortiz BL, Castillo-Pichardo L, Hernández E, Humphries-Bickley T, Mota-Peynado ADL, Cubano LA, et al. Characterization of EHop-016, Novel Small Molecule Inhibitor of Rac GTPase. *J Biol Chem*. 2012 Apr 13;287(16):13228–38.
168. Oprea TI, Bauman JE, Bologna CG, Buranda T, Chigaev A, Edwards BS, et al. Drug Repurposing from an Academic Perspective. *Drug Discov Today Ther Strateg*. 2011;8(3-4):61–9.
169. Bast RC, Hennessy B, Mills GB. The biology of ovarian cancer: new opportunities for translation. *Nat Rev Cancer*. 2009 Jun;9(6):415–28.
170. Matos P, Oliveira C, Velho S, Gonçalves V, da Costa LT, Moyer MP, et al. B-RafV600E Cooperates With Alternative Spliced Rac1b to Sustain Colorectal Cancer Cell Survival. *Gastroenterology*. 2008 Sep;135(3):899–906.
171. Lee K, Chen QK, Lui C, Cichon MA, Radisky DC, Nelson CM. Matrix compliance regulates Rac1b localization, NADPH oxidase assembly, and epithelial–mesenchymal transition. *Mol Biol Cell*. 2012 Oct 15;23(20):4097–108.
172. Liu J, Lee W, Jiang Z, Chen Z, Jhunjhunwala S, Haverly PM, et al. Genome and transcriptome sequencing of lung cancers reveal diverse mutational and splicing events. *Genome Res*. 2012 Dec 1;22(12):2315–27.
173. Hayball PJ, Wrobel J, Tamblyn JG, Nation RL. The pharmacokinetics of ketorolac enantiomers following intramuscular administration of the racemate. *Br J Clin Pharmacol*. 1994 Jan;37(1):75–8.
174. Mack NA, Whalley HJ, Castillo-Lluva S, Malliri A. The diverse roles of Rac signaling in tumorigenesis. *Cell Cycle*. 2011 May 15;10(10):1571–81.
175. Forget P, Machiels J-P, Coulie PG, Berliere M, Poncelet AJ, Tombal B, et al. Neutrophil:Lymphocyte Ratio and Intraoperative Use of Ketorolac or Diclofenac are Prognostic Factors in Different Cohorts of Patients Undergoing Breast, Lung, and Kidney Cancer Surgery. *Ann Surg Oncol*. 2013 Jul 25;20(3):650–60.

176. Kolluri SK, Corr M, James SY, Bernasconi M, Lu D, Liu W, et al. The R-enantiomer of the nonsteroidal antiinflammatory drug etodolac binds retinoid X receptor and induces tumor-selective apoptosis. *Proc Natl Acad Sci U S A*. 2005 Feb 15;102(7):2525–30.
177. Feng R, Lentzsch S. Treatment of multiple myeloma with SDX-308. *Drug News Perspect*. 2007 Sep;20(7):431–5.
178. Robak P, Smolewski P, Robak T. The role of non-steroidal anti-inflammatory drugs in the risk of development and treatment of hematologic malignancies. *Leuk Lymphoma*. 2008 Jan 1;49(8):1452–62.
179. Vakily M, Corrigan B, Jamali F. The problem of racemization in the stereospecific assay and pharmacokinetic evaluation of ketorolac in human and rats. *Pharm Res*. 1995 Nov;12(11):1652–7.
180. Buranda T, BasuRay S, Swanson S, Agola J, Bondu V, Wandinger-Ness A. Rapid parallel flow cytometry assays of active GTPases using effector beads. *Anal Biochem*. 2013 Nov 15;442(2):149–57.
181. Orlichenko L, Geyer R, Yanagisawa M, Khauv D, Radisky ES, Anastasiadis PZ, et al. The 19-Amino Acid Insertion in the Tumor-associated Splice Isoform Rac1b Confers Specific Binding to p120 Catenin. *J Biol Chem*. 2010 Jun 18;285(25):19153–61.